行政院國家科學委員會專題研究計畫 成果報告

鄰近傾斜岩石面對擋土牆主動土壓力之影響
研究成果報告(精簡版)

計 畫 類 別 ：個別型
計 畫 編 號 ：NSC 100-2221-E-009-128-
執 行 期 間 ：100 年 08 月 01 日至 101 年 07 月 31 日
執 行 單 位 ：國立交通大學土木工程學系（所）

計 畫 主 持 人：方永壽

計畫參與人員：碩士班研究生-兼任助理人員：劉政
碩士班研究生-兼任助理人員：黃昱銨
碩士班研究生-兼任助理人員：李易昌
碩士班研究生-兼任助理人員：李承祐
碩士班研究生-兼任助理人員：黃湘銘

報 告 附 件 ：出席國際會議研究心得報告及發表論文

公 開 資 訊 ：本計畫可公開查詢

中 華 民 國 101 年 11 月 26 日

中 文 摘 要 ： 本研究探討鄰近堅硬岩石面入侵回填土對擋土牆主動土壓力之影響。本研究以氣乾之渥太華砂為回填土，回填土高及牆高 H 皆為 0.5 公尺。量測於鬆砂(相對密度 Dr = 35%)狀態下，作用於剛性擋土牆的側向土壓力。本研究利用國立交通大學模型擋土牆設備，探討堅硬界面以不同傾角 beta 侵入回填土，對擋土牆主動土壓力影響。為模擬堅硬的岩石界面，本研究設計並建造一座鋼製界面板，及其支撐系統。本研究共執行五種岩石界面與水平面夾角 beta = 0、50、60、70 與 80 度五組實驗。依據實驗結果，獲得以下幾項結論。(1).當岩石界面傾角 beta = 0 度時，其主動土壓力係數 Ka,h 與 Coulomb 解相吻合，其主動合力作用於距擋土牆底部約 0.33H 處。(2)在岩石界面傾角 45、60、70 與 80 度狀況下，側向土壓力隨深度的增加而呈非線性分布，所獲得的側向土壓力低於 Jaky 解，側向土壓力隨界面傾角的增加而減少。(3)當界面傾角為 50 至 80 度，主動土壓合力隨岩石界面傾角的增加而逐漸減小。合力作用點的位置稍高於理論值 0.33H。(4)當傾斜岩石面入侵主動土楔時，造成擋土牆抗滑動之安全係數增加，因此根據 Coulomb 理論所求解之安全係數會偏向安全。(5)當傾斜岩石面入侵主動土楔時，使擋土牆抗傾覆之安全係數增加，所以依據 Coulomb 理論所求得之安全係數會趨於安全。

中文關鍵詞： 主動土壓力、回填土、擋土牆、土壓力

英 文 摘 要 ： In this report, the active earth pressure on retaining walls with the intrusion of an inclined rock face into the backfill is studied. The instrumented model retaining-wall facilities at National Chiao Tung University was used to investigate the active earth pressure induced by different interface inclination angle beta. Loose Ottawa sand was used as backfill material. The thickness of backfill and the wall height H were 0.5 m. To simulate an inclined rock face, a steel interface plate and its supporting system were designed and constructed. Base on the test results, the following conclusions were drawn. (1) Without the Stiff interface (beta = 0 degree), the active earth pressure coefficient Ka,h is in good agreement with Coulomb’s equation. The point of application of the active soil thrust is located at about 0.33H above the base of the wall. (2) For the interface

inclination angle beta = 50, 60, 70 and 80 degree, the distributions of active earth pressure are not linearly with depth. On the lower part of the model wall, the measured horizontal pressure is lower than Coulomb ‘s prediction. (3) For beta = 50 to 80 degree, the active earth pressure coefficient Ka,h decreases with increasing interface inclination angle. The point of application of the active thrust moves a location slight higher than h/H = 0.333. (4) For beta = 50 to 80 degree, the nearby inclined rock face would actually increase the factor of safety (FS) against sliding of the wall. The evaluation of FS against sliding with Coulomb’s theory would be on the safe side. (5) For beta = 50 to 80 degree, the intrusion of an inclined rock face into the active wedge would increase the FS against overturning of the retaining wall. The evaluation of FS against overturning with Coulomb ‘s theory would also be on the safe side.

英文關鍵詞： active earth pressure, backfill, retaining wall, earth pressure

行政院國家科學委員會 補助專題研究計畫
成果報告

鄰近傾斜岩石面對擋土牆主動土壓力之影響

計畫類別：■ 個別型計畫　　□ 整合型計畫
計畫編號：NSC 100-2221-E-009-128-
執行期間：100 年 08 月 01 日至 101 年 07 月 31 日

計畫主持人：　方永壽 教授
計畫參與人員：　鄭詠誠 劉政 黃昱銨 碩士班研究生

成果報告類型(依經費核定清單規定繳交)：□精簡報告　■完整報告

本成果報告包括以下應繳交之附件：
□赴國外出差或研習心得報告一份
□赴大陸地區出差或研習心得報告一份
■出席國際學術會議心得報告及發表之論文各一份
□國際合作研究計畫國外研究報告書一份

處理方式：除產學合作研究計畫、提升產業技術及人才培育研究計畫、列管計畫及下列情形者外，得立即公開查詢
□涉及專利或其他智慧財產權，□一年□二年後可公開查詢

執行單位：　國立交通大學土木工程學系

中 華 民 國　101　年　10　月　31　日

鄰近傾斜岩石面對擋土牆主動土壓力之影響

摘要

本研究探討鄰近堅硬岩石面入侵回填土對擋土牆主動土壓力之影響。本研究以氣乾之渥太華砂為回填土，回填土高及牆高 H 皆為 0.5 公尺。量測於鬆砂(相對密度 D_r = 35%)狀態下，作用於剛性擋土牆的側向土壓力。本研究利用國立交通大學模型擋土牆設備，探討堅硬界面以不同傾角β侵入回填土，對擋土牆主動土壓力影響。為模擬堅硬的岩石界面，本研究設計並建造一座鋼製界面板，及其支撐系統。本研究共執行五種岩石界面與水平面夾角β = 0^o、50^o、60^o、70^o 與 80^o 五組實驗。依據實驗結果，獲得以下幾項結論。

1. 當岩石界面傾角β = 0^o 時，其主動土壓力係數 $K_{a,h}$ 與 Coulomb 解相吻合，其主動合力作用於距擋土牆底部約 0.33H 處。
2. 在岩石界面傾角 45^o、60^o、70^o 與 80^o 狀況下，側向土壓力隨深度的增加而呈非線性分布，所獲得的側向土壓力低於 Jaky 解，側向土壓力隨界面傾角的增加而減少。
3. 當界面傾角為 50^o 至 80^o，主動土壓合力隨岩石界面傾角的增加而逐漸減小。合力作用點的位置稍高於理論值 0.33H。
4. 當傾斜岩石面入侵主動土楔時，造成擋土牆抗滑動之安全係數增加，因此根據 Coulomb 理論所求解之安全係數會偏向安全。
5. 當傾斜岩石面入侵主動土楔時，使擋土牆抗傾覆之安全係數增加，所以依據 Coulomb 理論所求得之安全係數會趨於安全。

關鍵字： 主動土壓力、回填土、擋土牆、土壓力

Active Earth Pressures on Retaining Walls adjacent to Inclined Rock Faces

Abstract

In this report, the active earth pressure on retaining walls with the intrusion of an inclined rock face into the backfill is studied. The instrumented model retaining-wall facilities at National Chiao Tung University was used to investigate the active earth pressure induced by different interface inclination angle β. Loose Ottawa sand was used as backfill material. The thickness of backfill and the wall height H were 0.5 m. To simulate an inclined rock face, a steel interface plate and its supporting system were designed and constructed. Base on the test results, the following conclusions were drawn.

1. Without the Stiff interface ($\beta = 0^o$), the active earth pressure coefficient $K_{a,h}$ is in good agreement with Coulomb's equation. The point of application of the active soil thrust is located at about 0.33H above the base of the wall.
2. For the interface inclination angle $\beta = 50^o$, 60^o, 70^o and 80^o, the distributions of active earth pressure are not linearly with depth. On the lower part of the model wall, the measured horizontal pressure is lower than Coulomb's prediction.
3. For $\beta = 50^o$ to 80^o, the active earth pressure coefficient $K_{a,h}$ decreases with increasing interface inclination angle. The point of application of the active thrust moves a location slight higher than h/H = 0.333.
4. For $\beta = 50^o$ to 80^o, the nearby inclined rock face would actually increase the factor of safety (FS) against sliding of the wall. The evaluation of FS against sliding with Coulomb's theory would be on the safe side.
5. For $\beta = 50^o$ to 80^o, the intrusion of an inclined rock face into the active wedge would increase the FS against overturning of the retaining wall. The evaluation of FS against overturning with Coulomb's theory would also be on the safe side.

Keywords: active earth pressure, backfill, retaining wall, earth pressure.

TABLE OF CONTENTS

1. INTRODUCTION

The NCTU model retaining wall facility was modified to study the effects of an adjacent inclined rock face on active earth pressure. A steel interface plate simulating the rock face was designed contracted. A top supporting beam, and a base supporting block was constructed to support the steel interface plate. Air-dry Ottawa sand was used as backfill material. For a loose backfill, the soil was placed behind the wall with air-pluviaiton method to achieve a relative density of 35%.

The main parameter considered for this study is the rock face inclination angles β = 0°, 50°, 60°, 70° and 80° as illustrated in Fig.1. The height of the wall H = 0.5 m. The variation of lateral earth pressure was measured with the soil pressure transducers (SPT) on the surface of the model wall. Based on experimental results, the distribution of earth pressure on the retaining wall adjacent an inclined rock face can be obtained. It is hoped that the findings of this study would provide valuable information for the geotechnical engineer to design the retaining structure near a inclined rock face more safely and more efficiently.

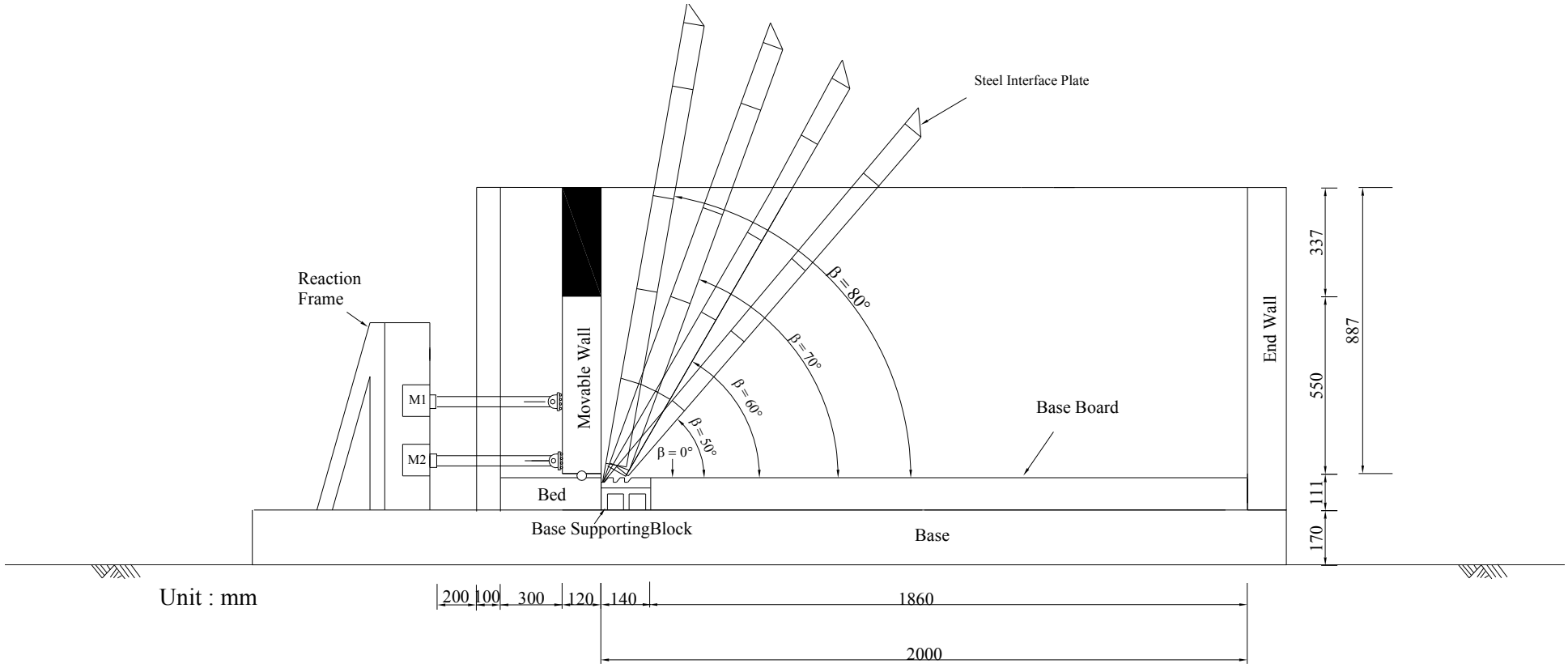

Fig. 1. Model wall test with different interface inclinations

2. LITERATURE REVIEW

It is common to all the theories that the soil mass be in a state of limiting equilibrium, and shear strength of the soil be expressed in terms of the Mohr-Coulomb failure criterion. However, they differ in the assumption about the shape of the failure surface. For example, Coulomb (1776) assumed that sliding occurs along a planar sliding surface. The method developed by Brinch Hansen (1953) assumed the soil wedge slip along a circular surface. Janbu's theory (1957) is not restricted to a particular shape of slip surface, but makes use of the method of slices and satisfied equilibrium in approximate manner. Terzaghi's general wedge theory (1941) is based on logarithmic spiral slip surface.

The coefficient of active earth pressure K_a computed from various theories was compared by Morgenstern and Eisenstein (1970). Fig. 2 shows the variation of K_a as a function of internal friction angle ϕ of backfill, where the wall friction angle δ is equal to ϕ and $\phi/2$. For the case $\delta = \phi/2$, the total range of variation of K_a is generally less than 15% from Rankine's solution. In this study, K_a values estimated with the Coulomb theory are compared with experiment results.

Fan and Chen (2006) used the non-linear finite element program PLAXIS to investigate the earth pressure from the at-rest to the active condition for a rigid wall close to an inclined rock face. In Fig. 3 the wall used for analysis is 5 m high, the back of the wall is vertical, and the surface of the backfill is horizontal. To investigate the influence of the adjacent rock face on the behavior of earth pressure, the inclination angle β of the rock face and the spacing d between the wall and the foot of the rock face were the parameters for numerical analysis. The wall was prevented from any movement during the placing of the fill. After the filling process, active wall movement was allowed until earth pressure behind the wall reached the active condition. The wall was assumed to be rigid. Fig. 4 shows the finite element mesh, which has been examined to eliminate the influence of size effect and boundary effects. The finite element mesh consists of 1,512 elements, 3,580 nodes, and 4,536 stress points. Base on the numerical analysis, the distribution of earth pressure at various wall displacements for translational mode (T mode) is shown in Fig. 5. The distribution of active earth pressure with depth is non-linear. The calculated active pressure is considerably less than that computed using the Coulomb's theory.

Fig. 6 shows the variation of the active earth pressure coefficient K_A computed with finite element analysis, as a function of the inclination β of the rock face and rock face-wall spacing d, for walls under T mode. The analytical active K values are less than those calculated with Coulomb's solution. The analytical K_A value decreased with decreasing β angle, for β angle less than 30°. Fig. 7 shows the variation of the K_A with the β angle at d = 0 with T, RT (rotation about top) and RB (rotation about base) modes.

Fig. 8 shows the variation of the point of application of the active soil thrust with the β angle for d = 0. The variation of the h/H value with the β for walls in RB and T modes are similar, where h is the vertical distance between the thrust and wall base. For walls in RB and T modes, the h/H decreased with increasing β angles, then it leveled off at h/H=0.333 for β angles greater than about 30°. However, the analytical h/H values were much higher than those for RB and T modes.

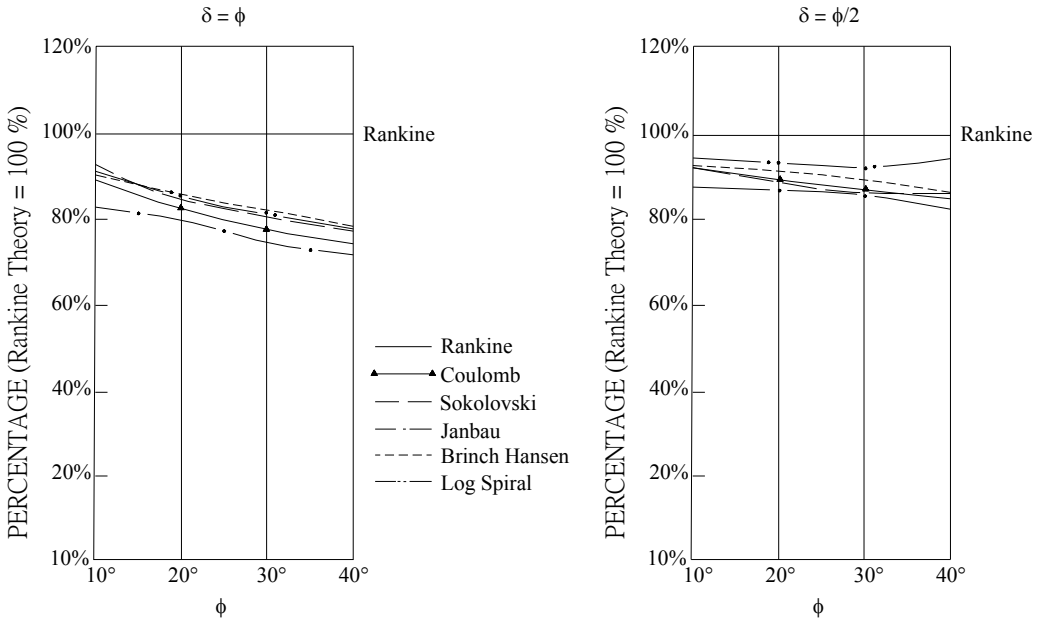

Fig. 2. Comparison of coefficient of horizontal component of active pressure for various theories (after Morgenstern and Eisenstein, 1970)

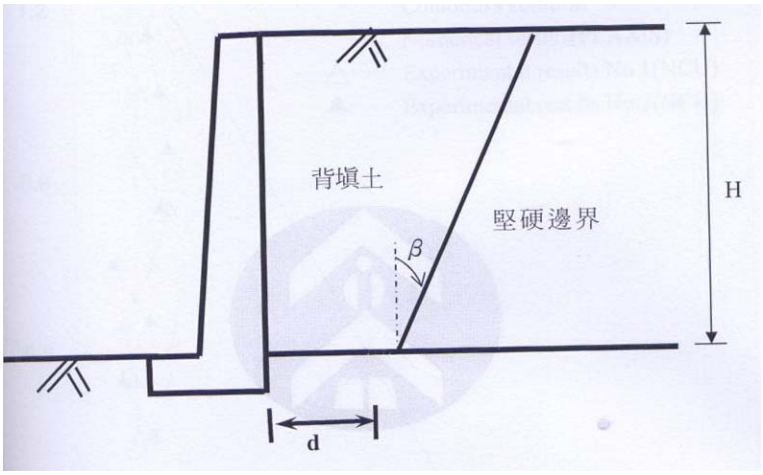

Fig. 3. Typical space of backfill behind a retaining wall (after Fan and Chen, 2006)

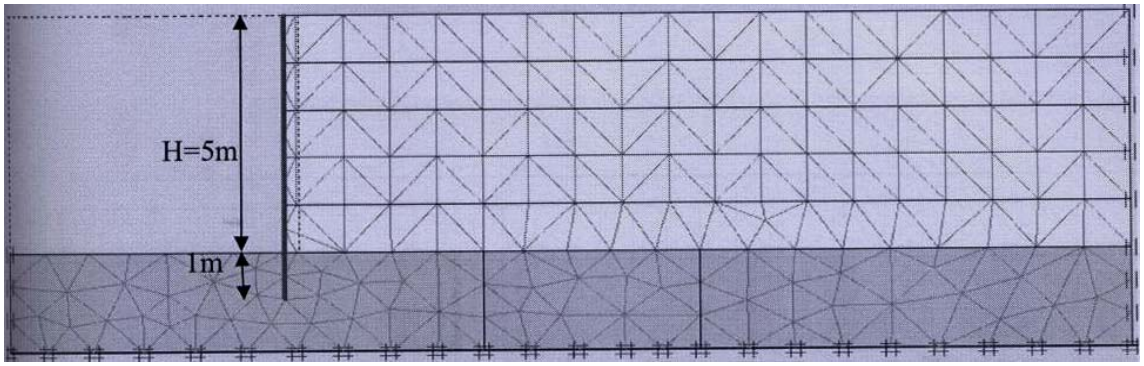

Fig. 4. Finite element mesh for a retaining wall with backfill (after Fan and Chen, 2006)

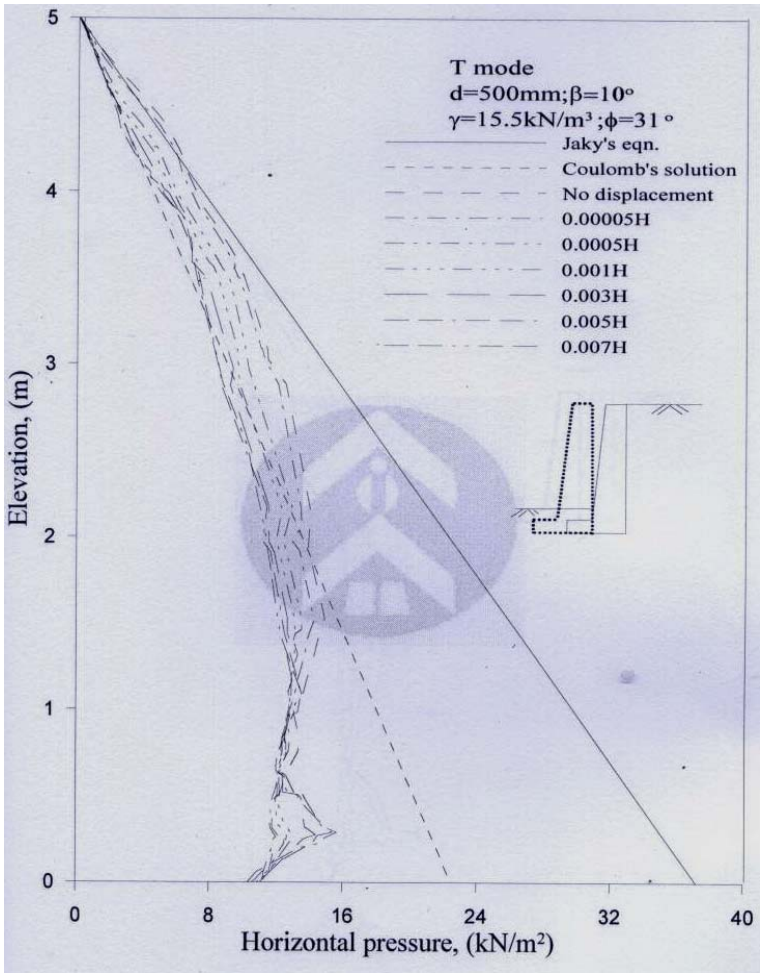

Fig. 5. Distribution of earth pressure at various wall displacements for T mode (after Fan and Chen, 2006)

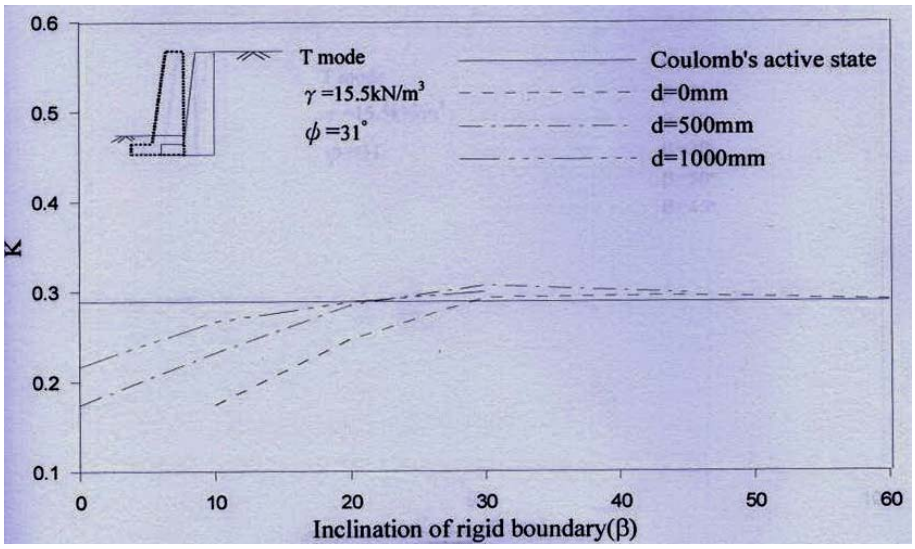

Fig. 6. Variation of K_A as a function of β and d for walls T mode (after Fan and Chen, 2006)

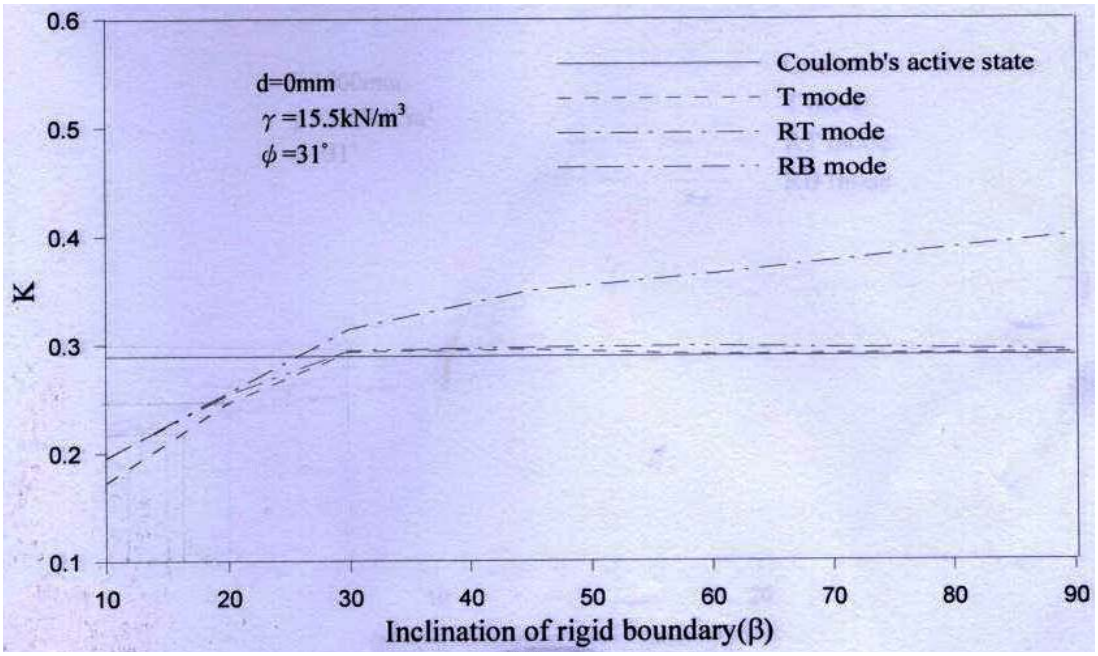

Fig. 7. Influence of type of wall movement on K_A with rock face inclination for d = 0 (after Fan and Chen, 2006)

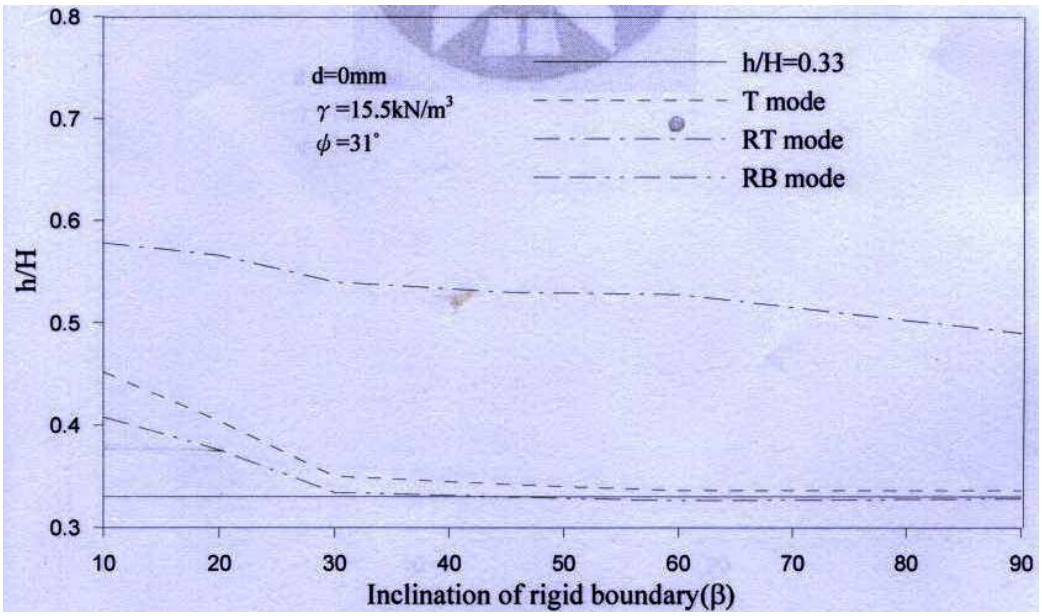

Fig. 8. Influence of types of wall movement on the location of resultant of active earth pressures for various inclinations of rock face at the backfill spacing d = 0 (after Fan and Chen, 2006)

3. EXPERIMENTAL APPARATUS

To study the earth pressure behind retaining structures, the National Chiao Tung University (NCTU) has built a model retaining wall facility which can simulate different kinds of wall movement. All of the investigations described in this report were conducted in this model wall system, which will be carefully discussed in this chapter. The entire system consists of the following components: (1) soil bin; (2) model retaining wall; (3) driving system; and (4) data acquisition system. The arrangement of the NCTU model retaining wall system is shown in Fig. 9.

3.1 Soil Bin

The soil bin is 2,000 mm in length, 1,000 mm in width and 1,000 mm in depth as shown in Fig. 10. Both side walls of the soil bin are made of 30 mm-thick transparent acrylic plates, through which the behavior of the backfill can be observed. Outside the acrylic plates, steel beams and columns are used to confine the side walls to ensure a plane strain condition.

3.2 Model Retaining Wall

The moveable retaining wall and its driving systems are shown in Fig. 9. The retaining wall is 1000 mm-wide, 550 mm-high, and 120 mm-thick, and is made of solid steel. The retaining wall is vertically supported by two unidirectional rollers and laterally supported by the steel frame through the driving system. Two separately controlled wall driving mechanism, one at the upper level, and the other at the lower level, provide various kinds of lateral wall movements.

A total of 9 earth pressure transducers have been arranged within a narrow central zone to avoid the friction that might exist near the side walls of the soil bin as shown in Fig. 12. The soil pressure transducers are strain-gage-type transducers (Kyowa PGM-02KG, capacity = 19.62kN/m^2) as shown in Fig. 11. To eliminate the soil arching effect, all soil pressure transducers are built quite stiff, and their measuring surfaces are flush with the face of the wall as shown in Fig. 13. They provide closely spaced data points for determining variation of the earth pressure distribution with depth.

3.3 Driving System

To achieve different modes of wall movement, two sets of driving rods are attached to the model wall. The upper driving rods are located 230 mm below the top of the wall, and the lower rods are located 236 mm below the upper rods as shown in Fig. 14. Two driving motors (ELECTRO, M-4621AB) supply the thrust to the upper and the lower driving rods independently. The wall speed and movement modes are controlled by the automatic motor speed control system (DIGILOK, DLC-300) shown in Fig. 15. By setting the same motor speed for the upper and lower driving rods, a translation mode can be achieved for the model wall test.

3.4. Data Acquisition System

Due to the considerable amount of data collected by the soil pressure transducers and displacement transducers, a data acquisition system shown in Fig. 16 was used for this study.

It is composed of the following four parts: (1) dynamic strain amplifiers (Kyowa DPM601A and DPM711B); (2) NI adaptor card; (3) AD/DA card; and (4) personal computers as indicated in Fig. 17. The analog signals obtained from the sensors are filtered and amplified by dynamic strain amplifiers. Analog experimental data are converted to digital data by the A/D - D/A card. The LabVIEW program is used to acquire test data, and experimental data are stored and analyzed with a personal computer.

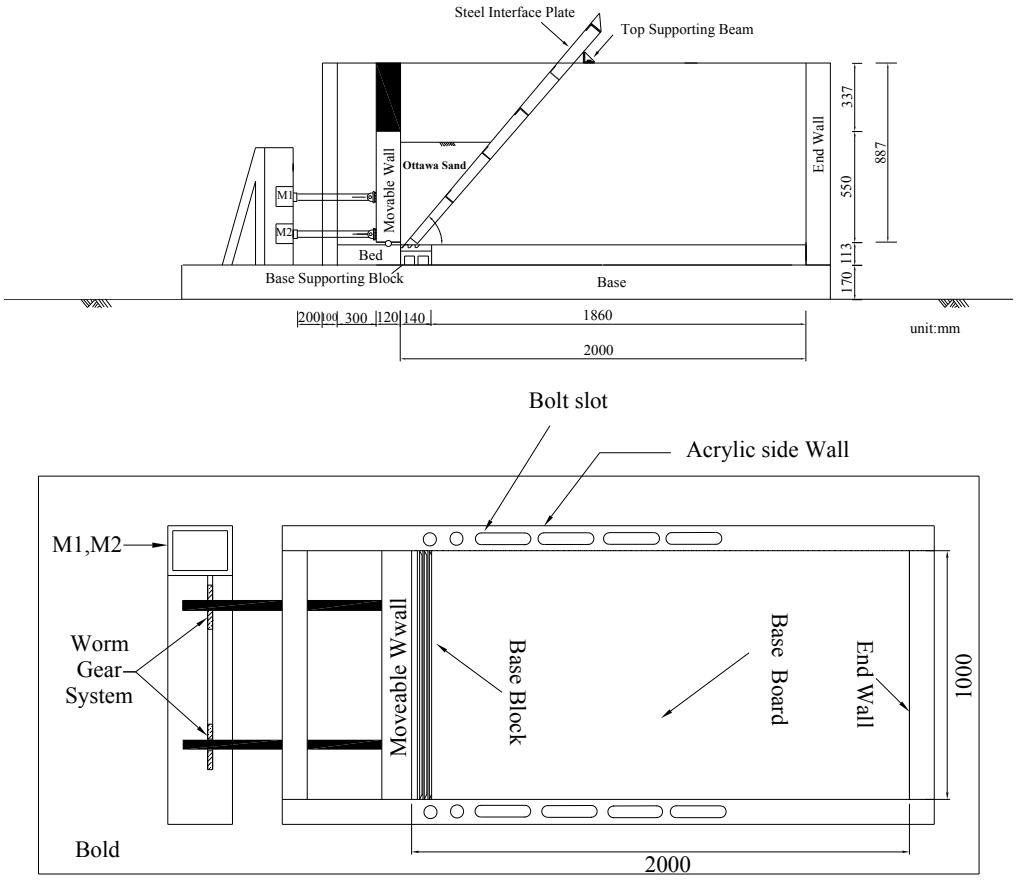

Fig. 9. NCTU model retaining wall

Fig. 10. Picture of NCTU model retaining wall

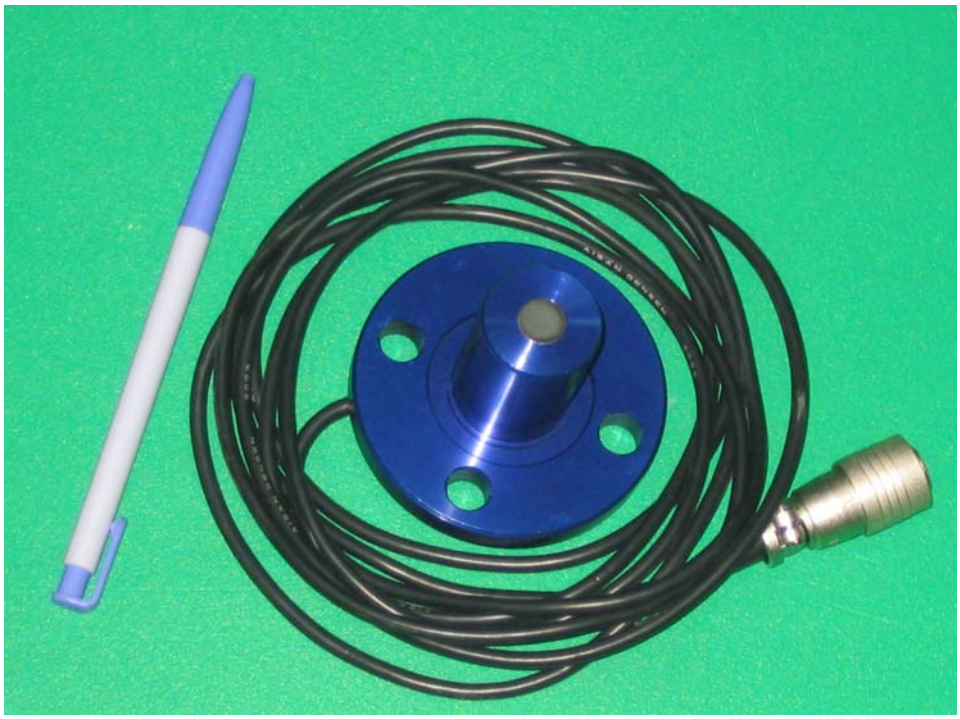

Fig. 11. Soil pressure transducer (Kyowa PGM-0.2KG)

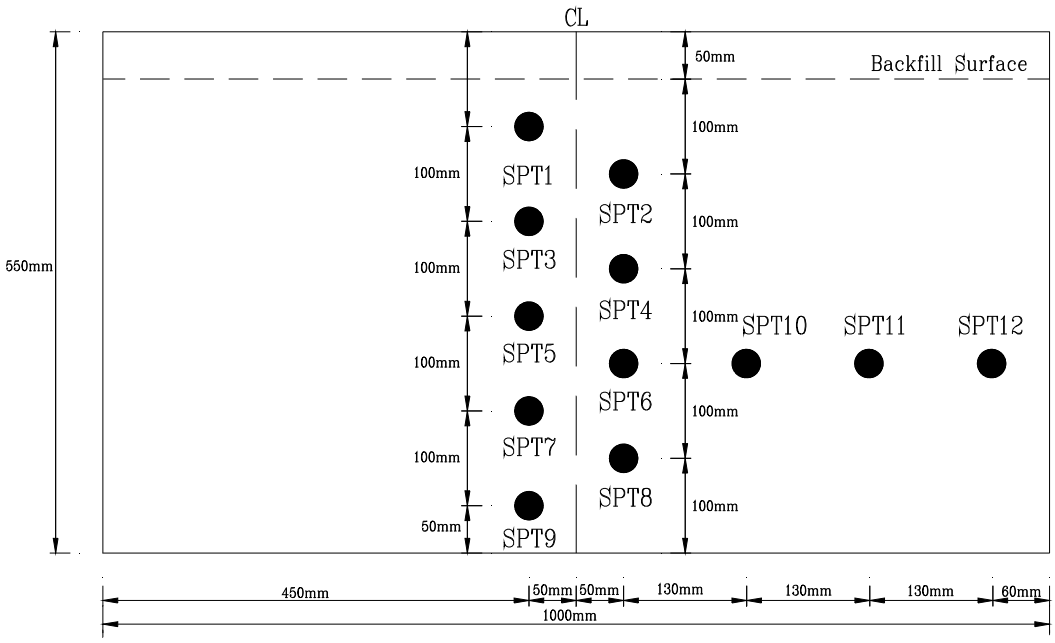

Fig. 12. Locations of pressure transducers on NCTU model wall

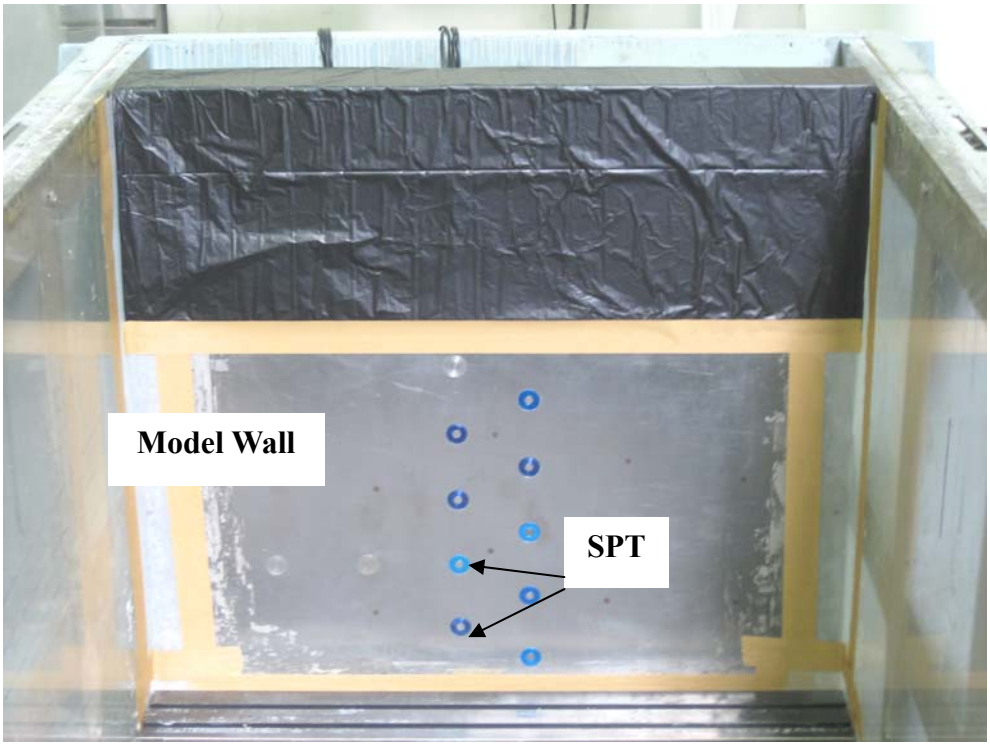

Fig. 13. Picture of pressure transducers on model wall

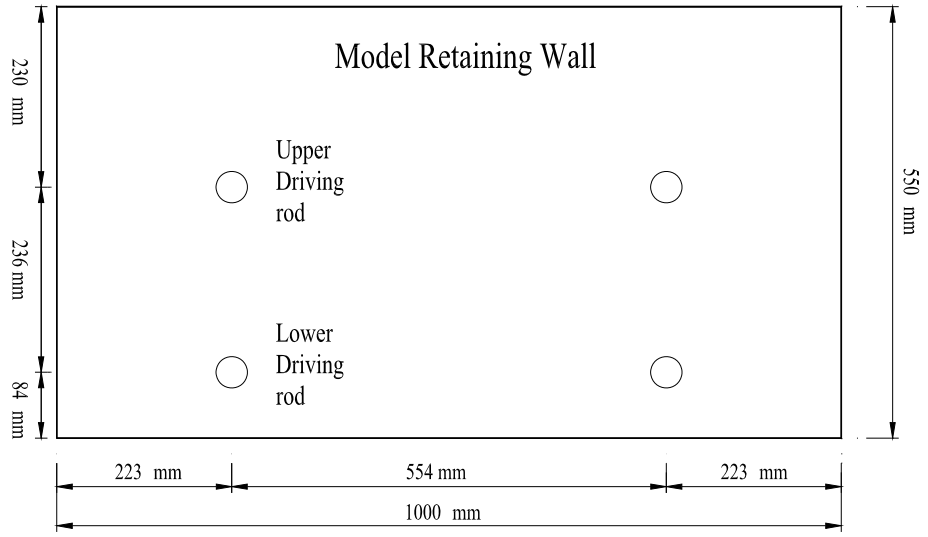

Fig. 14. Locations of driving rods

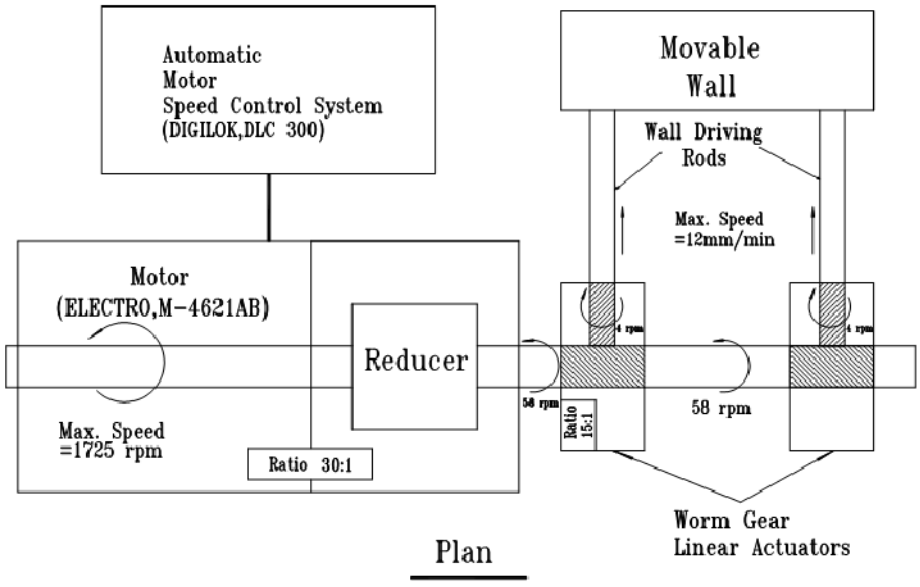

Fig. 15. Wall speed control system

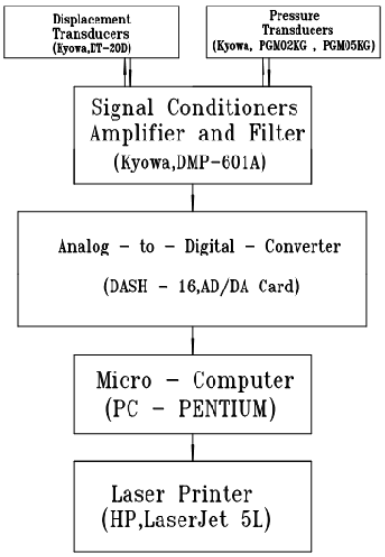

Fig. 16. Data Acquisition System

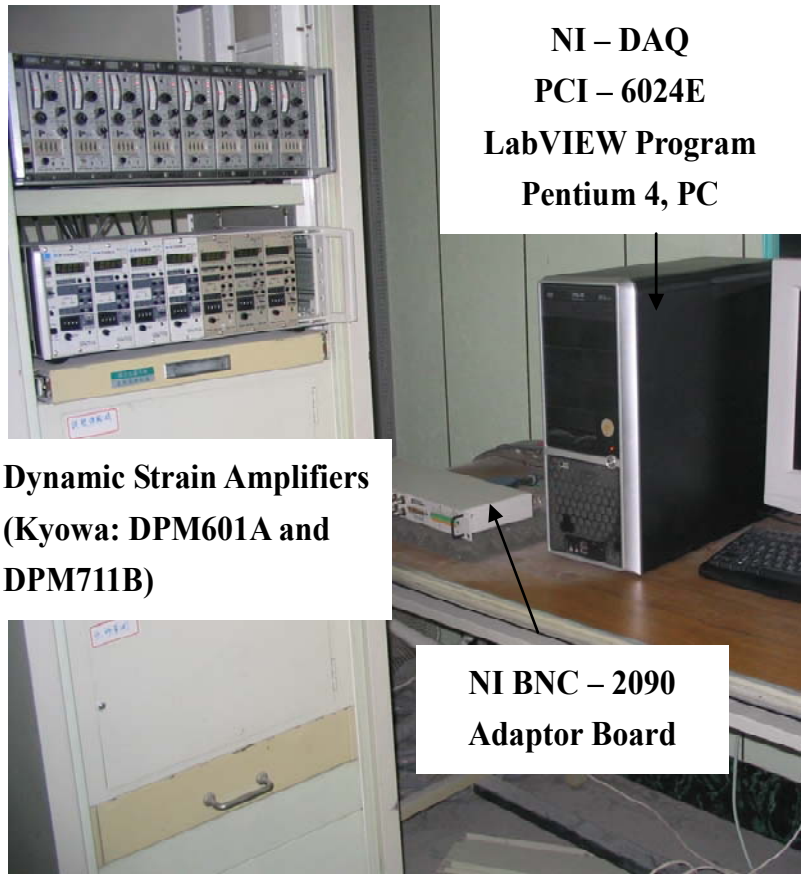

Fig. 17. Picture of data acquisition system

4. Interface Plate and Supporting System

4.1 Interface Plate

The steel plate is 1.370 m-long, 0.998 m-wide, and 5 mm-thick as shown in Fig. 18. The unit weight of the steel plate is 76.52 kN/m^3 and its total mass is 53.32 kg (0.523 kN). A layer of anti-slip material (Safety-walk, 3M) is attached on the steel plate to simulate the friction that acts between the backfill and rock face as illustrated in Fig. 18 (c) and Fig. 19 (a). For the inclination angle $\beta = 50^o$ shown in Fig. 1, the length of the interface plate should be at least 1.370 m. On the other hand, the inside width of the soil bin of the NCTU retaining wall facility is 1 m. To put the interface plate into the soil bin, the width of the steel plate has to less than 1.0 m. As a result, the steel plate was designed to be 1.370 m-long and 0.998 m-wide.

Section of the steel L-beam (30 mm x 30 mm x 3 mm) was chosen as the reinforced material. On top of the interface plate, a 65 mm x 65 mm x 8 mm steel L-beam was welded to reinforce the connection between the plate and the hoist ring shown in Fig. 19 (b).

4.2 Supporting System

In Fig. 20, the top supporting steel beam is placed at the back of the interface plate and fixed at the bolt slot of the side wall of the soil bin. Details of top supporting beam are illustrated in Fig. 21. The section of supporting steel beam is 65 mm $\times$ 65 mm $\times$ 8 mm and its length is 1,700 mm. Fig. 22 shows four bolt slots were drilled on each side of the U-shape steel beam on the side wall of the soil bin. Fig. 23 (b) shows the top supporting beam was fixed at the slots with bolts.

The base block used to support the steel interface plate is shown in Fig. 24. The supporting block is 1.00 m-long, 0.14 m-wide, and 0.113 m-thick. Fig. 24 (b) shows trapezoid grooves were caved to the face of the base supporting block. Fig. 20 shows the foot of the interface plate could be inserted into the groove at different distance from the model wall. Different horizontal spacing d could be adopted for testing includes: (1) d = 0 mm (2) d = 50 mm and (3) d = 100 mm. Fig. 20 shows 6 base boards are placed between the base supporting block and the end wall to keep the base block stable. Details of base boards are illustrated in Fig. 25. The base board is 1,860 mm-long, 1,002 mm-wide and 113 mm-thick. The surface of the top base board was cover with a layer of anti-slip material Safe-Walk.

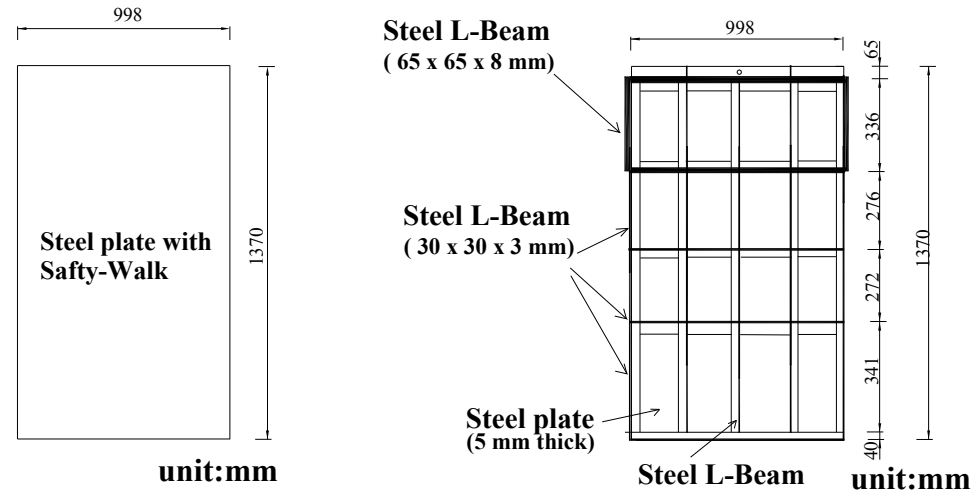

(a) Front-view (b) Back-view

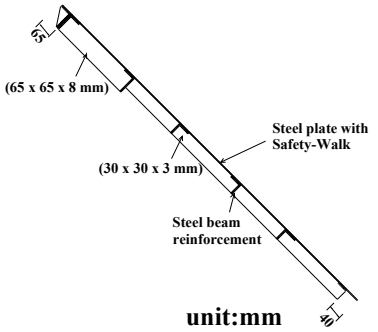

(c) Side-view

Fig. 18. Steel interface plate

(a) Front-view

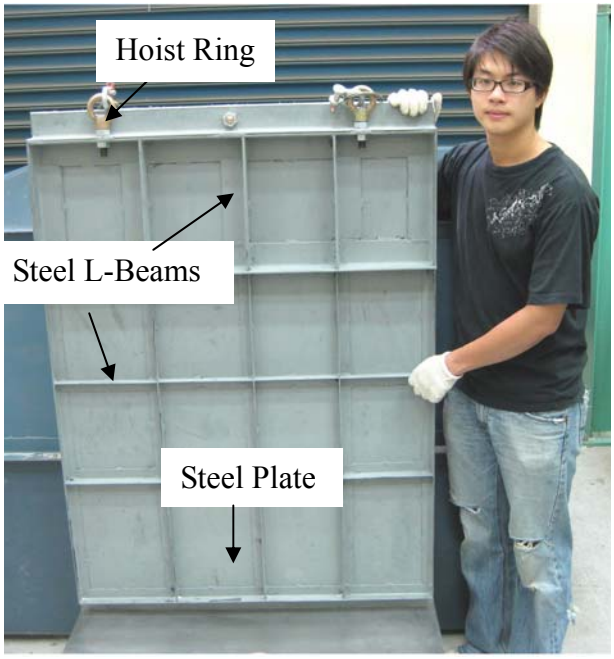

(b) Back-view

Fig. 19. Picture of steel interface plate

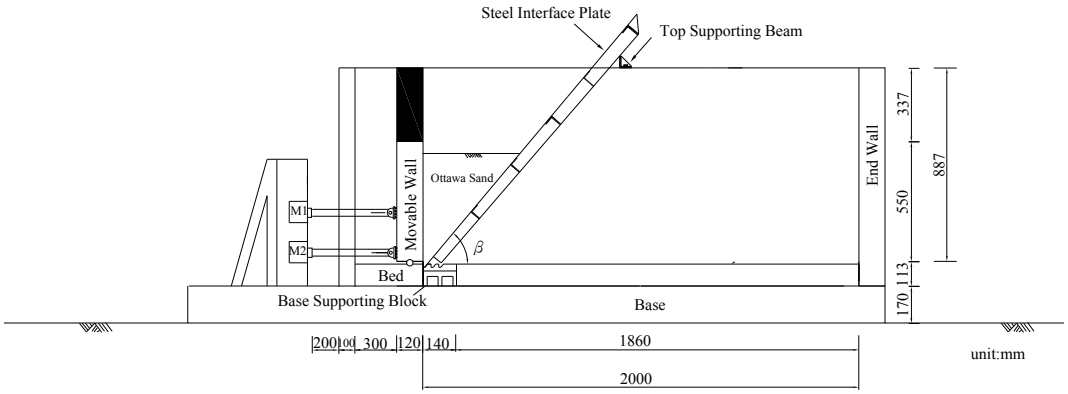

Fig. 20. Model retaining wall with interface plate and supports

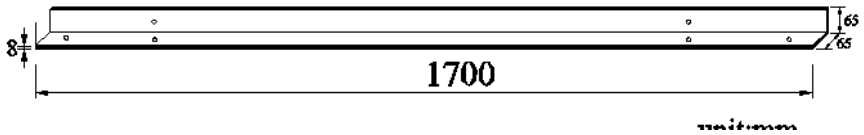

(a)

(b)

Fig. 21 Top supporting beam

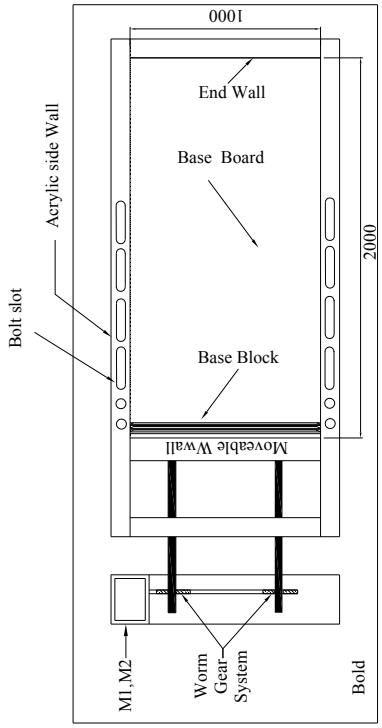

Fig. 22. Top-view of model wall

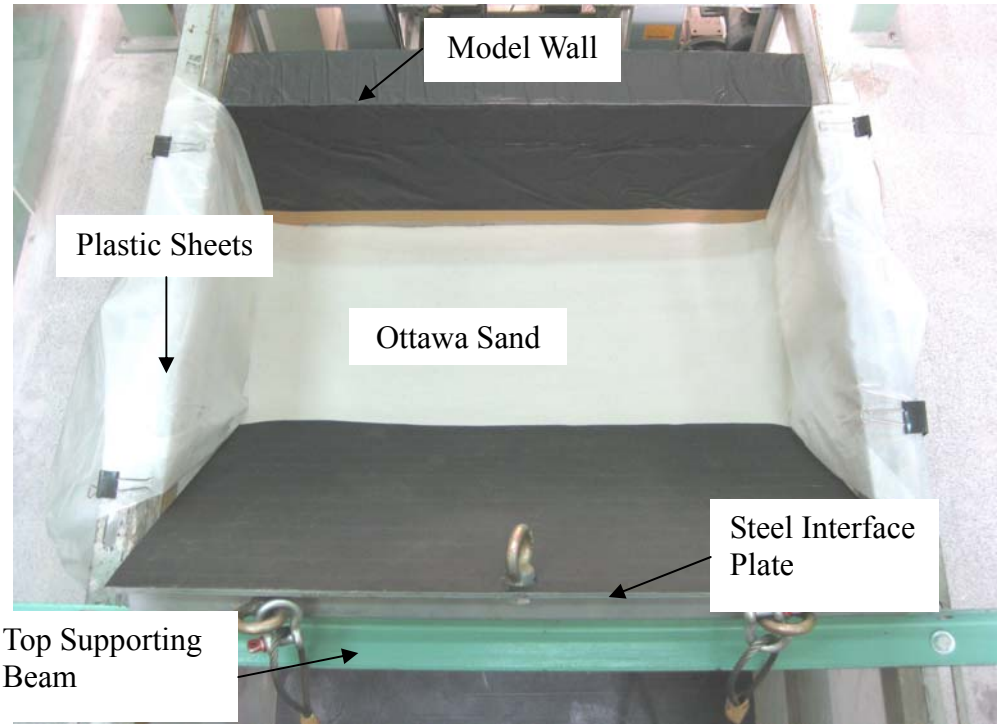

Fig. 23. Model retaining wall and steel interface plate

Fig. 24. Base supporting block

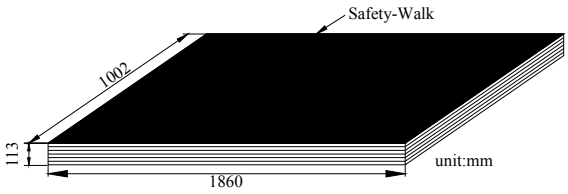

(a)

(b)

Fig. 25. Base supporting boards

5. BACKFILL AND INTERFACE CHARACTISTICS

5.1 Backfill Properties

Air-dry Ottawa silica sand (ASTM C-778) was used as backfill. Physical properties of Ottawa sand are listed in Table. 1 Grain-size distribution of the backfill is shown in Fig. 26.To establish the relationship between unit weight γ of backfill and its internal friction angle ϕ, direct shear tests have been conducted. The shear box used has a square (60 mm x 60 mm) cross-section, and its arrangements are shown in Fig. 27.

Chang (2000) established the relationship between the internal friction angle ϕ and unit weight γ of the ASTM C-778 Ottawa sand as shown in Fig. 28. It is obvious from the figure that soil strength increases with increasing soil density. For the air-pluviated backfill, the empirical relationship between soil unit weight γ and ϕ angle can be formulated as follows

$$\phi = 6.43\gamma - 68.99 \tag{5.1}$$

where

ϕ = angle of internal friction of soil (degree)

γ = unit weight of backfill (kN/m^3)

Eqn. (5.1) is applicable for γ= 15.45 ~ 17.4 kN/m^3 only.

5.2 Interface Characteristics between Model Wall and Backfill

To evaluate the wall friction angle δ_w between the backfill and model wall, special direct shear tests have been conducted. A 88 mm x 88 mm x 25 mm smooth steel plate, made of the same material as the model wall, was used as the lower shear box. Ottawa sand was placed into the upper shear box and vertical load was applied on the soil specimen. The arrangement of this test is shown in Fig. 29.

To establish the wall friction angles developed between the steel plate and sand, soil specimens with different unit weight were tested. Air-pluviation methods was used to achieve different soil densities, and the test result is shown in Fig. 30. For air-pluviation Ottawa sand, Lee (1998) suggested the following relationship:

$$\delta_w = 2.33\gamma - 17.8 \tag{5.2}$$

Eqn. (5.2) is applicable for γ = 15.5~17.5 kN/m^3 only. The ϕ angle and δ angle obtained in section 5.1 and 5.2 are used for calculation of active earth pressure for Coulomb, and Rankine's theories.

5.3 Side Wall Friction

To constitute a plane strain condition for model wall experiments, the shear stress between the backfill and sidewall should be minimized. A lubrication layer fabricated with plastic

sheets was equipped for all experiments to reduce the interface friction between the sidewall and the backfill. The lubrication layer consists of one thick and two thin plastic sheets as suggested by Fang et al. (2004). All plastic sheets had been vertically placed next to both side-walls before the backfill was deposited as shown in Fig. 31.

The friction angle between the plastic sheets and the sidewall was determined by the sliding block tests. The schematic diagram and the photograph of the sliding block test by Fang et al. (2004) are illustrated in Fig. 32 and Fig. 33. The sidewall friction angle δ_{sw} is determined based on basic physics principles. Fig. 34 shows the variation of interface friction angle δ_{sw} with normal stress σ based on the plastic sheet lubrication method. The friction angle measured was 7.5°. With the plastic-sheet lubrication method, the interface friction angle is almost independent of the applied normal stress. The shear stress between the acrylic side-wall and backfill could be effectively reduced with the plastic-sheet lubrication layer.

5.4 Interface Plate Friction

To evaluate the interface friction between the interface plate and the backfill special, direct shear tests were conducted as shown in Fig. 36. In Fig. 36(b), an 80 mm x 80 mm x 15 mm steel plate was covered with a layer of anti-slip material "Safety-Walk" to simulate the surface the interface plate. The interface plate was used to simulate the inclined stiff rock-face show in Fig. 35 Ottawa sand was placed in the upper shear box and vertical stress was applied on the soil specimen as shown in Fig. 36(a).

To establish the relationship between the unit weight γ of the backfill and the interface-plate friction angle δ_i, soil specimens with different unit weight were tested. Air-pluviation methods was used to achieve different soil densities, and the test result is shown in Fig. 37. For air-pluviation Ottawa sand, Wang (2005) suggested the following empirical relationship:

$$\delta_i = 2.7\,\gamma - 21.39 \qquad (5.3)$$

where

δ_i = interface-plate friction angle (degree)

γ = unit weight of backfill (kN/m^3)

Eqn. (5.3) is applicable for γ = 15.1 ~16.36 kN/m^3 only.

The relationships between backfill unit weight γ and different friction angles are summarized in Fig. 38. The internal friction angle of Ottawa sand ϕ, model wall-soil friction angle δ_w, interface-plate friction angle δ_i, and sidewall friction angle δ_{sw} as a function of soil unit weight are compared in the figure. It is clear in Fig. 38 that, with the same unit weight, the order of 4 different friction angles is $\phi > \delta_i > \delta_w > \delta_{sw}$.

Table 1. Properties of Ottawa sand (after Chen, 2003)

Shape	Rounded
e_{max}	0.76
e_{min}	0.50
G_s	2.65
D_{60} (mm)	0.39
D_{10} (mm)	0.26
C_u	1.5

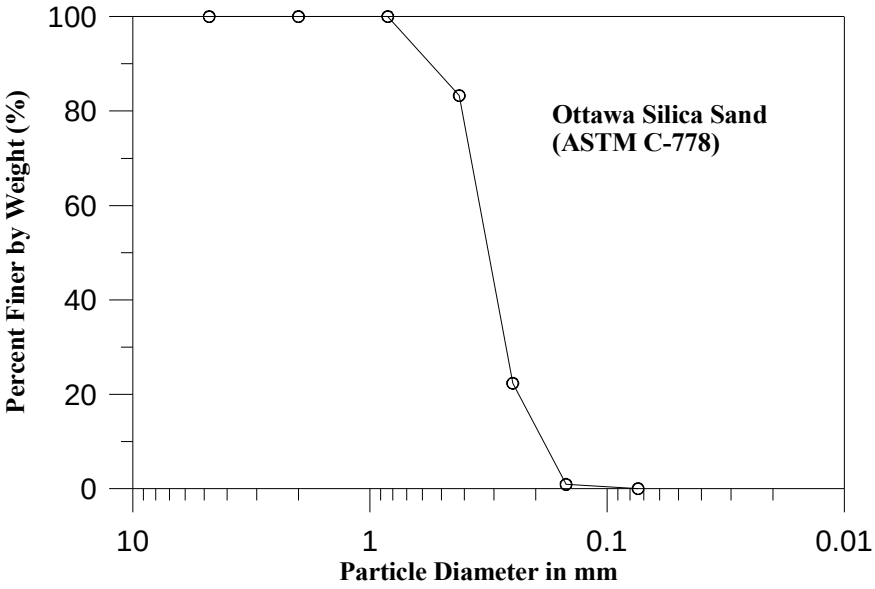

Fig. 26. Grain size distribution of Ottwa sand (after Hou, 2006)

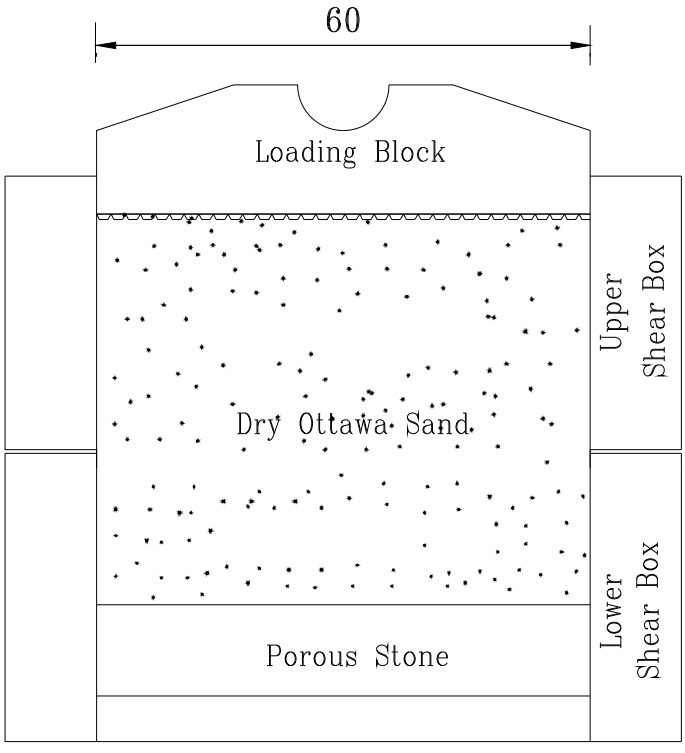

Fig. 27. Shear box of direct shear test device

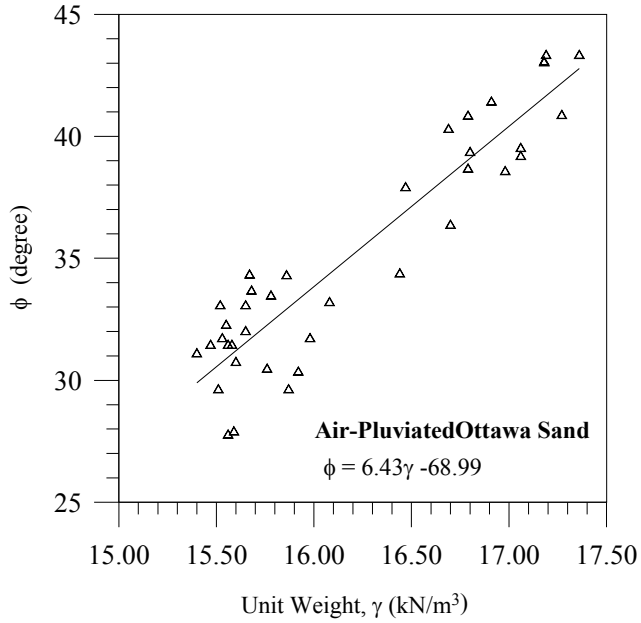

Fig. 28. Relationship between unit weight and internal friction angle (after Chang, 2000)

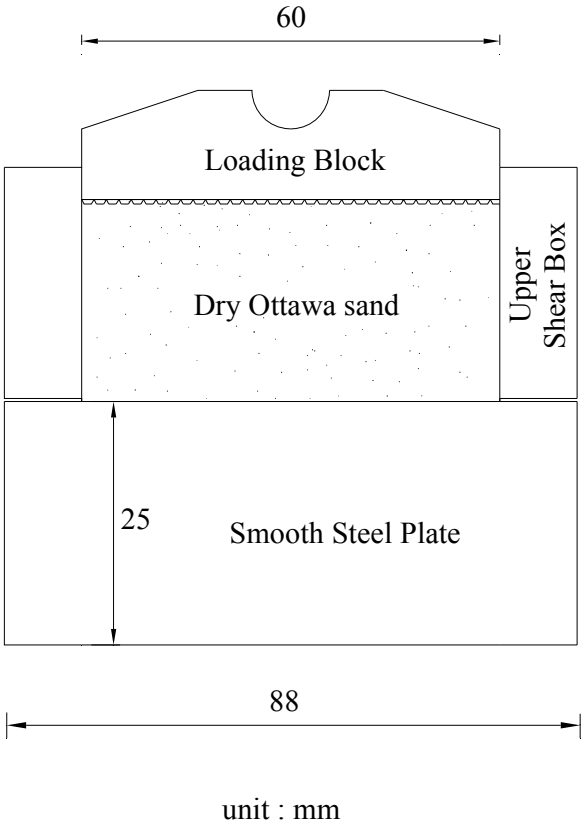

Fig. 29. Direct shear test arrangement to determinate wall friction

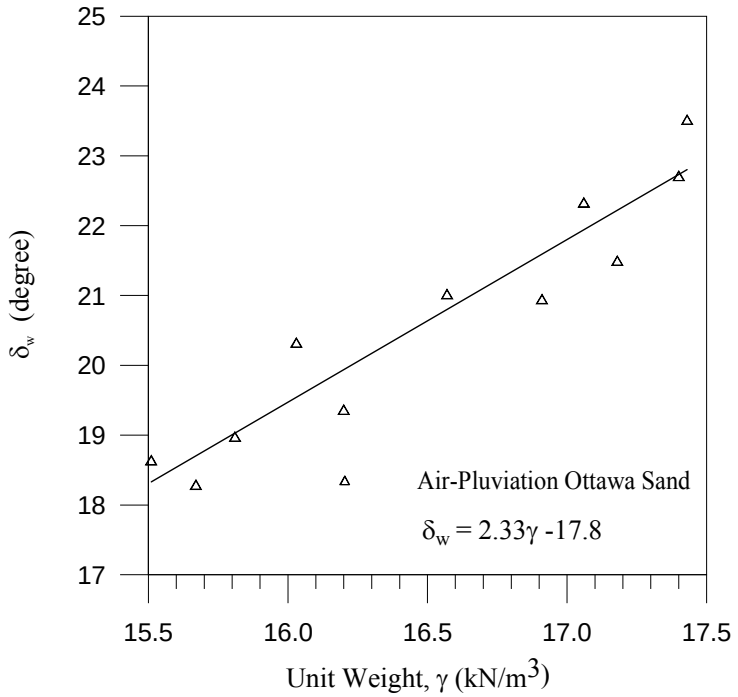

Fig. 30. Relationship between unit weight γ and wall friction angle δ_w (after Chang, 2000)

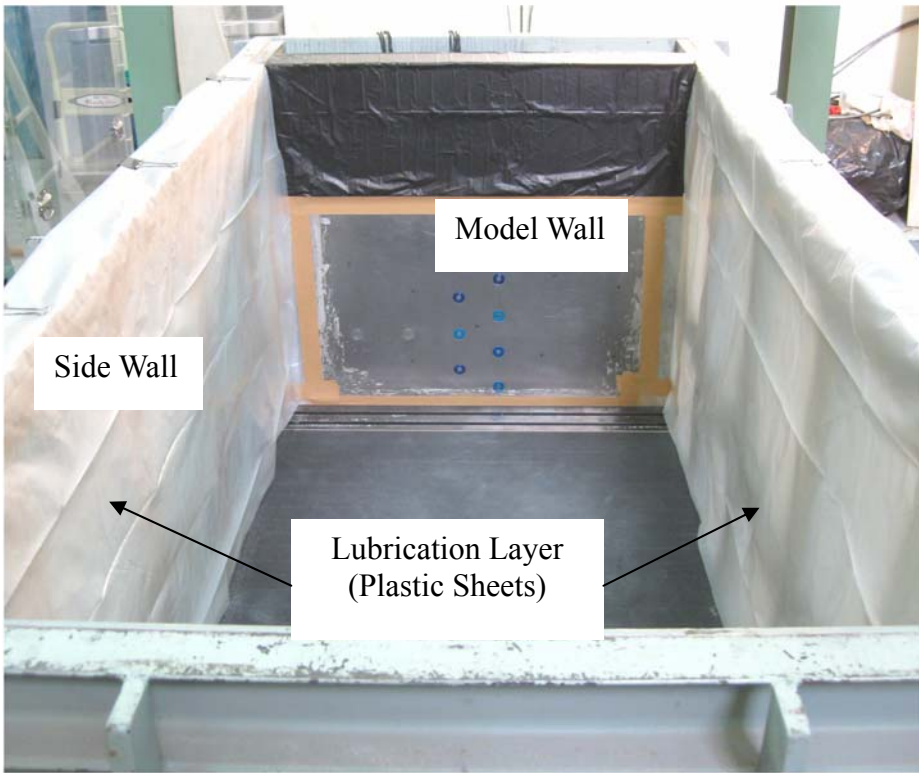

Fig. 31. Lubrication layers on side walls

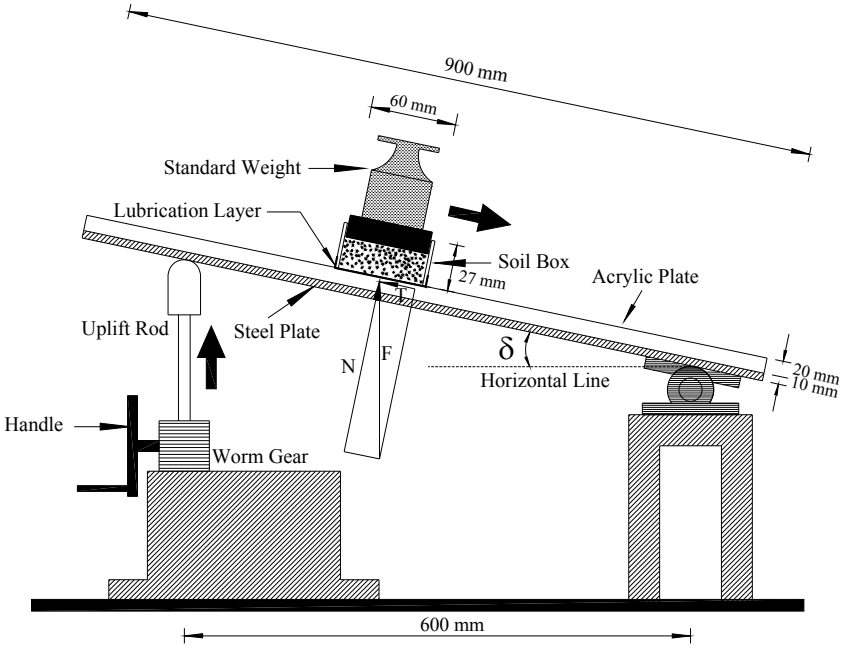

Fig. 32. Schematic diagram of sliding block test (after Fang et al., 2004)

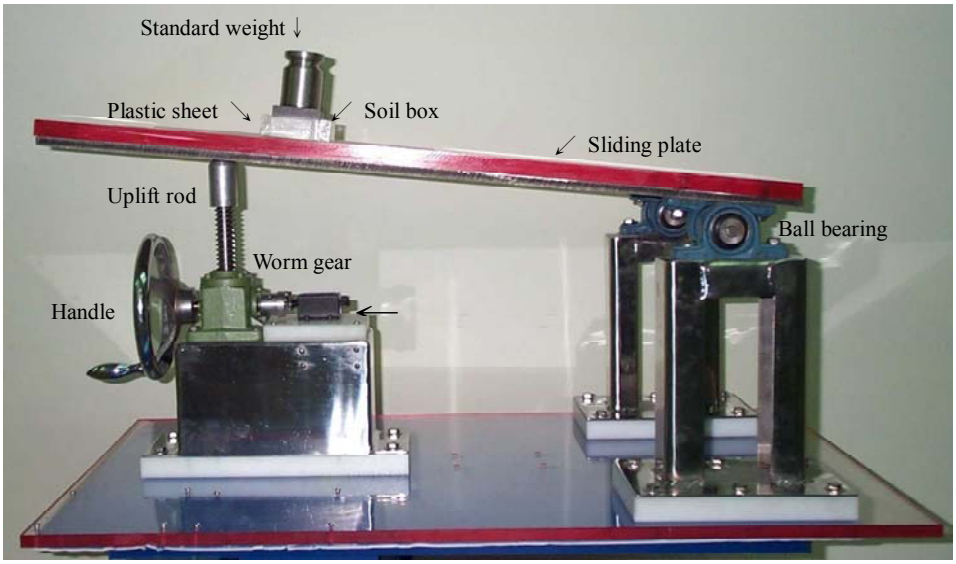

Fig. 33. Sliding block test apparatus (after Fang et al., 2004)

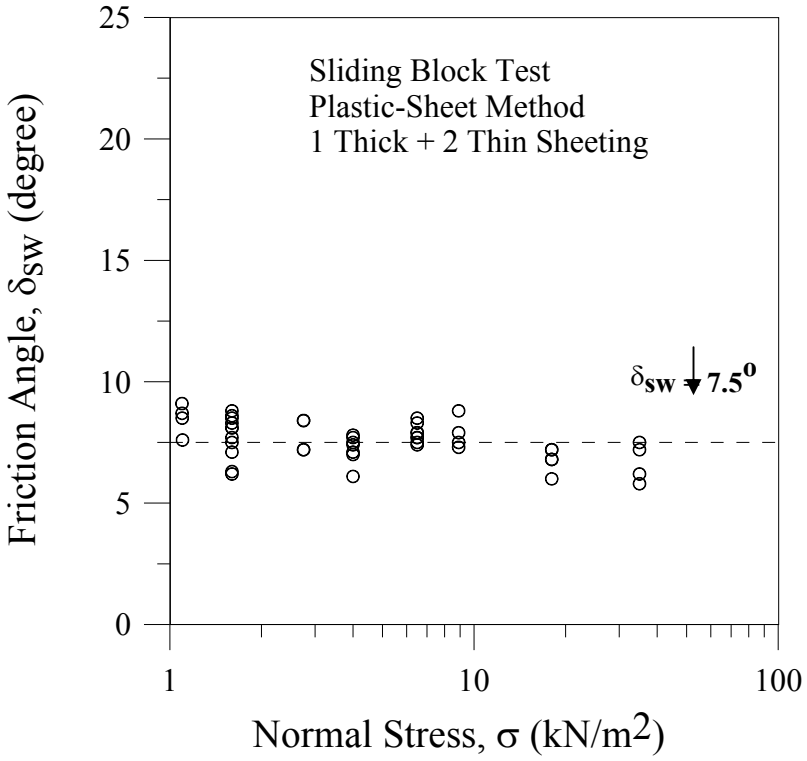

Fig. 34. Variation of interface friction angle with normal stress (after Fang et al., 2004)

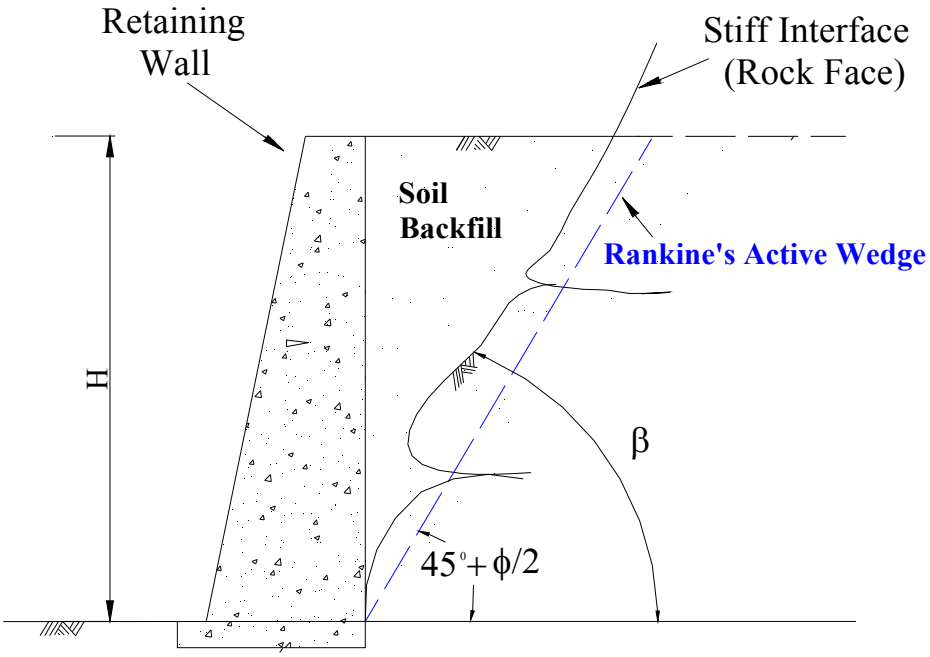

Fig. 35. Retaining wall with intrusion of a rock face into backfill

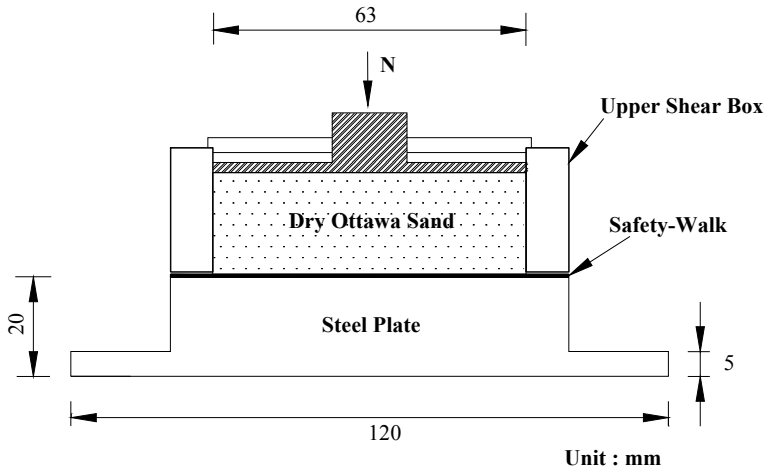

(a)

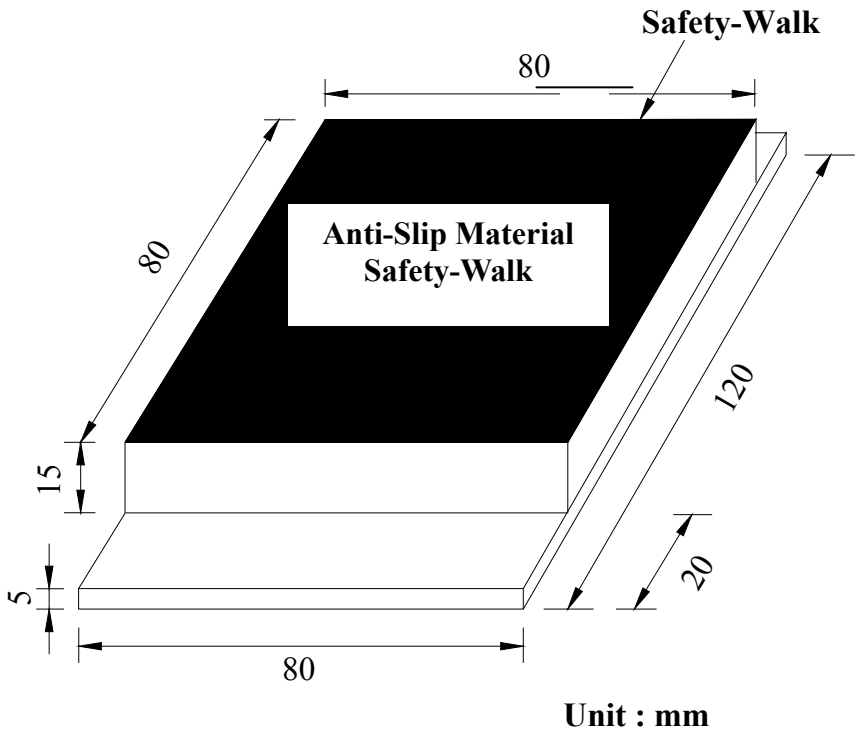

(b)

Fig. 36. Direct shear test arrangement to determine interface friction angle (after Wang, 2006)

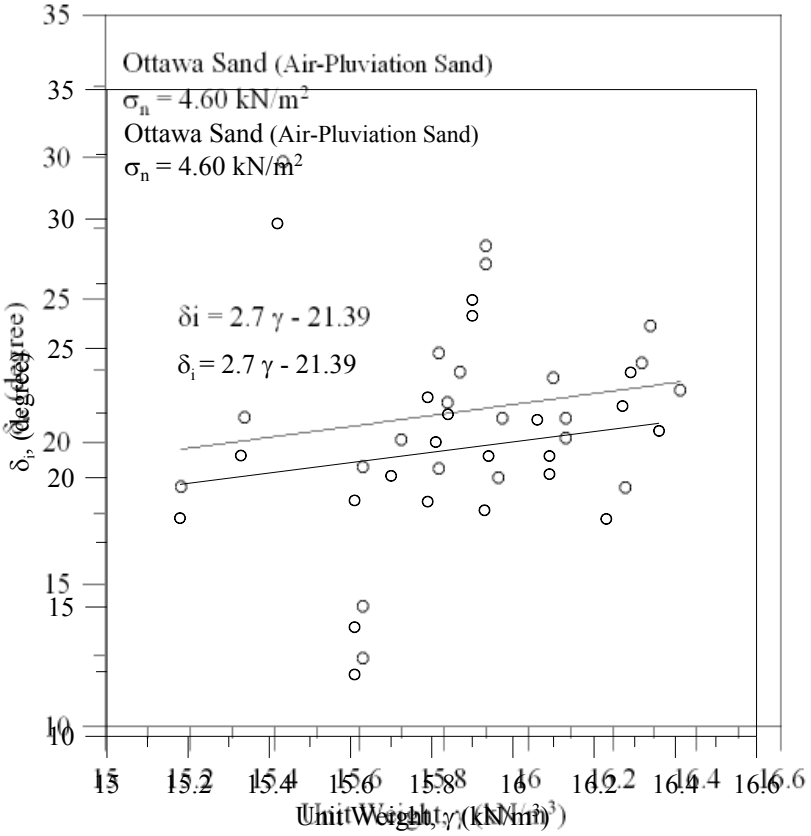

Fig. 37. Relationship between unit weight γ and interface plate friction angle δ_i (after Wang, 2005)

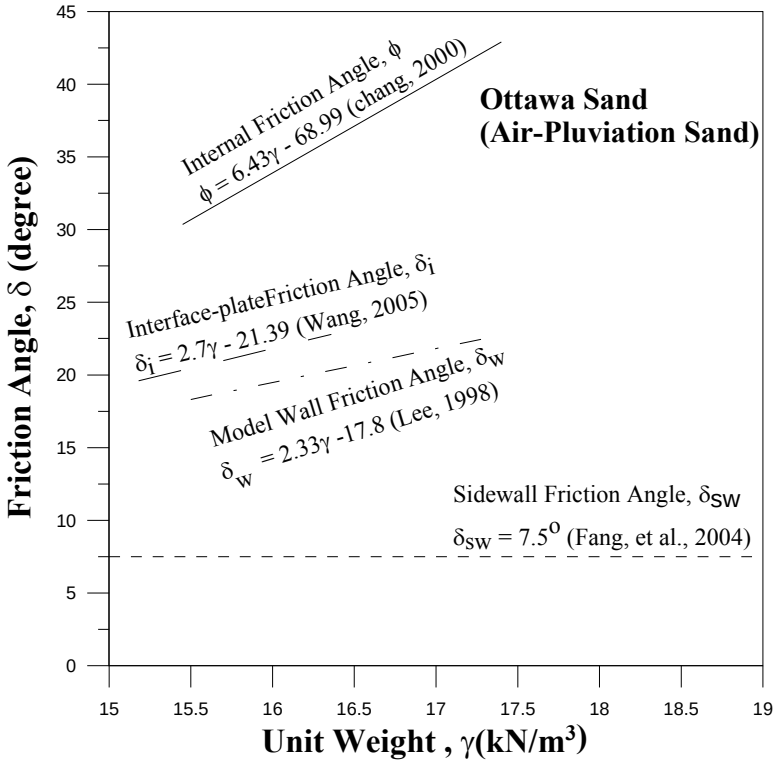

Fig. 38. Relationship between unit weight γ and different friction angles

6. TEST RESULTS

This chapter reports the experimental results regarding effects of an adjacent inclined rock face on the active earth pressure against a retaining wall filled with loose sand. The rock face interface inclination angles $\beta = 0^o$, 50^o, 60^o, 70^o and 80^o are illustrated in Fig. 1.

6.1 Earth Pressure Results

6.1.1 Earth Pressure for $\beta = 0°$

Distributions of horizontal earth pressure σ_h measured at different stages of wall displacements S/H are illustrated in Fig. 39. As the wall started to move, the earth pressure decrease, and eventually a limit active pressure was reached. The pressure distributions are essentially linear at each stage of wall movement. Active earth pressures calculated with Rankine and Coulomb theories are also indicated in Fig. 39. The ultimate experiment active pressure distribution is in fairly good agreement with that estimated with Coulomb and Rankine theories.

Fig. 40 shows a typical variation of horizontal earth pressure σ_h measured by different pressure transducer as a function of the wall movement, S/H (S : wall displacement, H : backfill height). In Fig. 40 the horizontal stress decreased with increasing active wall movements. The location for soil pressure transducer SPT1 through SPT9 is illustrated in Fig. 12. If the normal pressures at different depths are normalized by the soil unit weight γ and its depth z, the variation of $\sigma_h/\gamma z$ with S/H is shown in Fig. 41. In this figure, most of the data are concentrated. It seems possible that the active condition is reached at all depths simultaneously.

The variation of horizontal earth-pressure coefficient K_h as a function of wall displacement is shown in Fig. 42. The coefficient K_h is defined as the ratio of the horizontal coefficient component of total thrust to $\gamma H^2/2$. The horizontal thrust P_h was calculated by summing the pressure diagram shown in Fig. 39. The coefficient K_h decreased with increasing wall movement until a minimum value was reached, then remained approximately constant. The ultimate value of K_h is defined as the horizontal active earth-pressure coefficient $K_{a,h}$. In Fig. 43, the active condition was reached at approximately S/H = 0.0035.

As shown in Fig. 39, the distribution of earth pressure at different wall movements is almost linear. Therefore, the point of application of total thrust, h/H should remained at about H/3 above the wall base. Experimental results in Fig. 43 show that these points are located at a distance of about 0.331 H ~ 0.359 H above the wall base.

For Test 0825, the distributions of earth pressure at different stages of wall movement are shown in Fig. 44. As the wall starts to move, the earth pressure decrease. The pressure distribution is approximately linear with depth. Although the distribution is not strictly linear, such an assumption would not be far from reality.

In Fig. 42, the earth pressure coefficient, K_h decreases with increasing wall movement and finally a constant total thrust is reached. For Test 0825, the active condition occurred at the wall movement of approximately S/H= 0.003. It may be observed from Fig. 42 that

Coulomb theories ($\delta = 18.5^{\circ}$) provide a good estimate of the active earth pressure. In Fig. 42, data points obtained from Test 0809 and Test 0825, indicated that the experimental results were quite reproducible.

6.1.2 Earth Pressure for β = 50°

Fig. 45 shows the distribution of earth pressure at different stages of wall movement with presence of a stiff interface plate for an inclination angle $\beta = 50^{o}$. In Fig. 45, the measured stress at S/H= 0 is lower than Jaky's solution. The measured earth pressure at-rest is clearly affected by the intrusion of the rough interface inclined at $\beta = 50^{o}$. It is reasonable to expect the measured σ_h to be close to identical with Jaky's prediction. However, for the lower part of the model wall, the interface plate is quite close to the soil pressure transducers. As a result, the active earth pressure measured would be affected by the approaching of the interface plate.

Fig. 46 shows the typical variation of lateral pressure as a function of active wall movement. The horizontal stress decreases with increasing wall movement, then reaches a constant value. Fig. 47 shows the relationship between normalized earth pressure $\sigma_h/\gamma z$ and wall movement S/H. It is clear that σ_h measured at SPT1 to SPT9 decreases with the wall movement, then reach an active state.

Fig.48 presents the variation of lateral pressure as a function of active wall movement. As the wall starts to move, the lateral soil thrust decreases with increasing wall movement until a constant is reached, then remained approximate constant. The ultimate value of K_h is defined as the horizontal active earth-pressure coefficient $K_{a,h}$. In Fig. 48, the active condition was reached at approximately S/H = 0.003.

In Fig. 45, as the wall starts to translate, the earth pressure starts to decrease. This non-linear earth pressure distribution causes the total thrust to act at to higher location. Fig. 49 shows h/H reaches a constant value which is about 0.40 H ~ 0.42 H above the base of the wall.

For Test 0815, the distribution of earth pressure at different stages of wall movement for $\beta = 50^{o}$ is shown in Fig. 50. As the wall started to move, the earth pressure decrease and eventually a limiting active pressure was reached. The variation of K_h with S/H for Test 0814 and Test 0815 are summarized in Fig. 48. It can be seen from the figure that the two sets of test data concentrate in narrow strip. It can be concluded that the experimental results are highly reproducible.

6.1.3 Earth Pressure for β =60°

Fig. 51 shows the earth pressure distributions corresponding to different stages of wall displacements for the interface inclination angle β = 60°. At S/H = 0, the measured σ_h was significantly lower than Jaky's solution, especially the σ_h measured near the base of wall.

Fig. 52 shows the typical variation of lateral pressure as a function of active wall movement. The horizontal stress decreases with increasing wall movement, then reaches a constant value. Fig. 53 shows the relationship between normalized earth pressure $\sigma_h/\gamma z$ and wall movement S/H.

For $\beta = 60°$, the variation of earth pressure K_h with wall movement is shown in Fig. 54. The earth-pressure coefficient value K_h decreased with increasing wall movement until a constant value is reached. In Fig. 54 the active condition was reached at approximately at S/H = 0.003. Referring to Fig. 51, at S/H = 0.003 the active earth pressures measured near the base portion of the wall is much lower than Coulomb's prediction. The measured active earth pressure is clearly affected by the interface plate inclined at $\beta = 60°$. It is reasonable to expect the point of application of the active thrust would be located at a position higher than h/H = 0.333. Fig. 55 shows the experiment points of application the active thrusts were located at about 0.40H ~ 0.43H above the wall base.

For Test 0818, Fig. 54 shows the pressure distribution at various movement stages. The measured active earth pressure was lower than Coulomb's solution especially the pressure measured near the base of wall. This is most probably because the active earth pressure is affected by the intrusion of the inclined rock face.

6.1.4 Earth Pressure for $\beta = 70°$

The pressure distributions at various wall movements for $\beta = 70°$ are shown in Fig. 57. At S/H = 0, the measured earth pressure at rest was lower than Jaky's prediction, especially at the lower part of the model wall. This is because the interface plate is very close to the soil pressure transducers.

Fig. 58 shows the variation of horizontal earth pressure σ_h measured by different pressure transducer as a function of the wall movement. It is clear from the data shown in Fig. 59 that the horizontal stress decreases with increasing active wall movements. The variation of $\sigma_h/\gamma z$ with S/H is shown in Fig. 59.

Fig. 60 shows the variation of K_h with active wall movement for $\beta = 70°$. The coefficient K_h decreases with increasing wall movement. The wall movement needed for K_h to reach an active state is about S/H = 0.0035.

The variation of the location of to the active soil thrust with wall movement is shown in Fig. 61.Without the interface plate ($\beta = 0°$), the point of application h/H of the earth resultant is located at about 0.33H above the base of the wall. With the interface angle $\beta = 70°$, the earth pressure does not increase linearly with depth. This active earth pressure distribution shown in Fig. 57 causes the location of the total thrust to rise to a higher location. Experimental result in Fig. 61 shows the point of application of the active thrust was located at about 0.41H ~ 0.43H above the wall base.

Fig. 62 illustrates the distributions of earth pressure at different stages of wall movement for Test 0824. The active earth pressure measured near the base of the wall was much lower than Coulomb solution. In Fig. 60 and Fig. 61, data points obtained form Test 0822 and Test 0824 indicate that experimental results were in good agreement.

6.1.5 Earth Pressure for $\beta = 80°$

Fig. 63 shows the variation of the earth pressure distributions with depth at various wall

movements. At S/H = 0, the measured at-rest pressure distribution is not linearly with depth, and it is significantly less than the Jaky solution. For $\beta = 80°$, the interface plate was quite close to the wall surface. The amount of backfill sand withed between the rock face and the wall was very little. In this figure, the earth pressure slightly decreased with the active wall movement.

Fig.64 presents the variation of lateral pressure as a function of active wall movement. As the wall starts to move, the earth pressure decrease, and eventually a active pressure is reached. Fig. 65 shows the relationship between normalized earth pressure $\sigma_h/\gamma z$ and wall movement S/H.

In Fig. 66, the horizontal earth pressure coefficient K_h decrease with increasing wall movement, then a constant value $K_{a,h}$ is observed. The constant value $K_{a,h}$ is significantly lower than the value estimated with the Coulomb's theory. The location of total soil thrust versus the wall movements is shown in Fig. 67. Experimental results show that these points are located at a distance of about 0.42H ~ 0.43H above the wall base. This is most probably because the measure σ_h distribution is significantly affected by the presence of the nearby rock face.

The earth pressure distributions corresponding to different stages of wall displacement for $\beta = 80°$ are shown in Fig. 68. In this figure, the distributions of lateral earth pressure are non-linear with depth. This is probably because the interface plate is very close to the soil pressure transducers on the wall surface. In Fig. 66, the wall movement needed for the horizontal stress to reach a constant value is about S/H = 0.004. Similar variation of K_h with can be observed for Test 0825.and Test 0826.

6.2 Effects of Interface Inclination on Soil Thrusts

The variation of earth pressure coefficient K_h as a function of wall movement S/H is shown in Fig. 69. Without the interface plate ($\beta = 0°$), the active earth pressure coefficient $K_{a,h}$ is in good agreement with Coulomb's equation ($\delta = 18.5°$). However, with the approaching of the interface plate, the active earth pressure coefficient $K_{a,h}$ decreased with increasing interface inclination angle β.

The distributions of active earth pressure at the interface inclination angle $\beta = 0°$, 50°, 60°, 70° and 80° are shown in Fig. 70. In the figure, the active earth pressure decreases with increasing β angle. It would be reasonable to expect that the magnitude of active soil trust to decrease with increasing β angle. For β angle greater than 50°, the shape of the active pressure distribution implies that the point of application of the active soil thrust would not be affected by the rock face inclination angle β.

The point of application h/H of the soil thrust as a function of wall movement is discussed in this paragraph. Fig. 71 shows, without the interface plate ($\beta = 0°$), the point of application h/H of the earth pressure resultant is located at about 0.33H above the base of the wall. As the interface angle β increase up to 50°, the rock face started to intrude the active soil wedge, the earth pressure start to decrease near the base of the wall. This change of earth pressure distribution causes the active thrust to rise to a slightly higher location as shown in Fig. 70.

6.2.1 Magnitude of Active Soil Thrust

The variation of active earth pressure coefficient $K_{a,h}$ as a function of interface inclination angle β is shown in Fig. 72. For comparison purposes, the analytical results reported by Fan and Chen (2006) are also plotted in Fig. 72. Without the interface plate (β = 0°), the coefficient $K_{a,h}$ values is in fairly good agreement with Coulomb's prediction. However, with the intrusion of the rock face into the active soil wedge, the coefficient $K_{a,h}$ decrease with rock face inclination angle β. Although the tend was the same, the experimental $K_{a,h}$ was much lower than the numerical $K_{a,h}$ values.

6.2.2 Point of Application of Active Soil Thrust

Fig. 73 shows the variation of the point of application of active soil thrust with the β angle. For the β = 0°, no rock face was near the retaining wall, the $(h/H)_a$ value is located at about 0.33H above the base of the wall. As the interface angle β increase, the earth pressure measured near the base of the wall decreased. This change of earth pressure distribution causes the active total thrust to move to a slightly higher location as shown in Fig. 73. For β = 80°, the point of application of the active soil thrust is located at 0.425H above the base of the wall.

6.3 Design Considerations

In the design of a retaining structure, it is often necessary to check its adequacy. It is interesting to investigate how would the nearby inclined rock-face influence, the factor of Safety (FS) against sliding and overturning of the retaining wall.

6.3.1 Factor of Safety against Sliding

The factor of safety for sliding is defined as：

$$FS_{sliding} = \frac{\sum \text{Resisting Force}}{\sum \text{Driving Force}} \tag{6.1}$$

For the retaining wall shown in Fig. 35, the driving force comes from the active earth pressure acting on the face of the wall. Fig. 72 indicates, for β greater than 50°, the horizontal component of active soil thrust $P_{a,h}$ would decrease with increasing β angle. In Fig. 72 with the intrusion of the inclined rock face into the active soil wedge (β = 50° to 80°), the driving force acting on the wall would decrease to a value low than Coulomb's estimation. In equation 6.1, if the driving force on the wall is reduced, the FS against sliding would increase. The intrusion of the inclined rock face would actually increase the FS against sliding of the wall. The evaluation of FS against sliding with Coulomb's theory would be on the safe side.

6.3.2 Factor of Safety against overturning

The factor of safety against overturning of the retaining wall is defined as:

$$FS_{overturning} = \frac{\sum \text{Resisting moment}}{\sum \text{Driving moment}} \qquad (6.2)$$

The driving moment in equation 6.2 is the product of the horizontal soil thrust $P_{a,h} = K_{a,h} \times 0.5\, rH^2$ and the moment arm h. Fig. 72 shows, for β =50° to 80°, coefficient $K_{a,h}$ would decrease with increasing β angle. However, Fig. 73 shows, for β =50° to 80°, the moment arm h increases with increasing β angle. Fig. 74 shows the normalized driving moment $K_{a,h} \times \left(h/H\right)$ as a function of the rock face inclination angle β. It is clear that, for the result obtained with both the experimental and analytical methods, for β =50° ~ 80° the normalized driving moment would decrease with increasing β angle. In equation 6.2, if the driving moment is reduced, the FS against overturning would increase. The intrusion of an inclined rock face into the active soil wedge would increase the FS against overturning of the retaining wall. The evaluation of F.S. against overturning with Coulomb's theory would also be the safe side.

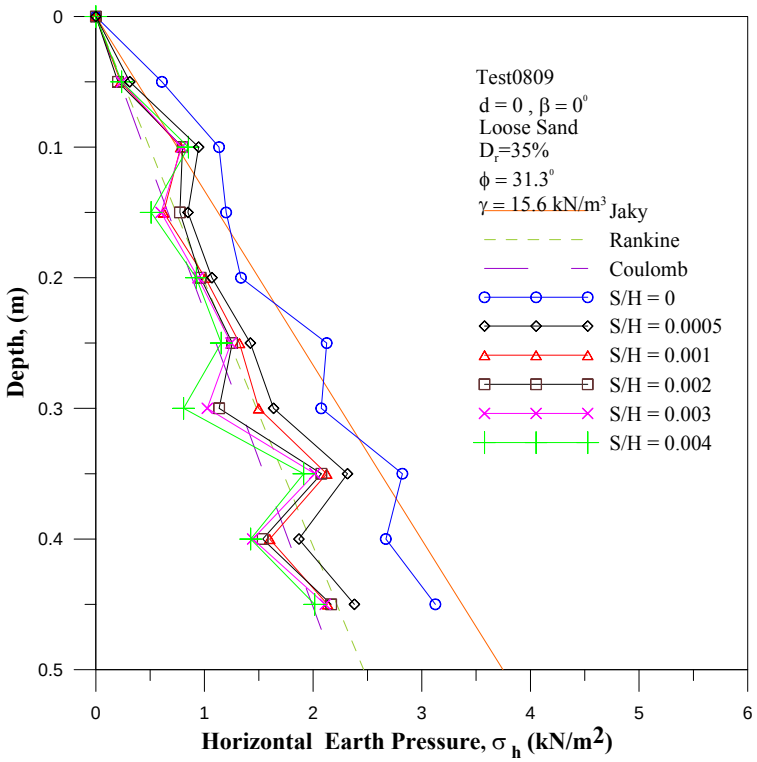

Fig. 39. Distribution of horizontal earth pressure for β = 0°

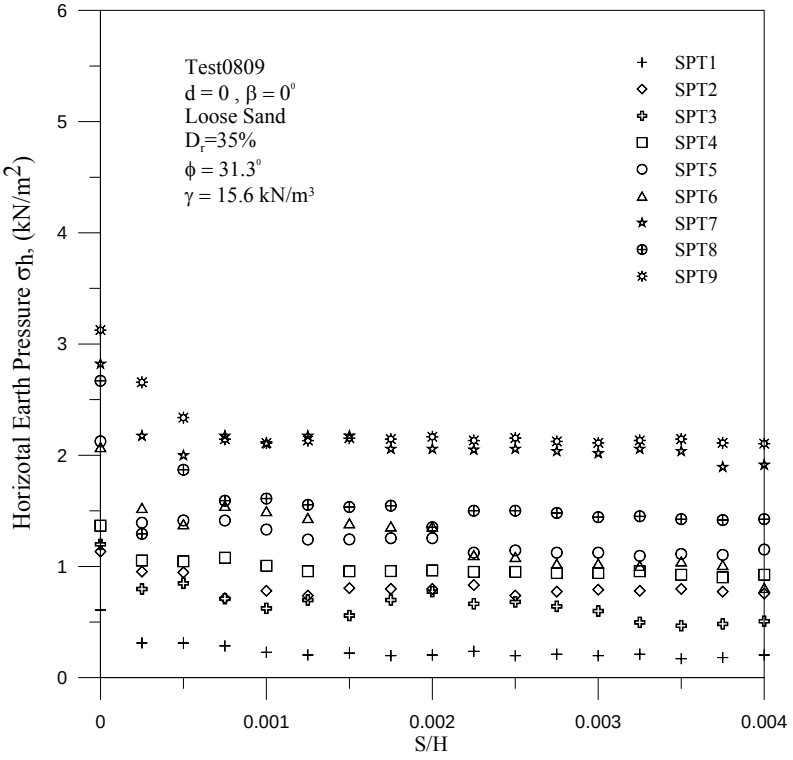

Fig. 40. Variation of horizontal earth pressure versus wall movement for β = 0°

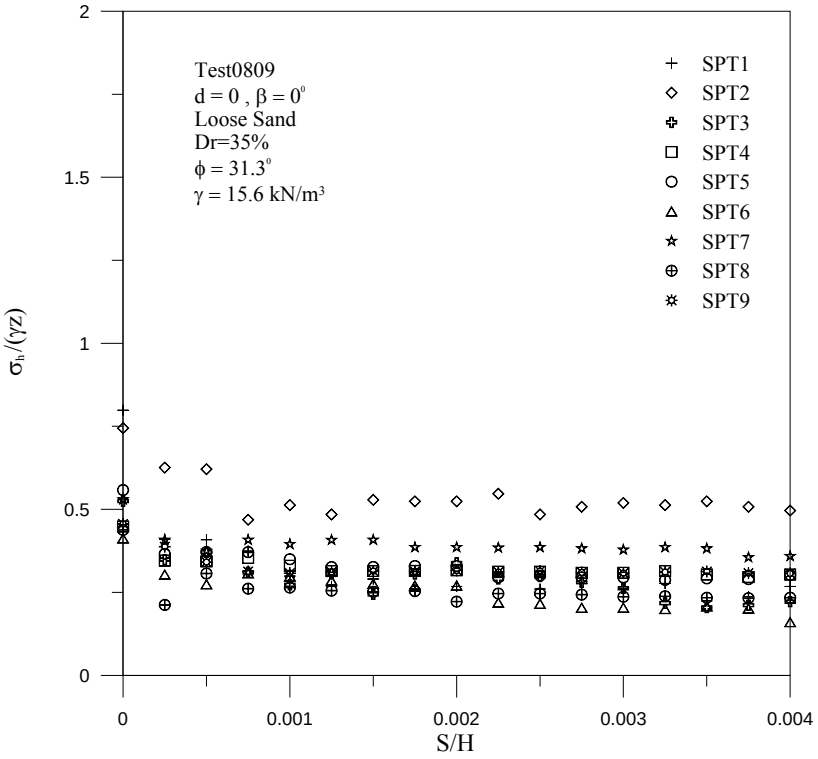

Fig. 41. Relationship between $\sigma_h/\gamma z$ and S/H for β = 0°

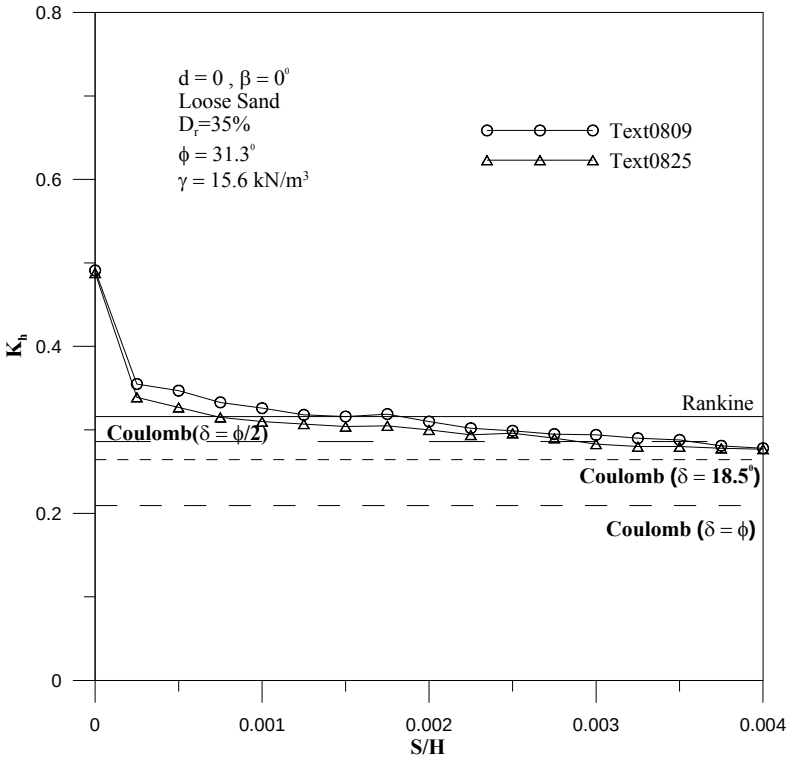

Fig. 42. Earth pressure coefficient K_h versus wall movement for $\beta = 0°$

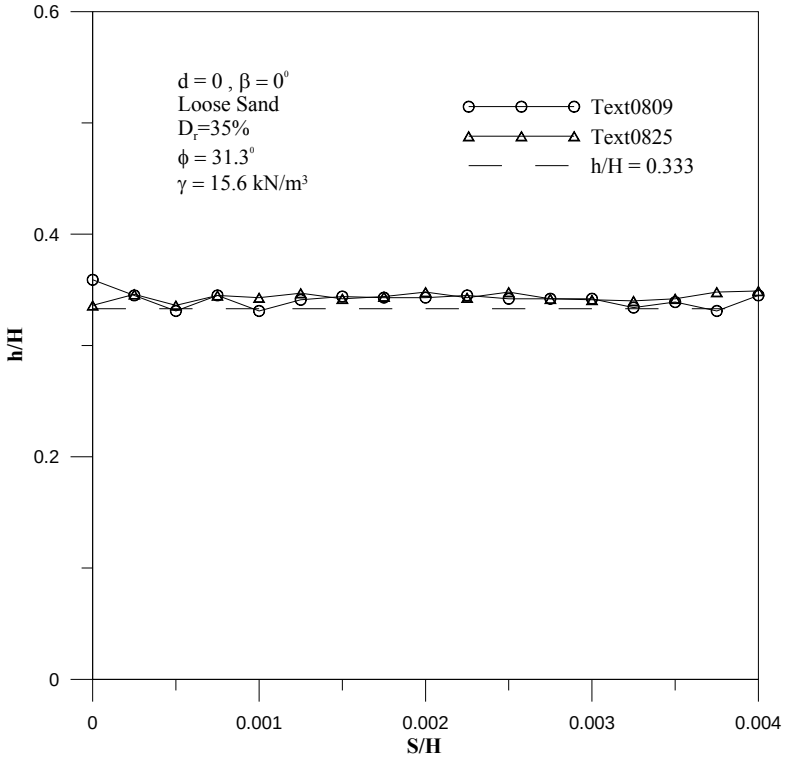

Fig. 43. Location of total thrust application for $\beta = 0°$

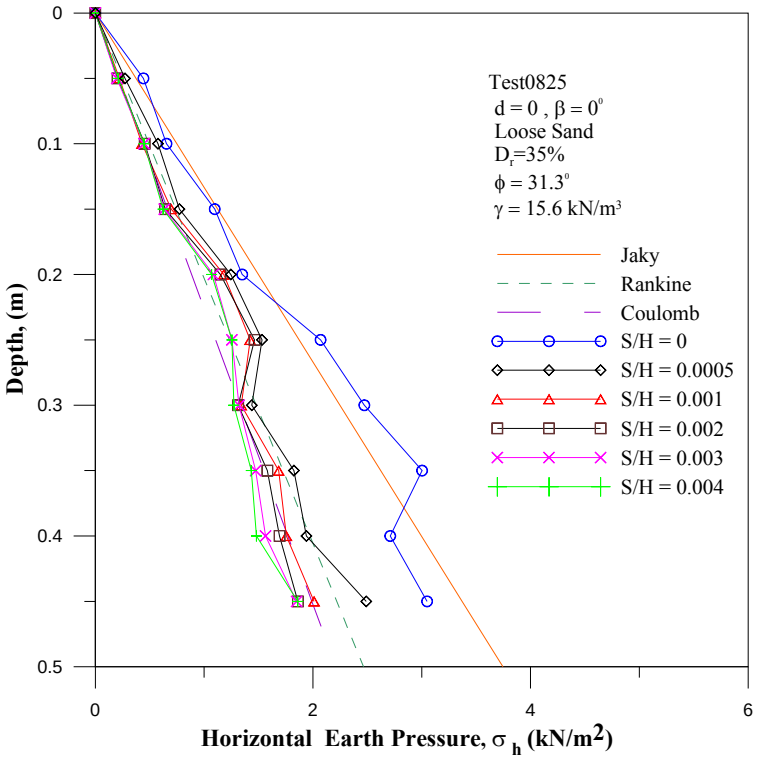

Fig. 44. Distribution of horizontal earth pressure for β = 0°

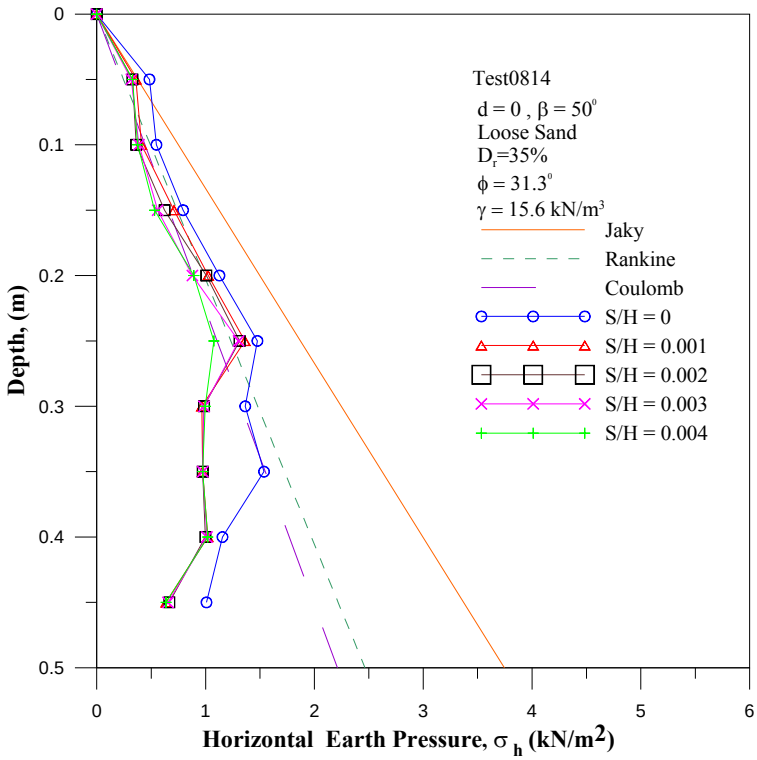

Fig. 45. Distribution of active earth pressure for β = 50°

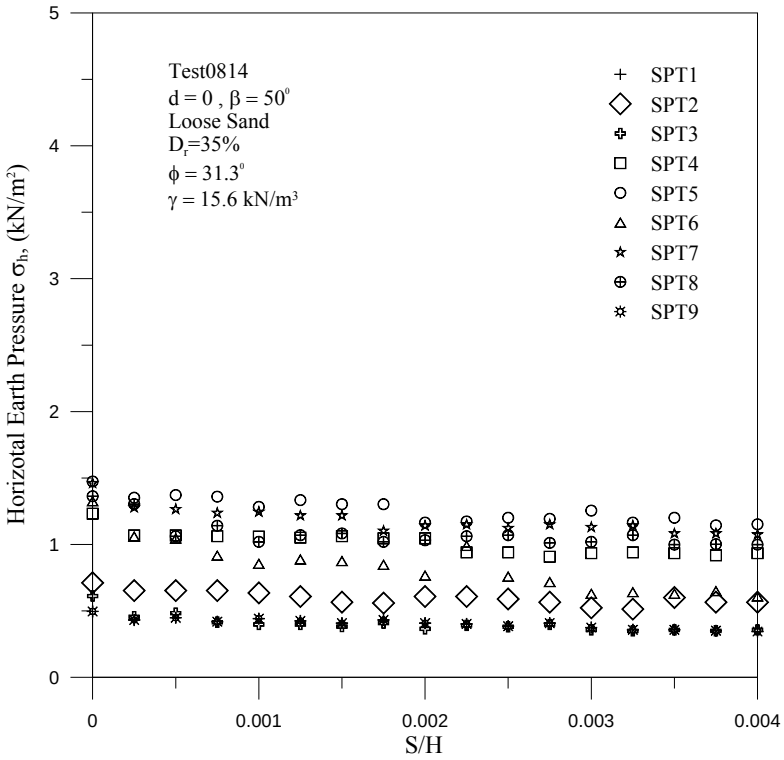

Fig. 46. Variation of horizontal earth pressure versus wall movement for β = 50°

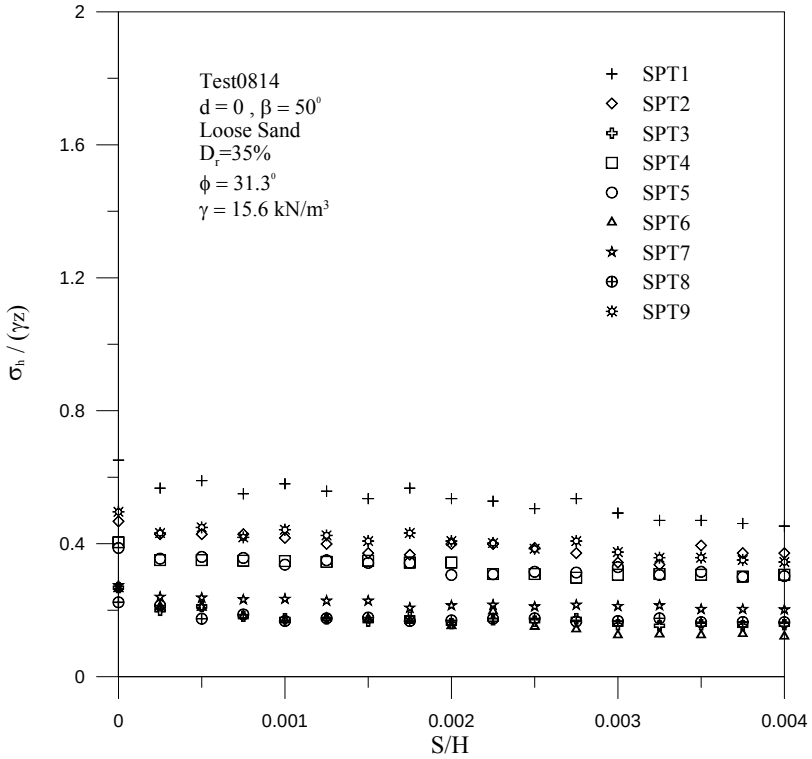

Fig. 47. Relationship between $\sigma_h/\gamma z$ and S/H for β = 50°

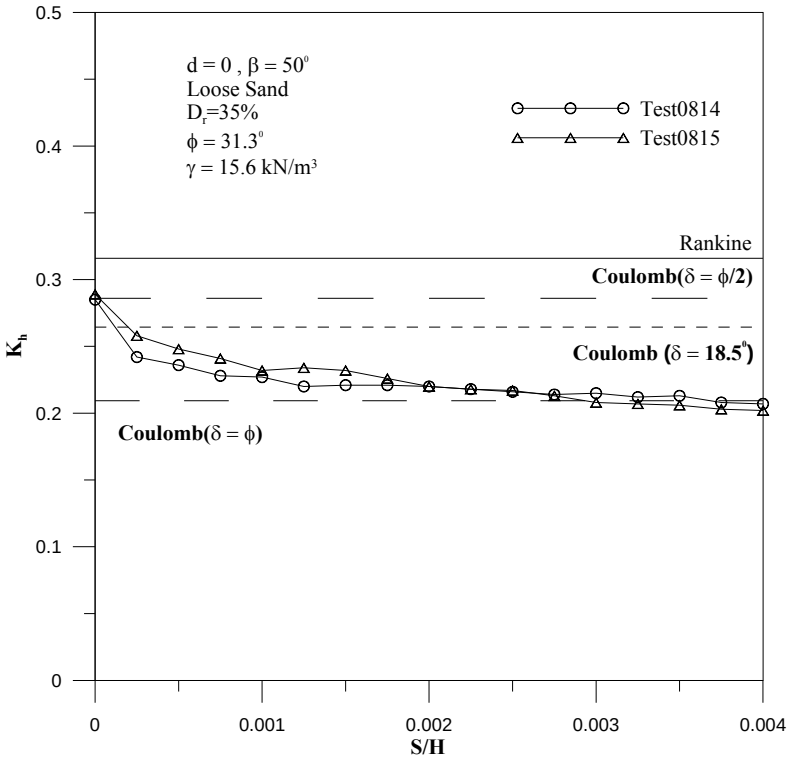

Fig. 48. Earth pressure coefficient K_h versus wall movement at $\beta = 50°$

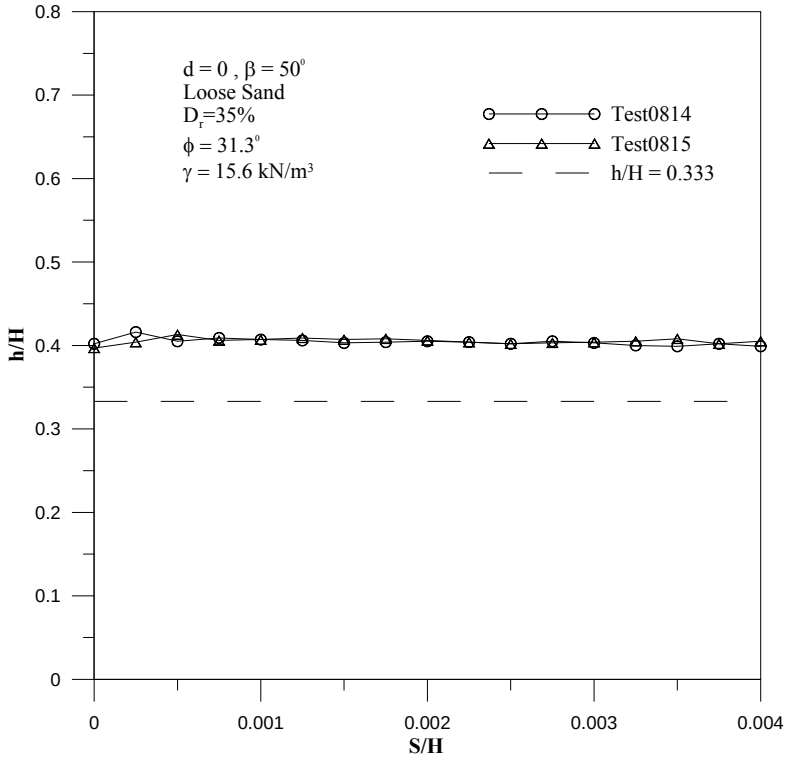

Fig. 49. Location of total thrust application for $\beta = 50°$

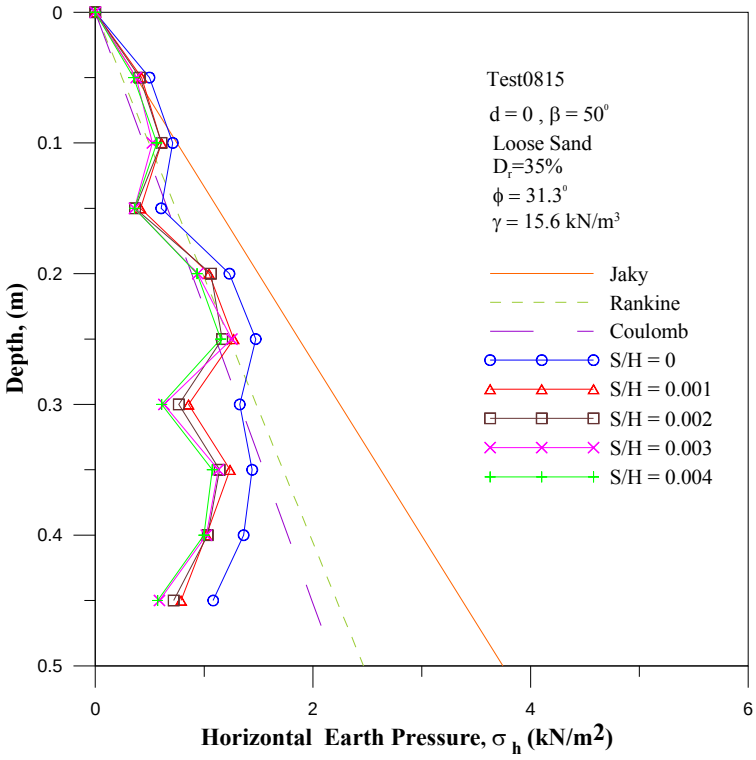

Fig. 50. Distribution of earth pressure for β = 50°

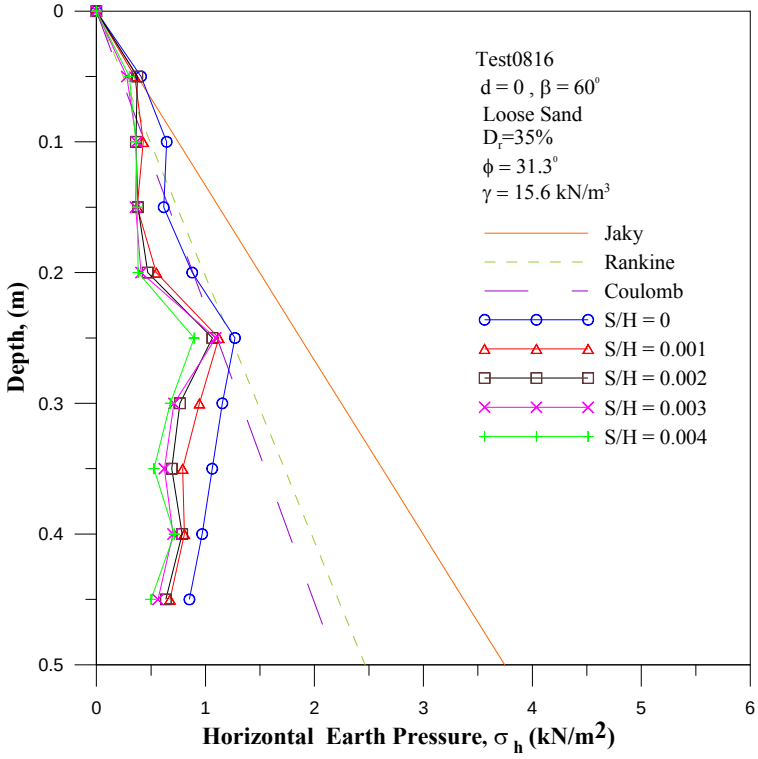

Fig. 51. Distribution of earth pressure for β = 60°

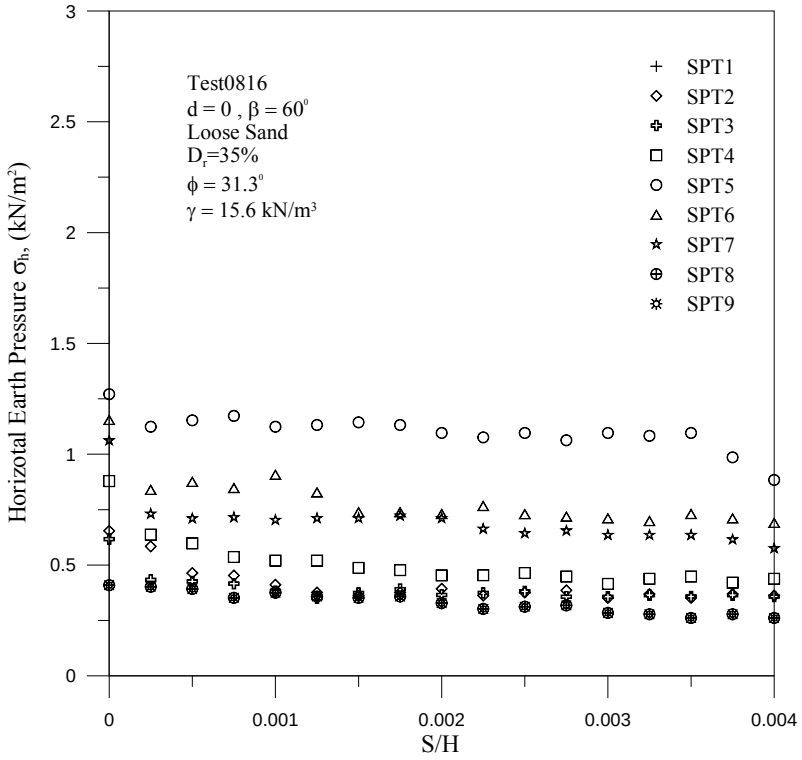

Fig. 52. Variation of horizontal earth pressure versus wall movement for β = 60°

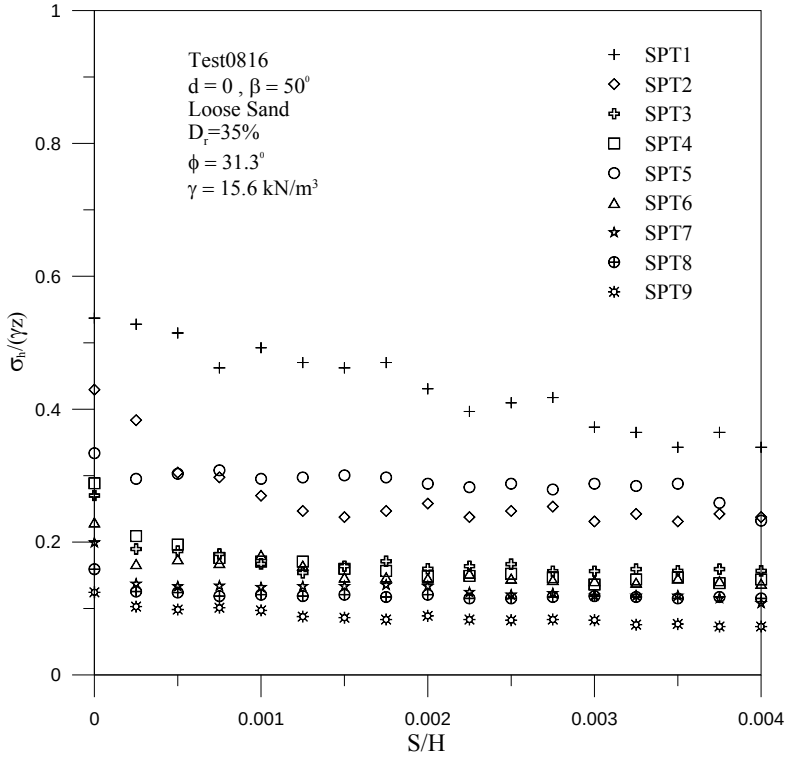

Fig. 53. Relationship between $\sigma_h/\gamma z$ and S/H at for β = 60°

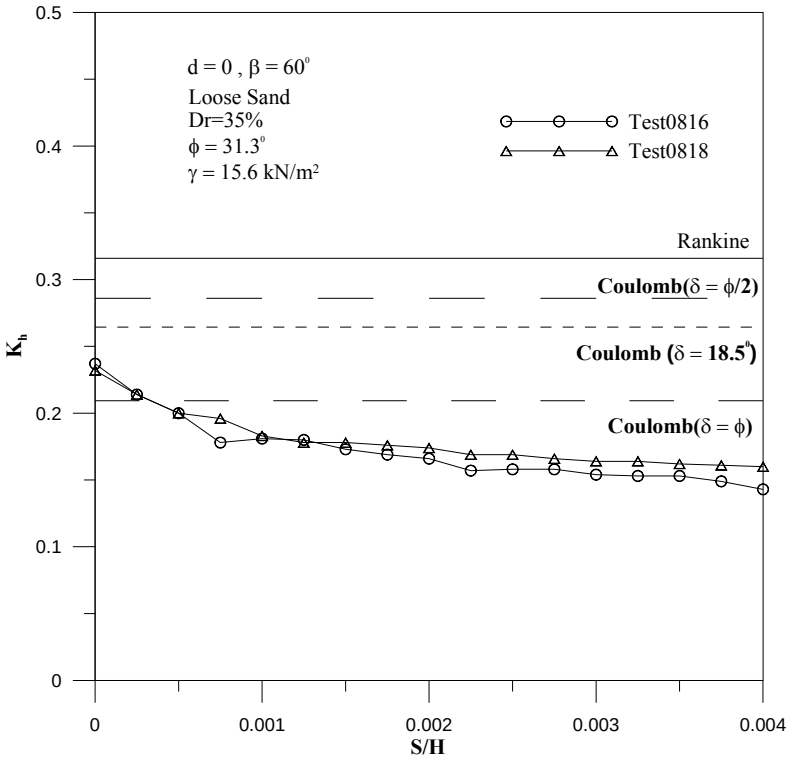

Fig. 54. Earth pressure coefficient K_h versus wall movement for β = 60°

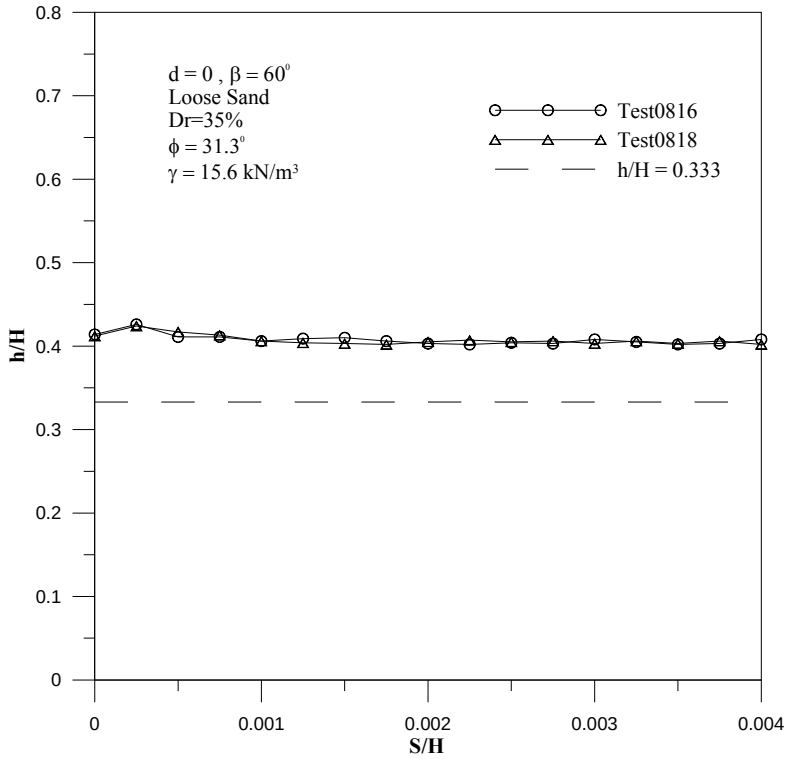

Fig. 55. Location of total thrust application forβ = 60°

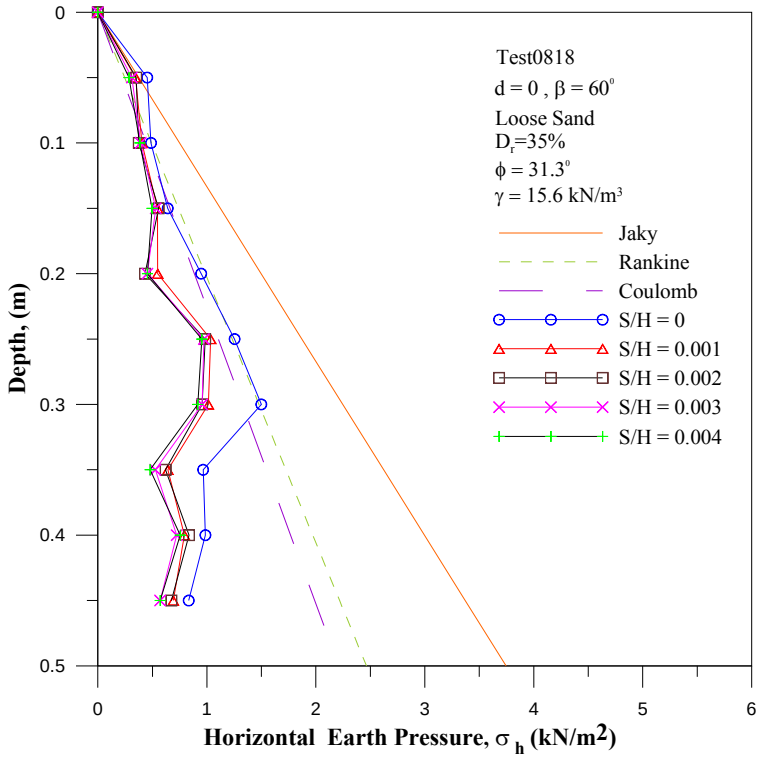

Fig. 56. Distribution of earth pressure for β = 60°

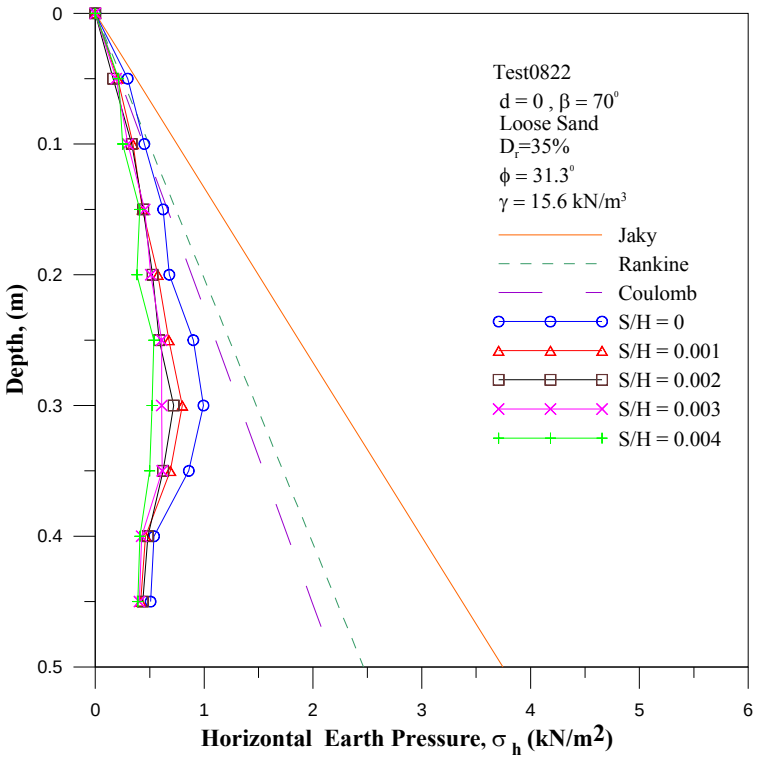

Fig. 57. Distribution of earth pressure for β = 70°

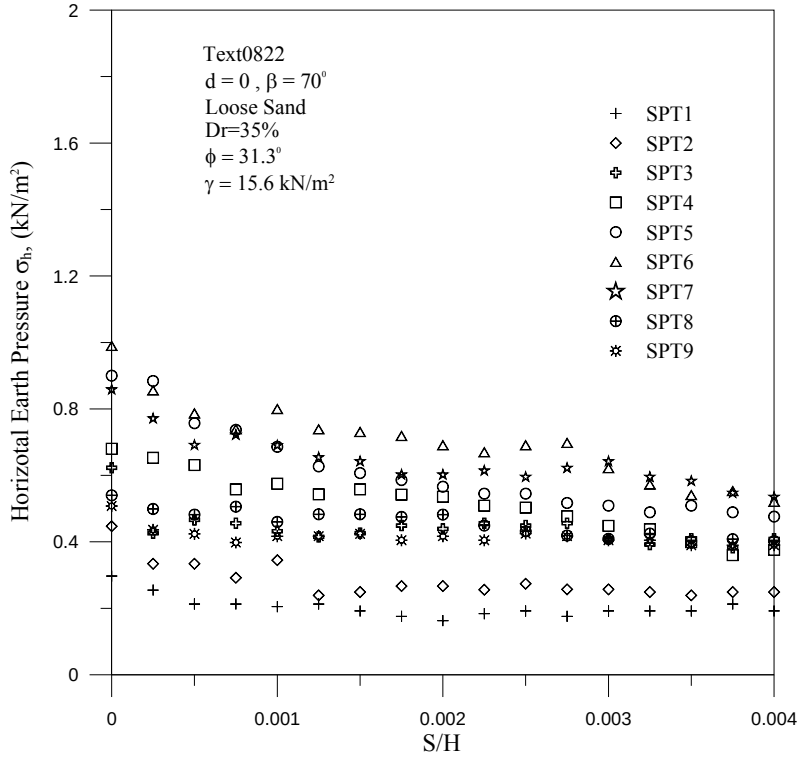

Fig. 58. Variation of the horizontal earth pressure versus wall movement for β = 70°

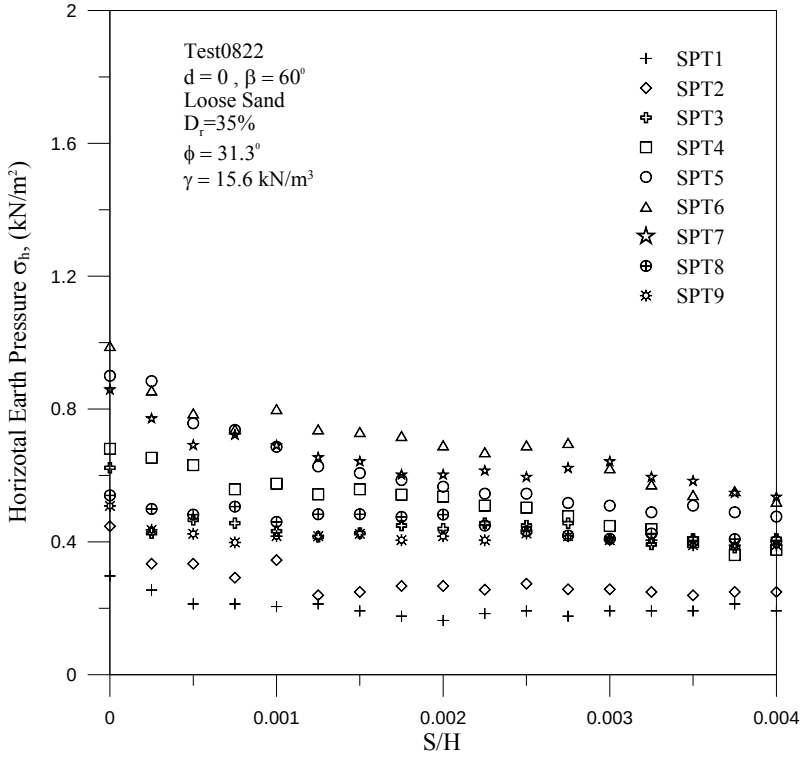

Fig. 59. Relationship between $\sigma_h/\gamma z$ and S/H for β = 70°

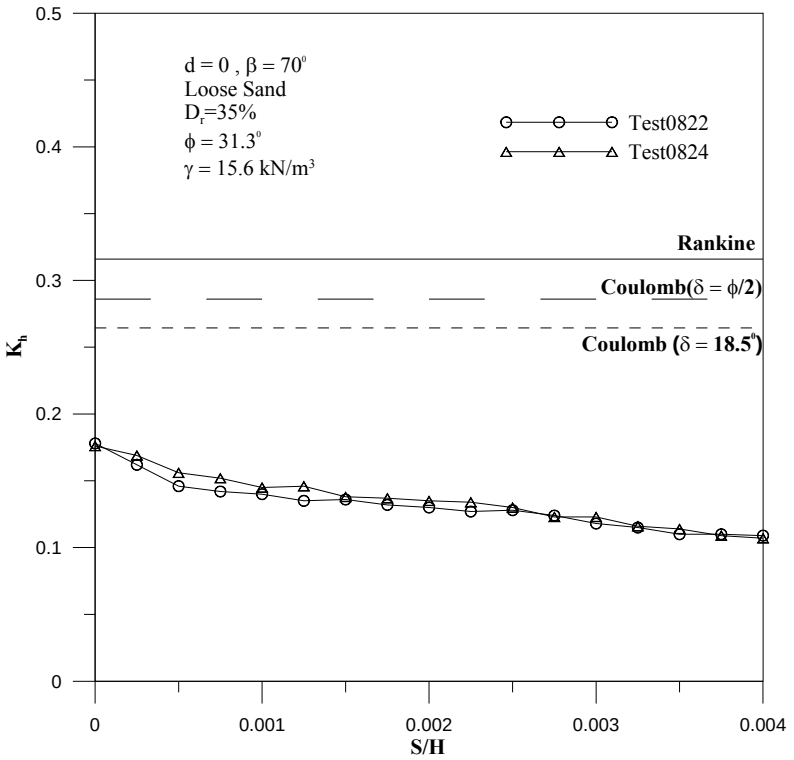

Fig. 60. Earth pressure coefficient K_h versus wall movement for β = 70°

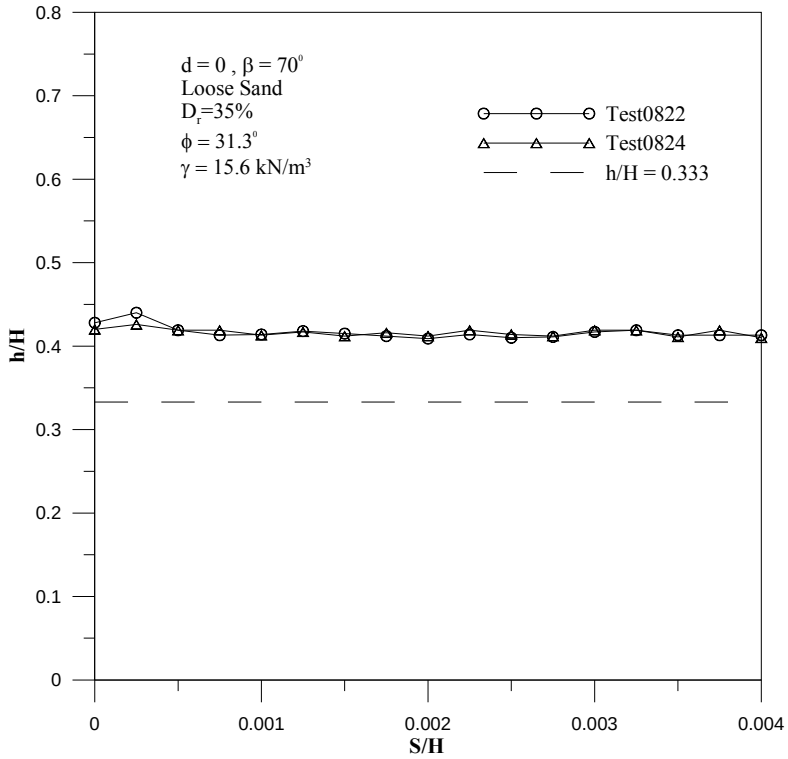

Fig. 61. Location of total thrust application for β = 70°

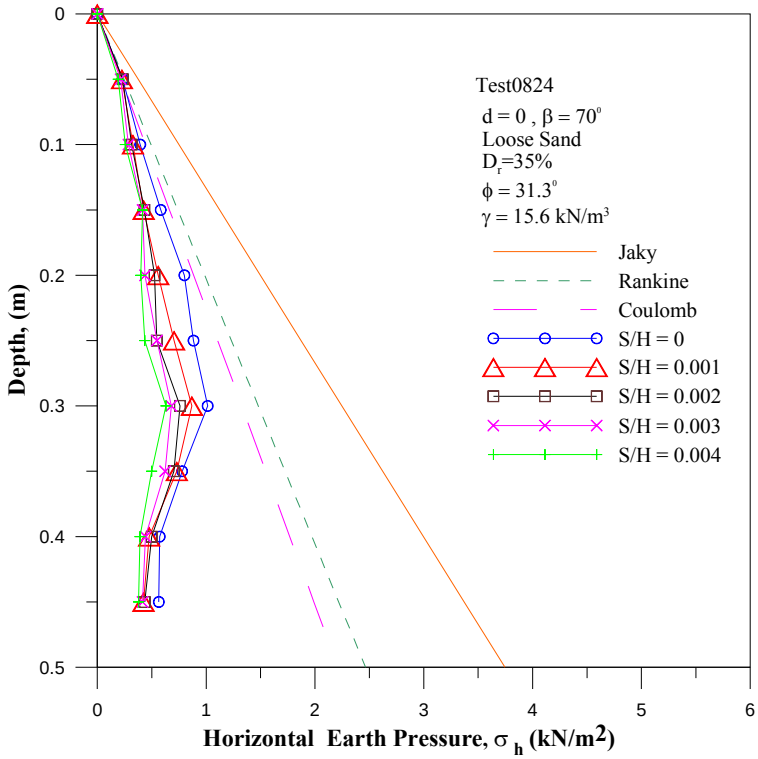

Fig. 62. Distribution of earth pressure for β = 70°

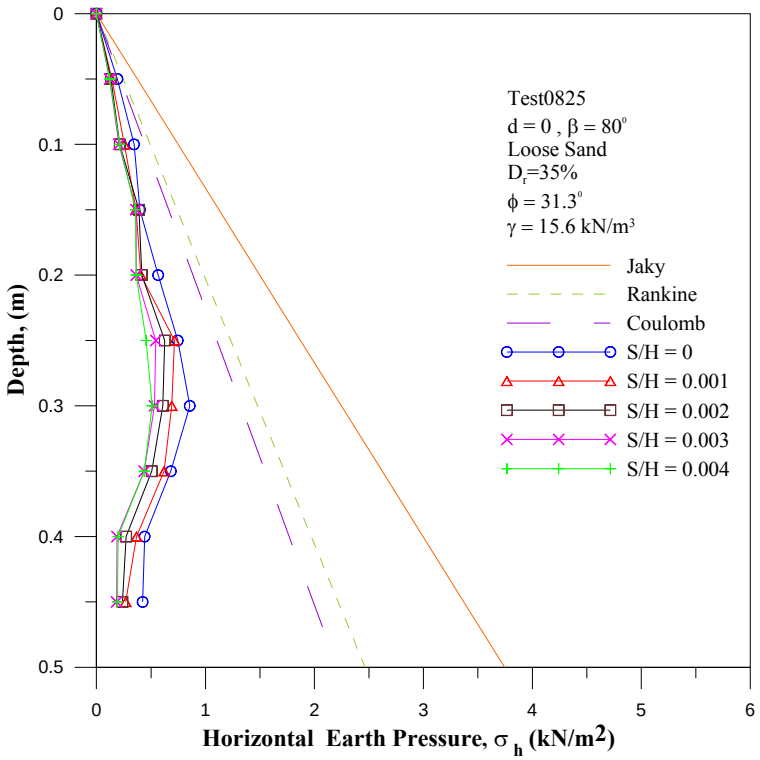

Fig. 63. Distribution of earth pressure for β = 80°

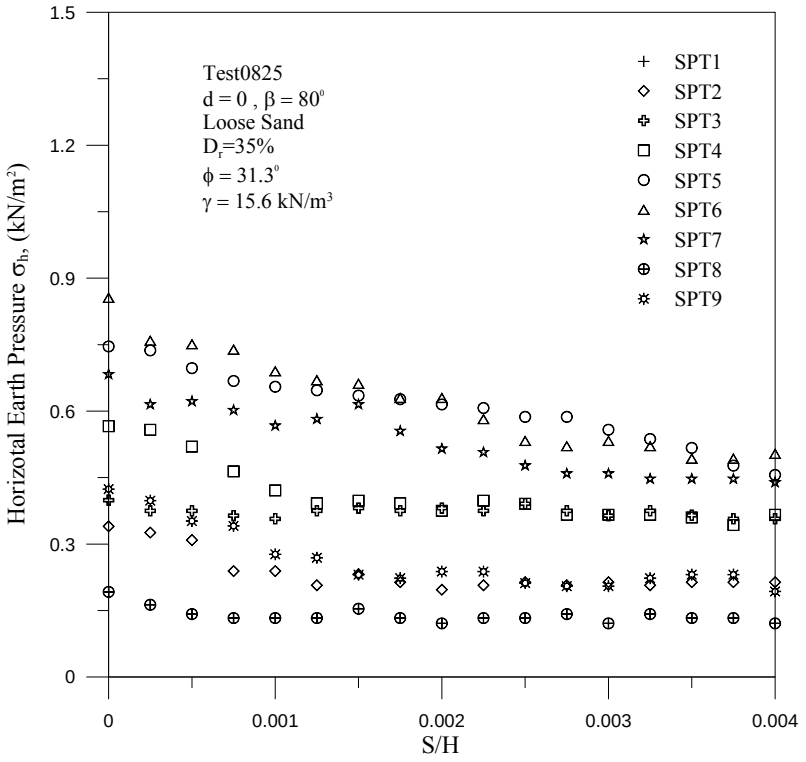

Fig. 64. Variation of horizontal earth pressure versus wall movement for β = 80°

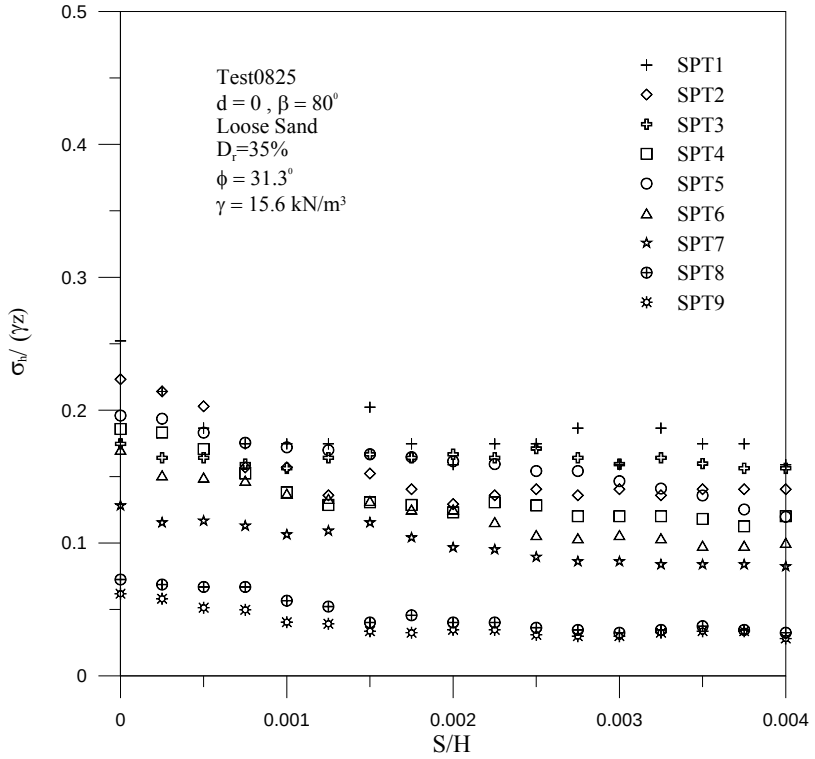

Fig. 65. Relationship between $\sigma_h/\gamma z$ and S/H for β = 80°

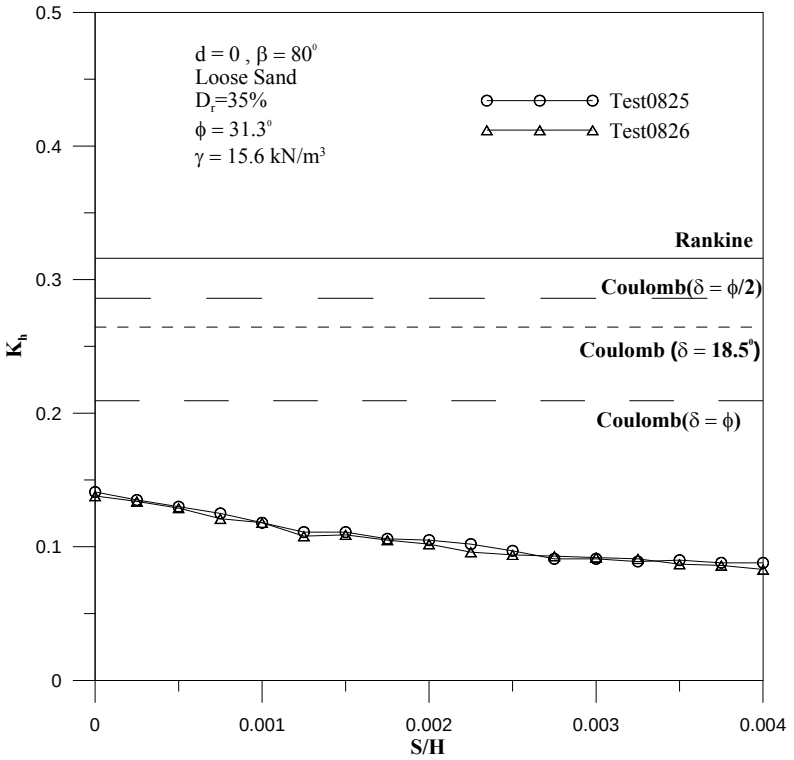

Fig. 66. Earth pressure coefficient K_h versus wall movement for β = 80°

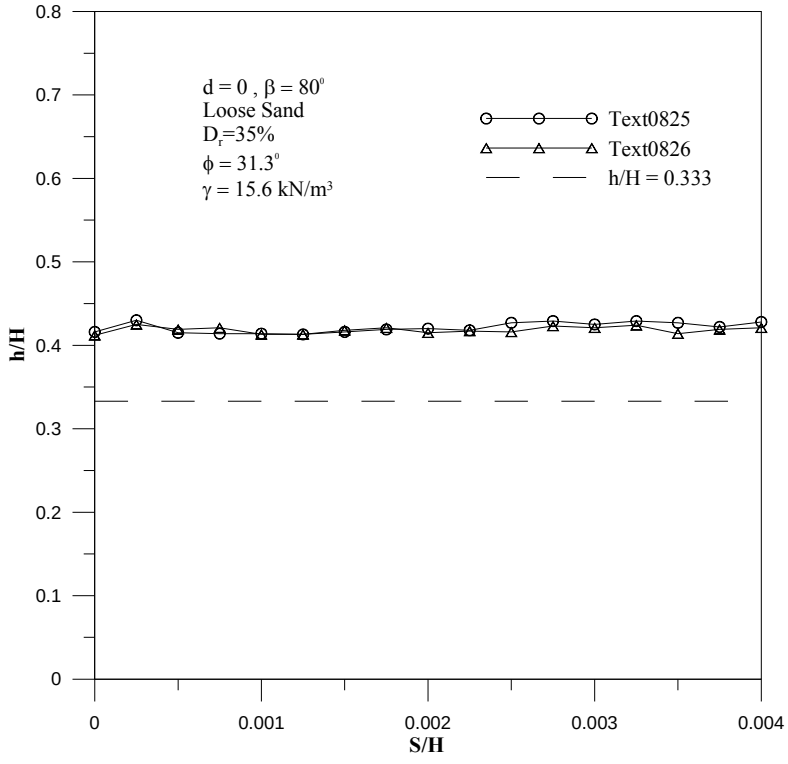

Fig. 67. Location of total thrust application forβ = 80°

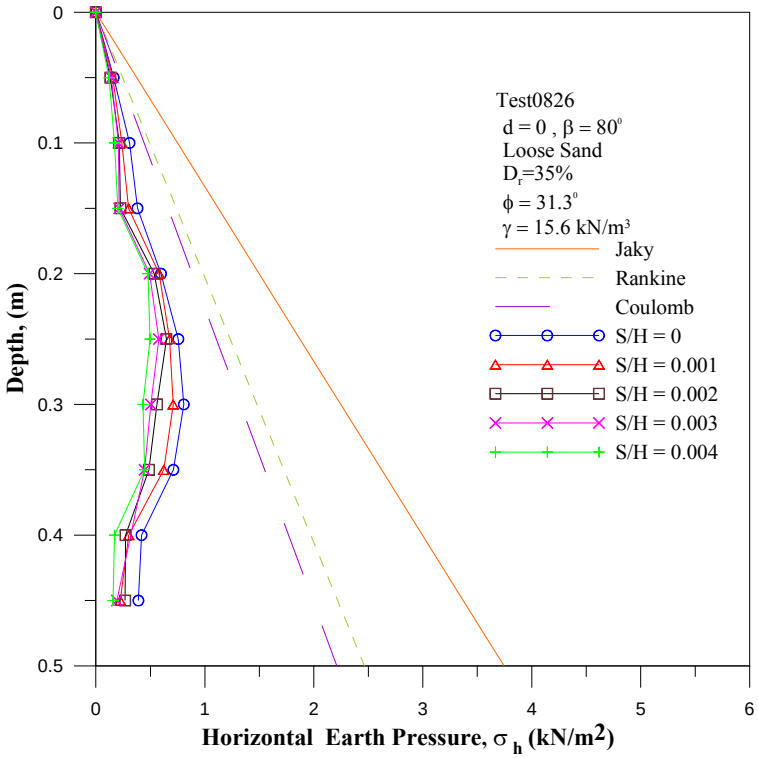

Fig. 68. Distribution of earth pressure for β = 80°

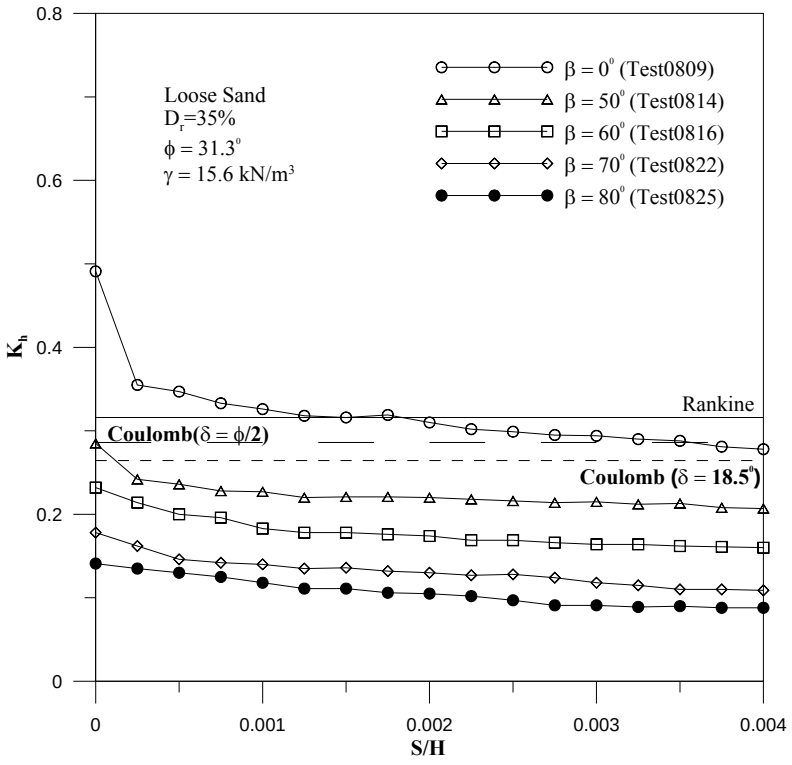

Fig. 69. Variation of earth pressure coefficient $K_{,h}$ with increasing wall movement

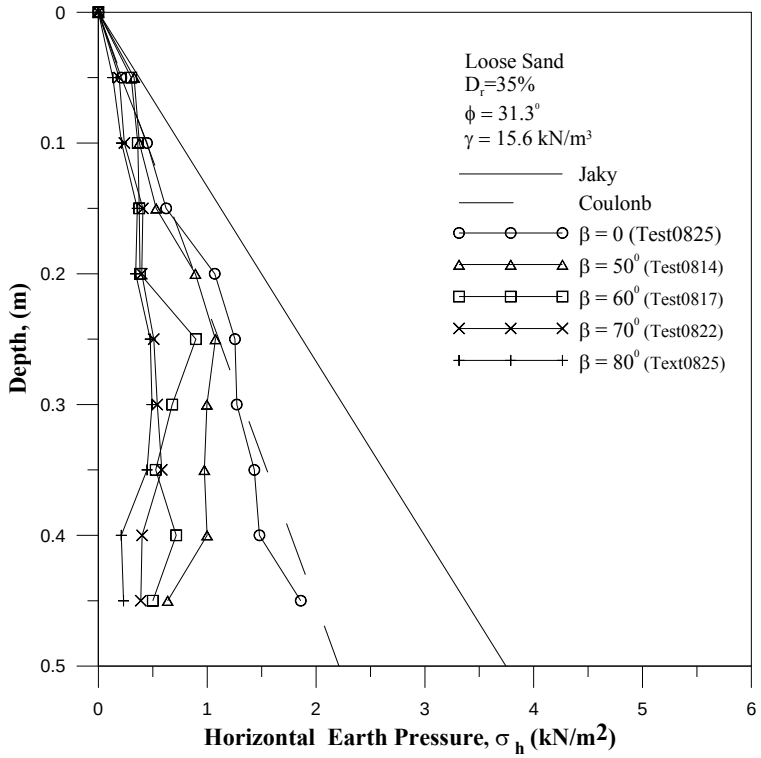

Fig. 70 Distribution of active earth pressure at different interface inclination angle β

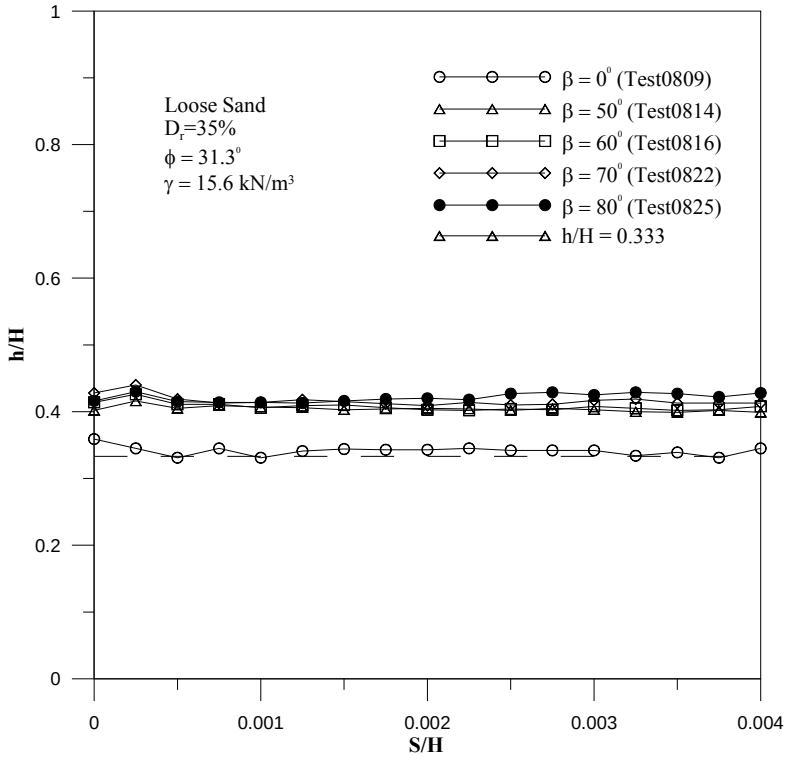

Fig. 71. Variation of total thrust location with increasing wall movement

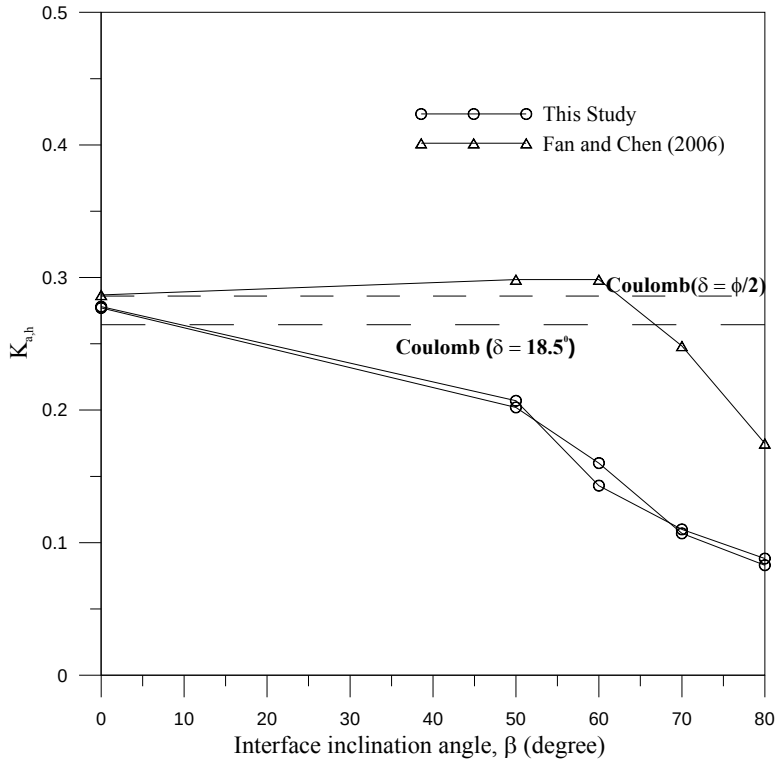

Fig. 72. Active earth pressure coefficient $K_{a,h}$ versus interface inclination angle β

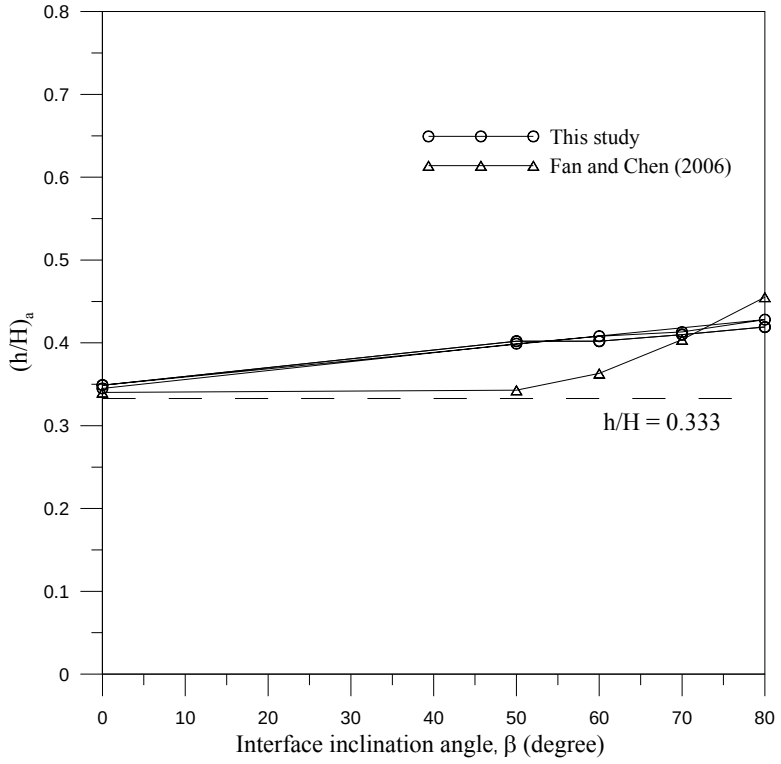

Fig. 73. Point of application of active soil thrust versus interface inclination angle β value

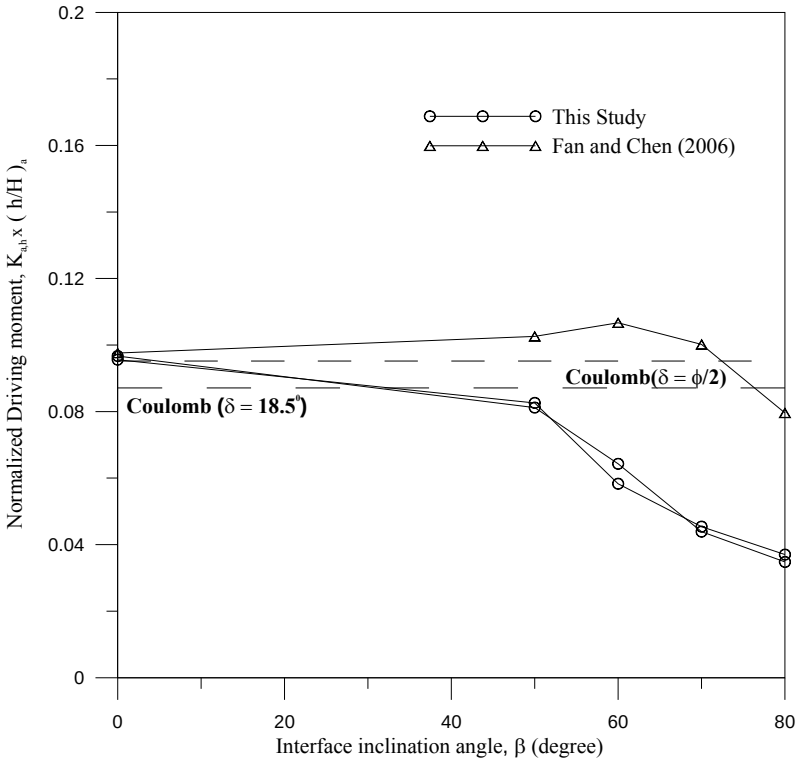

Fig. 74. Normalized driving moment versus interface inclination angle β

7. CONCLUSIONS

In this report, the effects of a nearby inclined rock face on the active earth against a rigid retaining wall are investigated. Based on the test results, the following conclusions are drawn.

1. Without the Stiff interface ($\beta = 0^o$), the active earth pressure coefficient $K_{a,h}$ is in good agreement with Coulomb's equation. The point of application h/H of the active soil thrust is located at about 0.33H above the base of the wall.
2. For the interface inclination angle $\beta = 50^o$, 60^o, 70^o and 80^o, the distributions of active earth pressure are not linearly with depth. On the lower part of the model wall the measured horizontal pressure is lower than Coulomb's solution.
3. For $\beta = 50^o \sim 80^o$, the active earth pressure coefficient $K_{a,h}$ decreases with increasing interface inclination angle. The point of application of the active total thrust move a location slight higher than h/H = 0.333.
4. For $\beta = 50^o \sim 80^o$, the nearby inclined rock face would actually increase the FS against sliding of the wall. The evaluation of FS against sliding with Coulomb's theory would be on the safe side.
5. For $\beta = 50^o \sim 80^o$, the intrusion of an inclined rock face into the active soil wedge would increase the FS against overturning of the retaining wall. The evaluation of FS against overturning with Coulomb's theory would also be on the safe side.

8. RERERENCES

1. Ang, A. H., and Tang, W. H., (1975) "Probability Concepts in Engineering Planning and Design, Volume Ⅰ - Basic Principles," John Wiley and Sons, Inc, New York, N.Y., pp. 286-294.
2. Bakeer, R. M., and Bhatia, S. K., (1989), "Earth Pressure Behind a Gravity Retaining Wall ," International Journal for Numerical and Analytical Methods in Geomechanics, Vol. 13, pp. 665-973.
3. Brinch Hansen, J., (1953), "Earth Pressure Calculation," Danish Technical Press, Copenhagen.
4. Bros, B., (1972), "The Influence of Model Retaining Wall Displacements on Active and Passive Earth Pressure in Sand," Proceedings, 5th European Conference on Soil Mechanics, Vol.1, Madrid, Spain, pp. 241-249.
5. Chen, C. Y., (1995), "Active Earth Pressure with Inclined Backfill," Master of Engineering Thesis, National Chiao Tung University, Hsinchu, Taiwan.
6. Chang, S. Y., (2000), "Effect of Backfill Density on Active Earth Pressure," Master of Engineering Thesis, Dept. of Civil Engineering, National Chiao Tung University, Hsinchu, Taiwan.
7. Chen, H. R., (1997), "Earth Pressure At-Rest with Different Soil Densities and Backfill Inclinations," Master of Engineering Thesis, National Chiao Tung University, Hsinchu, Taiwan.
8. Chen, T. J., (2003). "Earth Pressures Due to Vibratory Compaction." Ph.D. dissertation, National Chiao Tung University, Hsinchu, Taiwan.
9. Clough, G. W., and Duncan, J. M., (1971), "Finite Element Analysis of Retaining Wall Behavior," Journal of Geotechnical Engineering, ASCE, Vol. 87, No. SM12, pp. 1657-1673.
10. Das, B. M. (1994), "Principles of Foundation Engineering." PWS Publishing Company, Boston.
11. Dubrova, G. A., (1963), "Interaction of Soil and Structures," Izd. "Rechonoy Transport," Moxcow
12. Fan, C. C., and Chen K. H, (2006), "Earth Pressure of Retaining Walls near Faces" Master of Engineering Thesis, Department of Construction Engineering, National Kaohsiung First University of Science and Technology, Kaohsiung, Taiwan.
13. Fang, Y. S., and Ishibashi, I., (1986), "Static Earth Pressures with Various Wall Movements," Journal of Geotechnical Engineering, ASCE, Vol. 112, No. 3, Mar., pp. 317-333.
14. Fang, Y. S., Cheng F. P., Cheng, R. T., and Fan, C. C., (1993), "Earth Pressure under General Wall Movements," Geotechnical Engineering, SEAGS, Vol. 24, No. 2, December., pp. 113-131.
15. Fang, Y. S., Chen, J. M., and Chen, C. Y., (1997), "Earth Pressures with Sloping Backfill" Journal of Geotechnical and Geoenvironmental Engineering, ASCE, 123(3), March, 250-259.
16. Fang, Y. S., Chen, T. J., and Wu, B. F., (1994), "Passive Earth Pressure with Various Wall Movements," Journal of Geotechnical Engineering, ASCE, 120(8), Aug., 1307-1323.
17. Fang, Y. S., Chen, J. J., Holtz, R. D., and Lee, W. F. (2004), "Reduction of Boundary Friction in Model Tests," Geotechnical Testing Journal, ASTM, 27(1), 1-10.
18. Frydman. S., and Keissar, I. (1987). "Earth Pressure on Retaining Walls near Rock Faces." Journal of Geotechnical Engineering, ASCE, 113(6), 586-599.
19. Ho, Y. C., (1999), "Effects of Backfill Compaction on Passive Earth Pressure," Master

of Engineering Thesis, National Chiao Tung University, Hsinchu, Taiwan.
20. Ishibashi, I., and Fang, Y. S., (1987), "Dynamic Earth Pressures with Different Wall Movements Modes," Soils and Foundations, JSSMFE, 27(4), Dec., 11-22.
21. Lo Presti, D. C. F., Pedroni, S., and Crippa, V. (1992). "Maximum dry density of cohesionless soils by pluviation and by ASTM D 4253-83: A comparative study." Geotechnical Testing Journal, ASTM, 15(2), 180-189.
22. Mackey, R. D., and Kirk, D. P., (1967), "At Rest, Active and Passive Earth Pressures," Proceedings, South East Asian Conference on Soil Mechanics and Foundation Engineering, Bangkok, pp. 187-199.
23. Nakai, (1985), "Finite Element Computations for Active and Passive Earth Pressure Problems of Retaining Wall," Soils and Foundations, JSSMFE, 25(3), 98-112.
24. Naval Facilities Engineering Command. (1982). Foundations and earth structures design manual 7.2, NAVFAC DM-7.2, Dept. of the Navy, Naval Facilities Engineering Command, Virginia, NAVFAC DM-7.2.
25. Potts, D. M., and Fourie, A. B., (1986), "A Numerical Study of the Effects of Wall Deformation on Earth Pressures," International Journal for Numerical and Analytical Methods in Geomechanics, Vol. 10, pp. 383-405.
26. Rad, N.S., and Tumay, M. T. (1987). "Factors affecting sand specimen preparation by raining." Geotechnical Testing Journal, ASTM, 10(1), 31-37.
27. Rowe, P. W., and Barden, L. (1964). "Importance of Free Ends in Triaxial Testing." Journal of the Soil Mechanics and Foundations Division, ASCE, 90(SM1), 1-77.
28. Sherif, M. A., Fang, Y. S., and Sherif, R. I., (1984). "K_a and K_o behind Rotating and Non-Yielding Walls," Journal of Geotechnical Engineering, ASCE, 110(1), Jan., 41-56.
29. Tatsuoka, F., and Haibara, O., (1985), "Shear Resistance between Sand and Smooth or Lubricated Surface." Soils and Foundations, JSSMFE, 25(1), Mar., 89-98.
30. Tatsuoka, F., Molenkamp, F., Torii, T., and Hino, T. (1984). "Behavior of Lubrication Layers of Platens in Element Tests." Soils and Foundations, JSSMFE, 24(1), 113-128.
31. Tejchman, J., and Wu, W., (1995) "Experimental and Numerical Study of Sand-Steel Interfaces", International Journal for Numerical and Analytical Methods in Geotechanics, Vol. 19, No. 8, pp.513-536.
32. Terzaghi, K., (1932), "Record Earth Pressure Testing Machine." Engineering News-Record, Vol. 109, Sept., 29, pp. 365-369.
33. Terzaghi, K., (1941), "General Wedge Theory of Earth Pressure," ASCE Transaction, Vol. 106, pp. 68-80.
34. Terzaghi, K., and Peck, R. B.,(1967), Soil Mechanics in Engineering Practice, Wiley, New York.
35. Wang, F. J., (2005), "Effects of adjacent Rock Face Inclination on Earth Pressure At-Rest," Master of Engineering Thesis, National Chiao Tung University, Hsinchu, Taiwan.
36. Wu, B. F., (1992), "Design and Construction of National Chiao Tung University Model Retaining Wall," Master of Engineering Thesis, National Chiao Tung University, Hsinchu, Taiwan.

9. 計劃成果自評可供推廣之研發成果資料表

本研究探討鄰近堅硬岩石面入侵回填土對擋土牆主動土壓力之影響。本研究以氣乾之渥太華砂為回填土，回填土高及牆高 H 皆為 0.5 公尺。量測於鬆砂(相對密度 $D_r = 35\%$)狀態下，作用於剛性擋土牆的側向土壓力。本研究利用國立交通大學模型擋土牆設備，探討堅硬界面以不同傾角β侵入回填土，對擋土牆主動土壓力影響。為模擬堅硬的岩石界面，本研究設計並建造一座鋼製界面板，及其支撐系統。本研究共執行五種岩石界面與水平面夾角$\beta = 0^o$、50^o、60^o、70^o與80^o五組實驗。依據實驗結果，獲得以下幾項結論。

1.當岩石界面傾角$\beta = 0^o$時，其主動土壓力係數 $K_{a,h}$ 與 Coulomb 解相吻合，其主動合力作用於距擋土牆底部約 0.33H 處。

2.在岩石界面傾角 45^o、60^o、70^o與80^o狀況下，側向土壓力隨深度的增加而呈非線性分布，所獲得的側向土壓力低於 Jaky 解，側向土壓力隨界面傾角的增加而減少。

3.當界面傾角為 50^o至80^o，主動土壓合力隨岩石界面傾角的增加而逐漸減小。合力作用點的位置稍高於理論值 0.33H。

4.當傾斜岩石面入侵主動土楔時，造成擋土牆抗滑動之安全係數增加，因此根據Coulomb理論所求解之安全係數會偏向安全。

5.當傾斜岩石面入侵主動土楔時，使擋土牆抗傾覆之安全係數增加，所以依據 Coulomb 理論所求得之安全係數會趨於安全。

本研究獲得數項創新發現，研究成果具工程實用價值。參與研究的碩士班研究生藉此機會，獲得試驗儀器之設計與製作寶貴經驗，習得大型基礎模型實驗與資料擷取之操作，以及嚴謹審慎之實驗方法與獨立思考及創造的能力，獲益匪淺。

可供推廣之研發成果資料表

□ 可申請專利　　□ 可技術移轉　　日期：101 年 10 月 31 日

國科會補助計畫	計畫名稱：鄰近傾斜岩石面對擋土牆主動土壓力之影響 計畫主持人：方永壽 教授 計畫編號：NSC 100-2221-E-009-128- 學門領域：土木水利工程
技術/創作名稱	鄰近傾斜岩石面對擋土牆主動土壓力之影響
發明人/創作人	方永壽 教授
技術說明	中文: 本研究探討鄰近堅硬岩石面入侵回填土對擋土牆主動土壓力之影響。本研究以氣乾之渥太華砂為回填土，回填土高及牆高 H 皆為 0.5 公尺。量測於鬆砂(相對密度 $D_r = 35\%$)狀態下，作用於剛性擋土牆的側向土壓力。本研究利用國立交通大學模型擋土牆設備，探討堅硬界面以不同傾角β侵入回填土，對擋土牆主動土壓力影響。為模擬堅硬的岩石界面，本研究設計並建造一座鋼製界面板，及其支撐系統。本研究共執行五種岩石界面與水平面夾角$\beta = 0^o$、50^o、60^o、70^o 與 80^o 五組實驗。依據實驗結果，獲得以下幾項結論。(1).當岩石界面傾角$\beta = 0^o$時，其主動土壓力係數 $K_{a,h}$ 與 Coulomb 解相吻合，其主動合力作用於距擋土牆底部約 0.33H 處。(2)在岩石界面傾角 45^o、60^o、70^o 與 80^o 狀況下，側向土壓力隨深度的增加而呈非線性分布，所獲得的側向土壓力低於 Jaky 解，側向土壓力隨界面傾角的增加而減少。(3)當界面傾角為 50^o 至 80^o，主動土壓合力隨岩石界面傾角的增加而逐漸減小。合力作用點的位置稍高於理論值 0.33H。(4)當傾斜岩石面入侵主動土楔時，造成擋土牆抗滑動之安全係數增加，因此根據 Coulomb 理論所求解之安全係數會偏向安全。(5)當傾斜岩石面入侵主動土楔時，使擋土牆抗傾覆之安全係數增加，所以依據 Coulomb 理論所求得之安全係數會趨於安全。

	英文： In this report, the active earth pressure on retaining walls with the intrusion of an inclined rock face into the backfill is studied. The instrumented model retaining-wall facilities at National Chiao Tung University was used to investigate the active earth pressure induced by different interface inclination angle β. Loose Ottawa sand was used as backfill material. The thickness of backfill and the wall height H were 0.5 m. To simulate an inclined rock face, a steel interface plate and its supporting system were designed and constructed. Base on the test results, the following conclusions were drawn. (1) Without the Stiff interface ($\beta = 0^o$), the active earth pressure coefficient $K_{a,h}$ is in good agreement with Coulomb's equation. The point of application of the active soil thrust is located at about 0.33H above the base of the wall. (2) For the interface inclination angle $\beta = 50^o$, 60^o, 70^o and 80^o, the distributions of active earth pressure are not linearly with depth. On the lower part of the model wall, the measured horizontal pressure is lower than Coulomb's prediction. (3) For $\beta = 50^o$ to 80^o, the active earth pressure coefficient $K_{a,h}$ decreases with increasing interface inclination angle. The point of application of the active thrust moves a location slight higher than h/H = 0.333. (4) For $\beta = 50^o$ to 80^o, the nearby inclined rock face would actually increase the factor of safety (FS) against sliding of the wall. The evaluation of FS against sliding with Coulomb's theory would be on the safe side. (5) For $\beta = 50^o$ to 80^o, the intrusion of an inclined rock face into the active wedge would increase the FS against overturning of the retaining wall. The evaluation of FS against overturning with Coulomb's theory would also be on the safe side.
推廣及運用的價值	本研究屬於基礎學術性研究，一年計劃完成，所獲研究成果將有助於國內外重力式擋土牆設計之重要參考。

※ 1. 每項研發成果請填寫一式二份，一份隨成果報告送繳本會，一份送 貴單位研發成果推廣單位（如技術移轉中心）。

※ **2. 本項研發成果若尚未申請專利，請勿揭露可申請專利之主要內容。**

※ 3. 本表若不敷使用，請自行影印使用。

國科會補助專題研究計畫項下出席國際學術會議心得報告

報告日期：101 年 7 月 11 日

計畫編號	NSC 100-2221-E-009-128		
計畫名稱	鄰近傾斜岩石面對擋土牆主動土壓力之影響		
出國人員姓名	方永壽	服務機構及職稱	國立交通大學 土木工程系 教授
會議時間	2012 年 6 月 17 日 至 2012 年 6 月 22 日	會議地點	Rhodes, Greece
會議名稱	(中文) 第 22 屆國際近海與極區工程研討會 (英文) 22nd International Offshore and Polar Engineering Conference		
發表論文題目	(中文) 鄰近傾斜岩石面對擋土牆靜止土壓力之影響 (英文) Effects of Adjacent Rock Face Inclination on Earth Pressure at-rest		

一、參加會議經過

第 22 屆國際近海與極地工程研討會(The 22nd International Offshore and Polar Engineering Conference)是由 International Society of Offshore and Polar Engineers (ISOPE)主辦，過去 5 屆的舉行地點包含: 葡萄牙里斯本(2007)、加拿大溫哥華(2008)、日本大阪(2009)、中國北京(2010)、及美國 Maui(2011)，下一屆研討會預定 2013 年在美國 Anchorage 舉辦。本次國際會議有來自 52 個國家代表的參與，論文集共收錄 694 篇論文，編列為 4 大冊論文集，本研討會論文集被列為 indexed by Engineering Index, Compendex。報告人除以書面及口頭發表論文外，亦擔任本研討會的論文審查委員(Reviewer)，協助維持發表論文的學術水準。

本次研討會透過主題集中的 150 場技術討論場次(Technical session)，發表經詳細審查、具原創性與重要性的論文，進行國際水準的論文發表，促進學術界與工業界的跨領域交流。大會並邀請數位傑出的學者專家發表 Keynote 演講，大師級學者的報告內容精采，與會者收穫甚為豐富。上頁照片左起為台灣海洋大學河海工程系的陳俶季教授、計畫主持人方永壽、及考試院考試委員李雅榮博士合影於研討會場。研討會主辦單位為 International Society of Offshore and Polar Engineering (ISOPE) 及 Aristotle University of Thessaloniki

本次研討會，透過 150 個技術討論場次，由 Selected Authors 發表經詳細審查、具重要性的論文，進行國際水準的論文發表，促進學術界與工業界的跨領域交流。此次會議與大地工程相關的技術討論主題如下:

Soil Properties
Soil Improvement
Suction Piles
Offshore Foundations
Piles and Foundations
Cyclic Loading
Slope Stability
Consolidation and Seepage
Materials and Test

二、論文發表及刊出

報告人於 2012 年 6 月 20 日(星期三)下午 16:20 於 Session 107 發表論文，該 Session 主題為 Estuary Hydraulics，報告人發表的論文題目是: Effects of Adjacent Rock Face Inclination on Earth Pressure at-rest。本研究依據實驗結果，探討鄰近傾斜岩石面對擋土牆靜止土壓力之影響，報告引起與會者的興趣，與作者展開熱烈的討論，並有英國 University of Dundee 的 Professor Dong-Sheng Jeng 向作者索取更多研究資料。

上圖為 Session 107 參與者合影，左起中國南京河海大學陳永平教授、大連理工梁書秀副教授、主持人台灣海洋大學簡連貴教授、報告人、及日本廣島商船高等專門學校芝田浩講師。報告人與研究生王福駿及劉政合著之論文，被刊出在研討會論文集第 2 冊、第 836 至 841 頁。此項研究為國科會專題研究計畫 NSC 94-2211-E-009-042 之研究成果。

三、建議

除發表論文及參與研討外，報告人順便參觀考察雅典市便捷的都會區(Metro)地鐵系統 Syntagma 地下車站，如下圖所示。

雅典是西方古文明發源的重鎮，歷史悠久且各種古蹟林立。雅典捷運於開挖地下車站時，經常遭遇各種古蹟。為避免破壞古文物，施工單位必須非常小心、謹慎的開挖，並將挖掘到的古文物加以清洗整理，選取精品作為捷運地下車站的展覽藝術品(如下圖)，成為雅典捷運地下車站的一項特色，這項作法值得我們台北捷運施工遭遇古蹟時，處理方法的參考。

四、攜回資料名稱及內容

論文集光碟 1 片(The Proceedings of The Twenty-second (2012) International Offshore and Polar Engineering Conference)

Proceedings of the Twenty-second (2012) International Offshore and Polar Engineering Conference **www.isope.org**
Rhodes, Greece, June 17–22, 2012

ISBN 978-1-880653-94–4 (Set); ISSN 1098-6189 (Set)

Effects of Adjacent Rock Face Inclination on Earth Pressure At-Rest

Yung-Show Fang and Cheng Liu
Department of Civil Engineering, National Chiao Tung University, Hsinchu, TAIWAN, China

Fu-Jyun Wang
Department of Power Development, Taiwan Power Company, Taipei, TAIWAN, China

ABSTRACT

This paper studied the effects of an adjacent inclined rock face on the at-rest earth pressure acting on a rigid retaining wall. Horizontal earth pressures in loose (D_r = 35%) and compacted (D_r = 72%) dry Ottawa sand were measured. A steel interface plate with inclination angles 0^o, 45^o, 60^o, 70^o, and 80^o were used to simulate the inclined rock face. The measured distribution of earth pressure was not linearly with depth, and was mostly lower than Jaky's solution. As the rock face inclination angle increased, the magnitude of at-rest soil thrust decreased, and the total thrust rose to a higher location. With the inclination angle of 80^o, only a small amount of sand was filled in the narrow gap between the wall and the inclined interface. The vertical stress in the soil slice was partially resisted by the friction on the nearby inclined rock face. With decreasing vertical stress in the soil mass, the horizontal stress acting on the wall decreased.

KEY WORDS: Constrained backfill; earth pressure at-rest; model test; retaining wall; sand.

INTRODUCTION

In this study, the effects of an adjacent inclined rock face on the earth pressure at-rest on a rigid retaining wall were investigated. In traditional, earth pressure at-rest behind a non-yielding retaining wall was estimated with Jaky's Formula. However, if the retaining wall was constructed adjacent to an inclined rock face as shown in Fig. 1, the inclined face intruded the cohesionless backfill. In this figure, the rock face was excavated behind the bridge abutment, and soil was filled between the abutment and the inclined face. The lateral movement of the abutment was restrained by the bridge girder at the top and the piles below the abutment. The inclination angle between the rock face and horizontal is defined as α. Under this condition, can the Jaky's formula be used to evaluate the earth pressure at-rest on the abutment wall? Would the distribution of earth pressure at-rest still be linear?

The ratio of the horizontal stress σ_h to vertical stress σ_v is defined as the coefficient of earth pressure at-rest K_o, or $K_o = \sigma_h / \sigma_v$. Since $\sigma_v = \gamma z$,

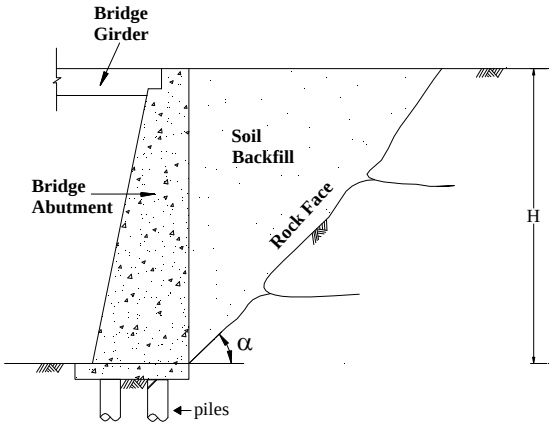

Fig. 1. Bridge abutment near inclined rock face

then $\sigma_h = K_o \gamma z$, where γ is the unit weight of soil. Mesri and Hayat (1993) reported that Jaky (1944) arrived at the relationship ($K_o = 1 - \sin\phi$) between K_o and the internal friction angle ϕ by analyzing a talus of granular soil freestanding at the angle of repose. Mayne and Kulhawy (1982) reported that, the approximate theoretical relationship for K_o for normally consolidated soils introduced by Jaky appears valid for cohesionless soils. Based on their experimental study, Sherif et al. (1984) reported that the earth pressure distribution for loose sand was in good agreement with Jaky's equation.

Spangler and Handy (1982) studied the distribution of soil pressure against a fascia wall built in front of a stable rock face. Granular backfill was placed in the relatively narrow gap between the wall and the natural outcrop. Spangler and Handy proposed an equation to estimate the lateral soil pressure against the wall. Frydman and Keissar (1987) used the centrifuge modeling technique to test a small model wall, and the rock face was modeled by a wooden block, which can be positioned at varying distances d from the wall. It was reported that Spangler and Handy's solution may be used for estimating lateral pressure for the no-movement K_o condition.

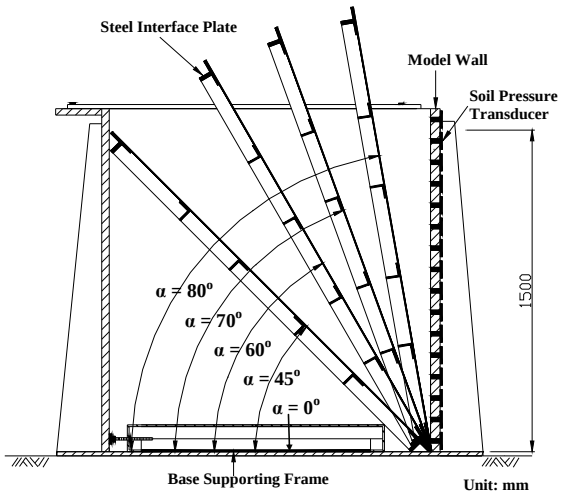

Fig. 2. Different interface inclinations for testing

In this study, the National Chiao Tung University (NCTU) model retaining wall was used to investigate the problem. A steel interface plate was designed and constructed to simulate the inclined rock face. Air-dry Ottawa sand was used as the backfill material. Parameters considered for this study included: (1) relative density, D_r = 35% for loose sand and D_r = 72% for compacted dense sand; (2) rock face inclination angles α = 0°, 45°, 60°, 70° and 80° as shown in Fig. 2. The height of the model wall was 1.5 m. The distribution of lateral earth pressure was measured with the soil pressure transducers mounted on the model wall.

EXPERIMENATL APPARATUS

The model wall shown in Fig. 3 is 1.5 m-wide and 1.6 m-high. The wall is 45 mm-thick and made of a solid steel plate. It is clear in Fig. 3 that the model wall is actually the front-side of the reinforced steel box. Outside the box, twenty four 20 mm-thick steel columns were welded on the walls to reduce any lateral displacement during loading. In addition, twelve channel section steel beams were welded horizontally around the box to further increase the stiffness of the soil bin.

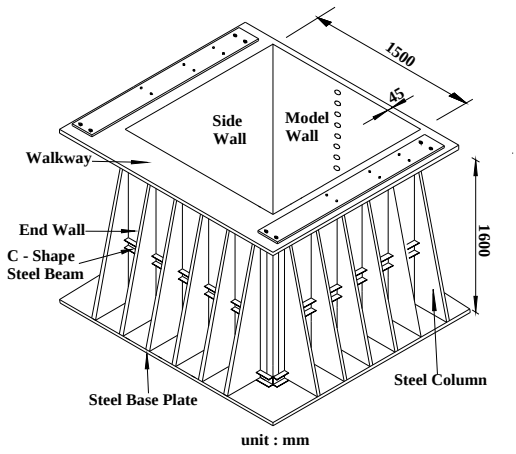

Fig. 3. NCTU non-yielding retaining wall and soil bin

Fig. 4. Strip vibratory soil compactor and model wall

The soil bin was fabricated of steel plates with inside dimensions of 1.5 m x 1.5 m x 1.6 m as illustrated in Fig. 3. The end-wall and sidewalls of the soil bin were made of 35 mm-thick steel plates. To constitute a plane-strain condition, the soil bin was built very rigid so that the lateral deformation of sidewalls under soil pressure would be negligible.

To investigate the variation of horizontal earth pressure σ_h at the wall-soil interface, soil pressure transducers (SPTs) were attached to the model wall. Fourteen transducers SPT1~SPT14 (Kyowa PGM-02KG, capacity = 19.6 kN/m^2) were mounted on the central zone of the model wall as indicated in Fig 2. For more information regarding the NCTU non-yielding retaining-wall facility, the readers are referred to Chen and Fang (2002).

A steel interface plate was designed and constructed to simulate the inclined rock face near the retaining wall. The steel interface plate shown in Fig. 2 is 1,370 mm-long, 998 mm-wide, and 5 mm-thick. A layer of anti-slip material (SAFETY-WALK, 3M) was attached to the plate surface to simulate the friction that might act between the backfill and the rough rock face. To increase the stiffness of the 5 mm-thick steel plate, 5 longitudinal and 5 transverse steel L-beams were welded to the back of the plate. The 30 mm x 30 mm x 3 mm steel beams were attached to establish a grid-beam system to reinforce the thin steel plate.

To achieve a dense backfill, two vibratory soil compactors were used for sample preparation. For large area compaction, the vibratory soil compactor with the base plate area of 225 mm x 225 mm was used. An acentric motor (Mikasa, KJ75-2P) was selected to be the source of vibration. The height of the handle was 1.0 m, and the mass of the compactor is 12.1 kg (0.119kN).

However, for α = 80° shown in Fig. 2, the fill sandwiched between the wall and the interface plate was narrow. A new strip vibratory soil compactor show in Fig. 4 was designed and constructed. The strip compacting plate was 90 mm-wide and 500 mm-long. An acentric motor was fixed on a steel plate on the top of compactor. The total mass of the compactor is 25 kg (0.245 kN).

.

BACKFILL AND INTERFACE CHARACTERISTICS

In this section, properties of the backfill, interface characteristics between the backfill and the sidewalls, and the interface plate

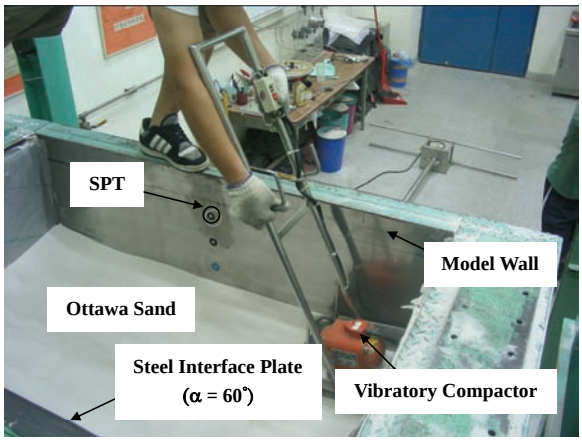

Fig. 5. Compaction of backfill with square vibratory compactor

were discussed. Air-dry Ottawa sand was used throughout this investigation. Physical properties of the soil include G_S = 2.65; e_{max} = 0.76; e_{min} = 0.50; D_{60} = 0.39 mm; and D_{10} = 0.26 mm. For the loose fill, the backfill was deposited by air-pluviation from the slit of a hopper into the soil bin. Rad and Tumay (1987) reported that pluviation is the method that provides reasonably homogeneous specimens with desired relative density. The drop distance was approximately 1.5 m to the soil surface and the slit opening was 18 mm. The soil unit weight γ achieved with the pluviation method was 15.6 kN/m^3, and its relative density D_r was 35%. The corresponding internal friction angle ϕ determined from direct shear tests was 31.3^o.

To obtain a dense condition to simulate field conditions, the loose backfill was densified with the vibratory compactors. For wide-area compaction, the surface of air-pluviated backfill was compacted with the 225 mm x 225 mm square vibratory compactor as shown in Fig. 5. Each compacted lift was 0.3 m-thick. For compaction in the narrow gap between the wall and the interface, the loose sand was compacted with the strip vibratory compactor. Each lane was densified with the vibratory compactor for a pass of 70 seconds. Fig. 6 illustrated the compaction of loose backfill with the 90 mm x 500 mm strip compactor. To achieve a similar dense condition, each compacted lift was 0.1 m-thick.

To observe the distribution of density in the soil sample, density measurements were made. The cylindrical density cup was made of acrylic with an inner diameter of 100 mm and height of 50 mm. The cups were placed in the soil mass at different elevations and locations. In Fig. 7, the distribution of relative density for sand compacted with the strip compactor was compared with that for sand compacted with the square vibratory compactor. The distributions of density obtained with two different compactors were in fairly good agreement (D_r = 72 %), and the density distribution in the soil bin was quite uniform. It may be seen in Fig. 7 that the soil density near the surface of fill was relatively loose.

D'Appolonia et al. (1969) reported that, due to the lack of confining pressure, the soil near the surface may not be dense even after compaction
To simulate a plane-strain condition, the shear stress between the backfill and sidewall should be minimized to be nearly frictionless. This was accomplished by creating a lubrication layer between the sidewalls and the soil. The lubrication layer suggested by Fang et al. (2004) consisted of two 0.009-mm thin plastic sheets and a 0.152-mm

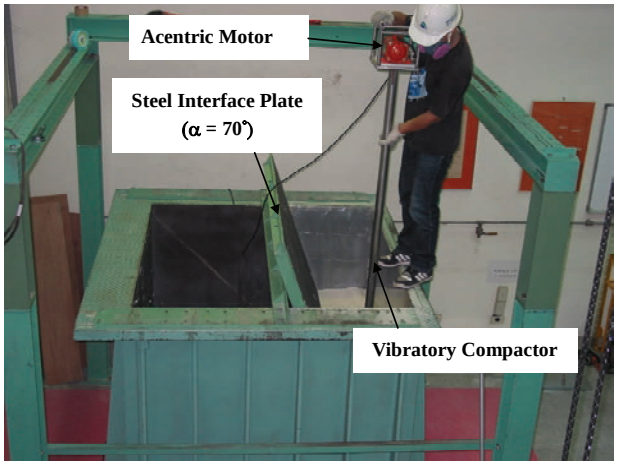

Fig. 6. Compaction of backfill with strip vibratory compactor

thick plastic sheet was used. With the lubrication layer, the sidewall friction angle was reduced to approximately 7.5^o.

To evaluate the interface friction angle δ_i between the backfill and the interface plate, special direct shear tests were conducted. In the test, the lower shear box was replaced with a steel plate covered with a layer of anti-slip material. The interface friction angle δ_i between Ottawa sand and the SAFETY-WALK covered interface plate was found to be 20.7^o.

TEST RESULTS FOR LOOSE BACKFILL

The interface inclination angles of rock face α = 0^o, 45^o, 60^o, 70^o, and 80^o with the horizontal were illustrated in Fig. 2. A loose backfill (D_r = 35%) was placed between the wall and the inclined rock face.

Distribution of Earth Pressure at-rest

The distribution of the lateral earth pressure σ_h against the non-yielding model wall for α = 0^o was illustrated in Fig. 8. In the figure, the

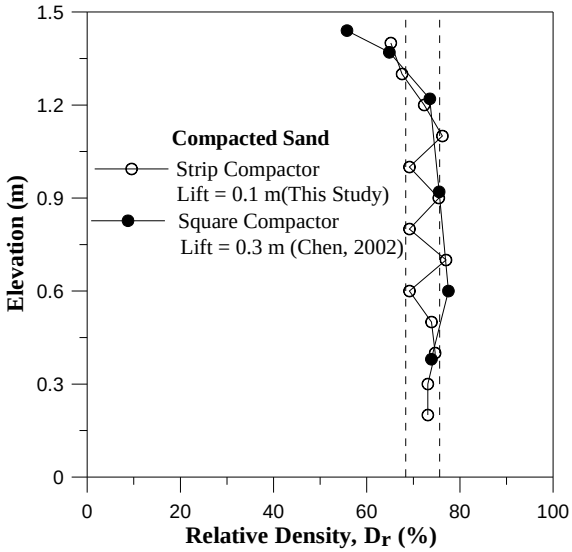

Fig. 7. Comparison of density distribution compacted with strip and square compactors

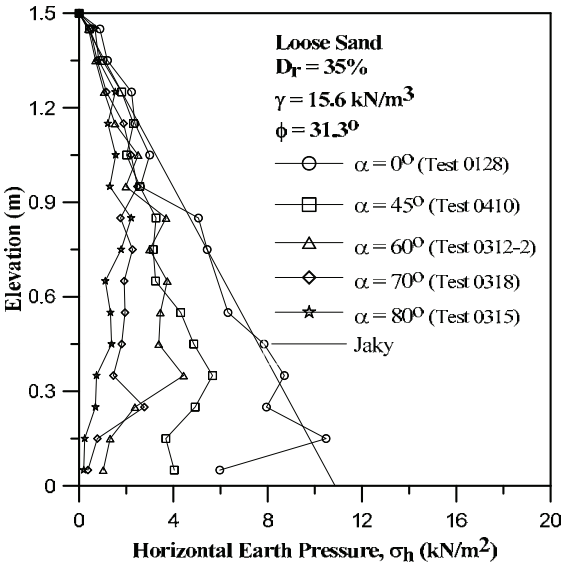

Fig. 8. Distribution of lateral earth pressure at various α angles for loose sand

experimental earth pressure was compared with Jaky's solution. At the elevation 0.15 m to 1.5 m, the distribution of earth pressure was nearly linear and in fairly good agreement with Jaky' solution. Mayne and Kulhawy (1982), Mesri and Hayat (1993) reported that Jaky's equation is suitable to estimate the earth pressure at-rest for backfill in its loosest state. However, the lateral earth pressures measured near the base of the wall are lower than Jaky's prediction. This is most probably due to the high stiffness of the steel base plate.

For $\alpha = 45^o$ in Fig. 8, at the elevation 1.5 m to 1.2 m the measured σ_h was not affected by the steel interface plate. The lateral earth pressure increased with the increasing depth at elevation 1.5 m to 0.35 m. The maximum horizontal earth pressure was measured at the elevation 0.35 m. However, the measured lateral pressure decreased slowly with depth from the elevation 0.35 m to 0. It was clear in Fig. 2 that, for the upper part of model wall, the interface plate was relatively far from the pressure transducer. It was reasonable to expect the measured pressure σ_h to be identical to Jaky's solution. However, for the lower part of the model wall, the interface plate was quite close to the pressure transducers. As a result, the σ_h measured was affected by the nearby interface plate.

For $\alpha = 60^o$ in Fig. 8, the measured stress were lower than Jaky's solution especially the pressure measured near the base of wall. It may be observed in Fig. 2, with the increase of α angle, the horizontal spacing between the model wall and the interface plate decreased. The measured earth pressure at rest was even lower than that for $\alpha = 45^o$. Maximum lateral stress was measured at the elevation of 0.65 m. The distributions of lateral stress measured with the interface inclined at $\alpha = 70^o$ and 80^o were also indicated in Fig. 8. It was obvious that the measured earth pressure decreased with the approaching of the inclined rock face, especially on the lower part of the wall.

In Fig. 8, it is obvious that the distributions of earth pressure were not linearly with depth. The measured horizontal pressure was mostly lower than Jaky's solution. The magnitude of lateral pressure decreased with increasing α angle. The measured earth pressure at-rest was significantly affected by the presence of the nearby rock face. It would be reasonable to expect that the resultant soil thrust P_h acting on the

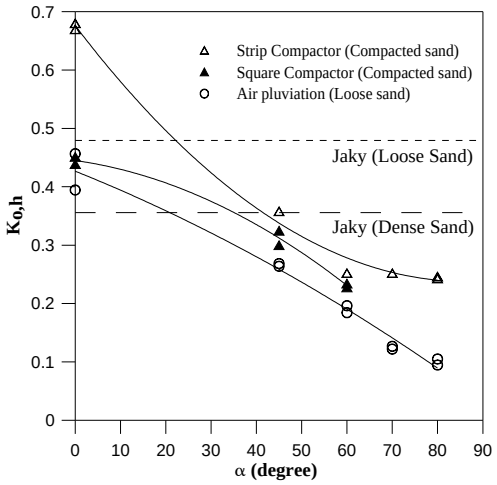

Fig. 9. Variation of $K_{o,h}$ at various α angeles

wall to decrease with increasing α angle. It may also be expected that the point of application of the total soil thrust would rise with increasing α angle.

Magnitude of at-rest Soil Thrust

The variation of horizontal at-rest pressure coefficient $K_{o,h}$ as a function of interface inclination angle α was shown in Fig. 9. The coefficient $K_{o,h}$ was defined as the ratio of the horizontal soil thrust. P_h to $\gamma H^2/2$. The horizontal soil thrust P_h was calculated by summing the pressure diagram shown in Fig. 8. Without the interface plate ($\alpha = 0^o$), the coefficient $K_{o,h}$ was slightly less than Jaky's solution. However, after the steel interface plate was placed in soil bin. The coefficient $K_{o,h}$ decreased with increasing rock face inclination angle. The measured coefficient $K_{o,h}$ was apparently less than the Jaky's solution. Based on the test results, an empirical relationship between the coefficient $K_{o,h}$ and the interface inclination angle α was be established:

$$K_{o,h,\alpha} = K_{o,h,Jaky} - (0.00462 - \alpha) \quad (1)$$

Where $K_{o,h} = 1 - \sin\phi$; α = interface inclination angle in degree. Eqn. (1) was only applicable for loose sand at $0° \leqq \alpha \leqq 80°$.

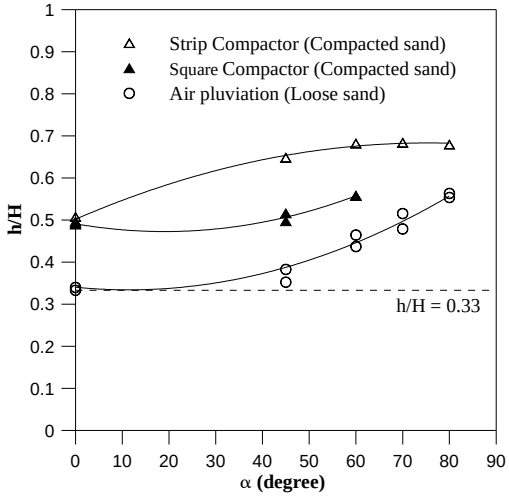

Fig. 10. Point of application of resultant force at various α angles

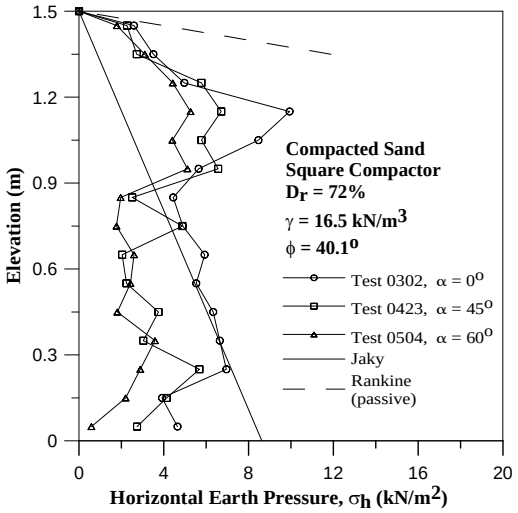

Fig. 11. Distribution of lateral earth pressure at various α angles for sand compacted with square compactor

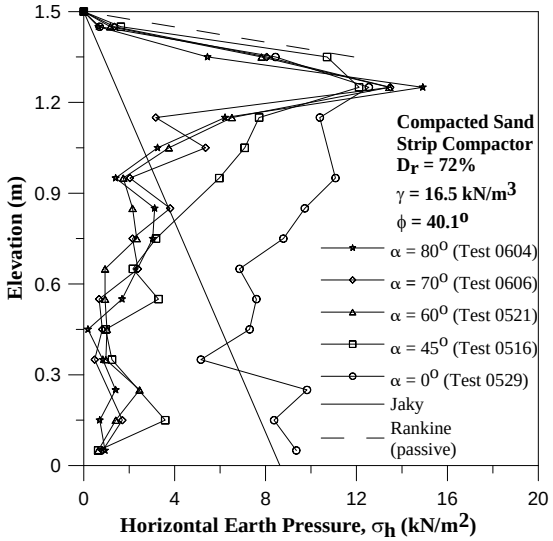

Fig. 12. Distribution of lateral earth pressure at various α angles for sand compacted with strip compactor

Point of Application of at-rest Soil Thrust

The point of application h/H of the total soil thrust as a function of the α angle was illustrated in Fig. 10. Note h is the vertical distance between the total thrust and the base of wall. In the figure, without the interface plate ($\alpha = 0^o$), the point of application of the at-rest soil thrust was located at about 0.33 H above the base of the wall. As the interface angle increased, the earth pressure gradually decreased near the base of the wall as seen in Fig. 8. This change of earth pressure distribution caused the total thrust to rise to higher locations as shown in Fig. 10. For $\alpha = 80^o$, the point of application of the total thrust was located at 0.55 H above the base of the wall.

TEST RESULTS FOR DENSE BACKFILL

This section reported the experimental results regarding effects of an adjacent inclined rock face on the earth pressure against a non-yielding wall with compacted backfill. The rock face inclination angle considered were $\alpha = 0^o$, 45^o, 60^o, 70^o and 80^o. To obtain the expected dense condition, the cohesionless backfill was compacted with two different vibratory compactors to reach the relative density $D_r = 72\%$, and the unit weight of 16.5 kN/m^3. Based on the results obtained with direct shear tests (Ho, 1999), the corresponding internal friction angle ϕ for the dense backfill was 40.1^o.

Distribution of Earth Pressure at-rest

Fig. 11 showed the distributions of lateral earth pressure against the non-yielding wall, after the backfill was compacted in five 0.3 m-thick lifts with the square vibratory compactor (see Fig. 5). Before compaction, the earth pressure at-rest could be properly estimated with Jaky's equation. After compaction, Fig. 11 showed that for $\alpha = 0^o$ an extra horizontal stress was induced by compaction at the upper part of wall surface. The compaction-influenced zone extended from the compacted surface to the depth of approximately 0.7 m. Peck and Mesri (1987) reported that the compaction induced lateral pressure near the surface was limited by the passive Rankine earth pressure. In Fig. 11,the lateral stress measured near the top of backfill was almost identical to the passive pressure. For more information regarding the compaction induced earth pressure, the reader is referred to Chen and Fang (2008). However, the lateral stresses measured below the compaction-influenced zone converged to the earth pressure at-rest based on Jaky's equation.

Fig. 12 showed the distributions of lateral earth pressure for the backfill compacted with the strip vibratory compactor (see Fig. 4). The 1.5 m-thick backfill was compacted in fifteen 0.1 m-thick lifts. The relative density of soil obtained was also 72%. For $\alpha = 0^o$, the compaction-influenced zone extended from the surface to the depth of approximately 1.1 m. It was obvious in Fig. 12 that the peak lateral earth pressure induced by the strip compactor was higher than that induced by the square compactor. It should be mentioned that, to achieve the same relative density, the backfill was compacted in 15 lifts and each lift was compacted in 15 lanes by the strip compactor. The amount of energy input by the strip compactor was much higher than that by the square compactor.

Fig. 11 showed the distribution of lateral earth pressure for the dense backfill compacted with the square compactor for the rock face inclination angles $\alpha = 0^o$, 45^o, and 60^o. In this Figure, the lateral earth pressures measured for $\alpha = 45^o$ and 60^o were less than Jaky's solution at the lower part of the wall. The magnitude of earth pressure decreased with increasing α angle. The compaction-influenced zone extended from the surface to the depth of approximately 0.6 m.

Fig. 12 showed the distribution of lateral stress for the dense backfill compacted with the strip compactor. In this Figure, at the lower part of the wall, the measured lateral stresses for $\alpha = 45^o$, 60^o, 70^o, and 80^o were lower than Jaky's solution. For $\alpha = 60^o$, 70^o and 80^o, the distributions of lateral stress were similar. The depth of compaction-influenced zone decreased with increasing interface inclination angle. This phenomenon may be explained with the help of Fig. 2. For $\alpha = 0^o$, compaction was compacted all over the soil layer. However, for $\alpha = 80^o$, compaction was carried out only on the surface of the narrow fill sandwiched between the wall and inclined plate. The effective compaction depth was significantly influenced by the amount of energy input.

Magnitude of at-rest Soil Thrust

The variation of horizontal at-rest pressure coefficient $K_{o,h}$ as a function

of interface inclination angle was shown in Fig. 9. The coefficient $K_{o,h}$ for loose sand was compared with that for the backfill compacted with two different compactors. It was seen that, at the same inclination angle α, the order of the coefficient was $K_{o,h,strip} > K_{o,h,square} > K_{o,h,loose}$. In Fig. 9, the coefficient $K_{o,h}$ for the backfill compacted with the square compactor, the coefficient $K_{o,h}$ decreased with increasing rock face inclination angle. The coefficient $K_{o,h}$ for sand compacted with the strip compactor was approximately 0.67 at $\alpha = 0^o$. Due to the compaction effect, the coefficient $K_{o,h}$ was clearly higher than Jaky's prediction. However, the coefficient $K_{o,h}$ decreased with increasing rock face inclination angle.

Spangler and Handy (1984) indicated granular backfill placed in the relatively narrow gap between the wall and the natural rock face was partly supported by friction on each side, from the wall and form the rock face. Since the friction acted nearly vertically, it reduced vertical stresses in the soil mass, which in turn reduced the horizontal stress. In this study, for $\alpha = 80^o$ as shown in Fig. 2, only a small amount of sand was filled in the narrow gap between the lower part of the wall and the inclined plate. The vertical stress in the soil slice was partially supported by the friction on the nearby inclined rock face. As a result, with decreasing vertical stress, the horizontal stress acting on the wall face decreased as indicated in Fig. 12.

Point of Application of at-rest Soil Thrust

The point of application of the at-rest soil thrust as a function of the rock face inclination angle was shown in Fig. 10. Without the interface plate ($\alpha = 0^o$), due to the compaction induced stresses near the top of the wall, the point of application of the at-rest soil thrust was located at about 0.49 H to 0.50 H above the base of the wall. Fig. 12 indicated that as the interface angle increased, the earth pressure on the lower part of the wall decreased. This change of earth pressure distribution caused the total thrusts to rise to higher locations as shown in Fig. 10. For $\alpha = 80^o$, the point of application of the at-rest soil thrust for the backfill compacted with a strip compactor was located at 0.68 H above the base of the wall. Due to the compaction effect, at the same inclination angle α, the order of h/H for compacted and loose fills was $(h/H)_{strip} > (h/H)_{square} > (h/H)_{loose}$.

CONCLUSIONS

For the wall backfilled with a loose fill, the distribution of earth pressure was not linearly with depth. The measured horizontal pressure was mostly lower than Jaky's solution. The magnitude of lateral pressure decreased with increasing α angle. The measured earth pressure at-rest was significantly affected by the presence of the nearby inclined rock face.

The magnitude of at-rest soil thrust decreased with increasing rock face inclination angle. The at-rest earth pressure coefficient $K_{o,h}$ was apparently less than the Jaky's solution. As the interface angle increased, the total thrust rose to higher locations. For $\alpha = 80^o$, the point of application of the total thrust was located at 0.65 H above the base of the wall.

For the wall backfilled with a compacted fill, an extra horizontal stress was induced by compaction at the upper part of wall surface. For $\alpha = 45^o$ and 60^o, the lateral pressures were less than Jaky's solution at the lower part of the wall. The magnitude of earth pressure decreased with the approach of the inclined rock face.

The magnitude of at-rest soil thrust decreased with increasing rock face inclination angle. Due to the compaction effect, the coefficient $K_{o,h}$ was clearly higher than Jaky's prediction. However, the coefficient $K_{o,h}$ decreased with increasing rock face inclination angle. In this study, for $\alpha = 80^o$, only a small amount of sand was filled in the narrow gap between the lower part of the wall and the inclined plate. The vertical stress in the soil slice was partially supported by the friction on the nearby inclined rock face. As a result, with decreasing vertical stress, the horizontal stress acting on the wall face decreased.

Without the interface plate, due to the compaction induced stresses near the top of the wall, the point of application of the at-rest soil thrust was located at about 0.49 H to 0.50 H above the base of the wall. As the interface angle α increased, the earth pressure on the lower part of the wall decreased. This change of earth pressure distribution caused the total thrust to rise to a higher location. For $\alpha = 80^o$, the point of application of the at-rest soil thrust for the backfill compacted with a strip compactor was located at 0.68 H above the base of the wall.

ACKNOWLEDGEMENTS

The writers wish to acknowledge the National Science Council of the Republic of China government (Grant No. : NSC 94-2211-E-009-042) for the financial assistance that made this investigation possible.

REFERENCES

Chen, TJ and Fang, YS (2002). "A New Facility for Measurement of Earth Pressure at Rest," *Geotech Eng J*, SEAGS, Vol 33, No 3, pp 153-159.

Chen, TJ, and Fang, YS (2008). "Earth Pressure Due to Vibratory Compaction," *J of Geotech and Geoenvironmental Eng*, ASCE, Vol 134, No 4, pp 437-444.

D'Appolonia, DJ, Whitman, RV and D'Appolonia, E (1969). "Sand Compaction with Vibratory Rollers," *J of Soil Mech and Found Div*, ASCE, Vol 95, No SM1, pp 263-284.

Fang, YS, Chen, TJ, Holtz, RD, and Lee, WF (2004). "Reduction of Boundary Friction in Model Tests," *Geotech Testing J*, ASTM, Vol 27, No 1, pp 1-10.

Frydman, S, and Keissar, I (1987). "Earth Pressure on Retaining Walls near Rock Faces," *J of Geotech Eng*, ASCE, Vol 113, No 6, pp 586-599.

Ho, YC (1999). "Effects of Backfill Compaction on Passive Earth Pressure," *Master Thesis*, Dept of Civil Eng, National Chiao Tung Univ, Hsinchu, Taiwan.

Jaky, J (1944). "The Coefficient of Earth Pressure at Rest," *J for Society of Hungarian Architects and Engineers*, Budapest, Hungary, pp 355-358.

Mayne, PW, and Kulhawy, FH (1982). "K_o - Relationships in Soil," *J of Geotech Eng Div*, ASCE, Vol 108, No GT6, pp 851-872.

Mesri, G, and Hayat, TM (1993). "The Coefficient of Earth Pressure at Rest," *Canadian Geotech J*, Vol 30, No 4, pp 647-666.

Peck, RB, and Mesri, G (1987). Discussion of "Compacted-Induced Earth Pressures under K_o - onditions," *J of Geotech Eng*, ASCE, Vol 113, No 11, pp 1406-1408.

Rad, NS, and Tumay, MT (1987). "Factors Affecting Sand Specimen Preparation by Raining," *Geotech Testing J*, ASTM, Vol 10, No 1, pp 31-37.

Sherif, MA, Fang, YS and Sherif, RI (1984). "K_a and K_o behind Rotating and Non-Yielding Walls," *J of Geotech Eng*, ASCE, Vol 110, No 1, pp 41-56.

Spangler, MG, and Handy, RL (1984). *Soil Engineering*, Harper and Row, New York, NY

國科會補助計畫衍生研發成果推廣資料表

日期:2012/11/26

國科會補助計畫	計畫名稱: 鄰近傾斜岩石面對擋土牆主動土壓力之影響
	計畫主持人: 方永壽
	計畫編號: 100-2221-E-009-128- 學門領域: 大地工程

無研發成果推廣資料

100 年度專題研究計畫研究成果彙整表

計畫主持人：方永壽	計畫編號：100-2221-E-009-128-
計畫名稱：鄰近傾斜岩石面對擋土牆主動土壓力之影響	

成果項目			量化			單位	備註（質化說明：如數個計畫共同成果、成果列為該期刊之封面故事...等）
			實際已達成數（被接受或已發表）	預期總達成數(含實際已達成數)	本計畫實際貢獻百分比		
國內	論文著作	期刊論文	0	0	100%	篇	
		研究報告/技術報告	1	1	100%		
		研討會論文	1	1	100%		
		專書	0	0	100%		
	專利	申請中件數	0	0	100%	件	
		已獲得件數	0	0	100%		
	技術移轉	件數	0	0	100%	件	
		權利金	0	0	100%	千元	
	參與計畫人力（本國籍）	碩士生	5	5	100%	人次	
		博士生	0	0	100%		
		博士後研究員	0	0	100%		
		專任助理	0	0	100%		
國外	論文著作	期刊論文	1	1	100%	篇	
		研究報告/技術報告	0	0	100%		
		研討會論文	1	1	100%		
		專書	0	0	100%	章/本	
	專利	申請中件數	0	0	100%	件	
		已獲得件數	0	0	100%		
	技術移轉	件數	0	0	100%	件	
		權利金	0	0	100%	千元	
	參與計畫人力（外國籍）	碩士生	0	0	100%	人次	
		博士生	0	0	100%		
		博士後研究員	0	0	100%		
		專任助理	0	0	100%		

其他成果 (無法以量化表達之成果如辦理學術活動、獲得獎項、重要國際合作、研究成果國際影響力及其他協助產業技術發展之具體效益事項等，請以文字敘述填列。)	1.擔任國內外知名期刊主編/編輯委員/客座編輯 (1) Editorial Board Member, Journal of GeoEngineering (EI) (2) Editorial Board Member, ISRN Civil Engineering-An Open Access Journal (3) 總編輯, 地工技術 2.大型產學計畫與具體成果 (1)計畫名稱：大斷面潛盾隧道技術與應用 (2)執行單位：中華民國隧道協會 (3)贊助單位: 台灣世曦工程顧問公司 (4)說明: 本大型產學計畫由方永壽教授擔任計劃主持人，台北市捷運局鄭國雄副局長、及台灣世曦陳福勝副總經理擔任共同主持人，邀請國內外學者專家，組成研究團隊，評析大斷面潛盾隧道在公路、軌道、維生管線等運用案例之特色，並導引大斷面潛盾隧道之淨空、線形，覆土、環境保護、維護等隧道規劃設計需考量之要點。 3. 計畫主持人榮獲國立交通大學100學年度優良教學獎

	成果項目	量化	名稱或內容性質簡述
科教處計畫加填項目	測驗工具(含質性與量性)	0	
	課程/模組	0	
	電腦及網路系統或工具	0	
	教材	0	
	舉辦之活動/競賽	0	
	研討會/工作坊	0	
	電子報、網站	0	
	計畫成果推廣之參與（閱聽）人數	0	

國科會補助專題研究計畫成果報告自評表

請就研究內容與原計畫相符程度、達成預期目標情況、研究成果之學術或應用價值（簡要敘述成果所代表之意義、價值、影響或進一步發展之可能性）、是否適合在學術期刊發表或申請專利、主要發現或其他有關價值等，作一綜合評估。

1. 請就研究內容與原計畫相符程度、達成預期目標情況作一綜合評估

■達成目標

□未達成目標（請說明，以 100 字為限）

□實驗失敗

□因故實驗中斷

□其他原因

說明：

2. 研究成果在學術期刊發表或申請專利等情形：

論文：□已發表 □未發表之文稿 ■撰寫中 □無

專利：□已獲得 □申請中 ■無

技轉：□已技轉 □洽談中 ■無

其他：(以 100 字為限)

研究成果已撰寫為學術論文,投稿至加拿大的 SCI 學術期刊 Canadian Geotechnical Journal

3. 請依學術成就、技術創新、社會影響等方面，評估研究成果之學術或應用價值（簡要敘述成果所代表之意義、價值、影響或進一步發展之可能性）(以 500 字為限)

本研究探討鄰近堅硬岩石面入侵回填土對擋土牆主動土壓力之影響。本研究以氣乾之渥太華砂為回填土,回填土高及牆高 H 皆為 0.5 公尺。量測於鬆砂(相對密度 Dr = 35%)狀態下，作用於剛性擋土牆的側向土壓力。本研究利用國立交通大學模型擋土牆設備，探討堅硬界面以不同傾角侵入回填土，對擋土牆主動土壓力影響。為模擬堅硬的岩石界面，本研究設計並建造一座鋼製界面板，及其支撐系統。依據實驗結果，獲得以下幾項結論。(1).當岩石界面傾角為 0 度時，其主動土壓力係數 Ka,h 與 Coulomb 解相吻合，其主動合力作用於距擋土牆底部約 0.33H 處。(2)在岩石界面傾角 45、60、70 與 80 度狀況下，側向土壓力隨深度的增加而呈非線性分布，所獲得的側向土壓力低於 Jaky 解，側向土壓力隨界面傾角的增加而減少。(3)當界面傾角為 50 至 80 度，主動土壓合力隨岩石界面傾角的增加而逐漸減小。合力作用點的位置稍高於理論值 0.33H。(4)當傾斜岩石面入侵主動土楔時，造成擋土牆抗滑動之安全係數增加，因此根據 Coulomb 理論所求解之安全係數會偏向安全。(5)當傾斜岩石面入侵主動土楔時，使擋土牆抗傾覆之安全係數增加，所以依據 Coulomb 理論所求得之安全係數會趨於安全。

研究成果有助於大地工程師對作用於鄰近傾斜岩石介面擋土結構物的主動土壓力分布，主動土壓合力的大小與作用位置，可以促進更經濟安全合理的重力式擋土牆設計。